

See discussions, stats, and author profiles for this publication at: <https://www.researchgate.net/publication/301788303>

Space-time observations for city level air quality modelling and mapping

Research · May 2016

DOI: 10.13140/RG.2.1.3950.1685

CITATION

1

READS

300

1 author:



Ipsit Dash

CGI Nederland

7 PUBLICATIONS 1 CITATION

SEE PROFILE

Some of the authors of this publication are also working on these related projects:

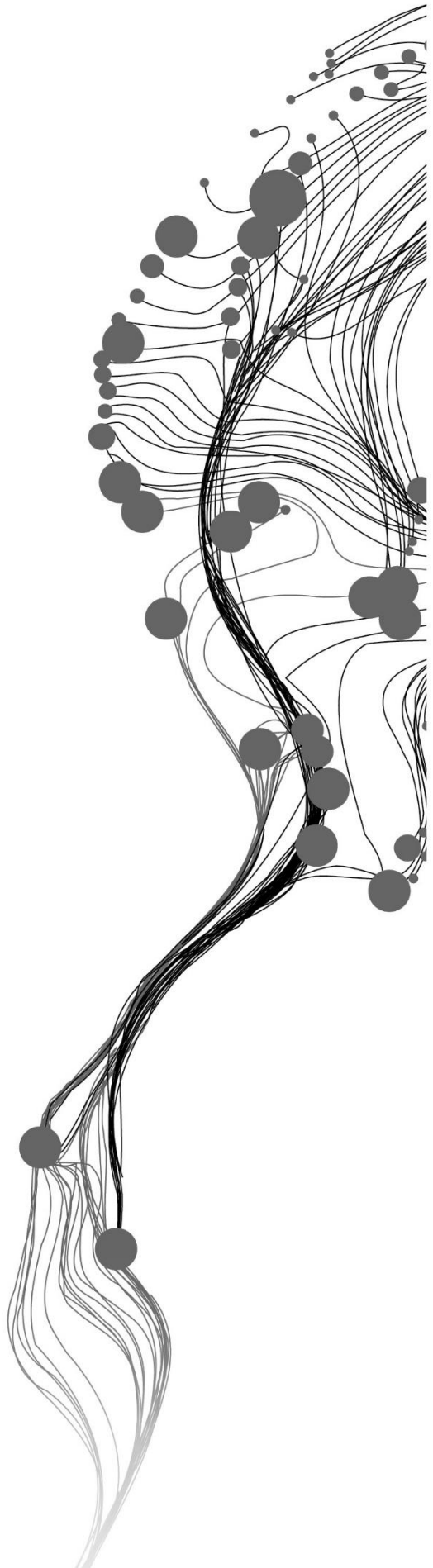


Space-time observations for city level air quality modelling and mapping [View project](#)

SPACE-TIME OBSERVATIONS FOR CITY LEVEL AIR QUALITY MODELLING AND MAPPING

IPSIT DASH
February, 2016

SUPERVISORS:
Dr. N.A.S. Hamm
Prof. Dr. Ir. A. Stein



SPACE-TIME OBSERVATIONS FOR CITY LEVEL AIR QUALITY MODELLING AND MAPPING

IPSIT DASH

Enschede, The Netherlands, February, 2016

Thesis submitted to the Faculty of Geo-Information Science and Earth Observation of the University of Twente in partial fulfilment of the requirements for the degree of Master of Science in Geo-information Science and Earth Observation.
Specialization: Geoinformatics

SUPERVISORS:

Dr. N.A.S. Hamm

Prof. Dr. Ir. A. Stein

THESIS ASSESSMENT BOARD:

Prof. Dr. Ir. M.G. Vosselman (Chair)

Dr. Ir. G. Hoek (External Examiner, IRAS, Utrecht University)

DISCLAIMER

This document describes work undertaken as part of a programme of study at the Faculty of Geo-Information Science and Earth Observation of the University of Twente. All views and opinions expressed therein remain the sole responsibility of the author, and do not necessarily represent those of the Faculty.

ABSTRACT

Spatiotemporal characterization of ambient air quality in a city is an important issue from epidemiological and regulatory standpoint. Observations in form of air quality model predictions and ground based measurement networks can be integrated to model the space-time behaviour of pollutants such as particulate matter and facilitate predictions at unmeasured locations. Prior using model predictions, it is imperative to evaluate their performance against measurements while considering uncertainty levels associated in them. This study firstly, assesses the prediction performance of PM₁₀ and PM_{2.5} from a downscaled city level dispersion model, URBIS against measurements from low cost sensor network ILM at different temporal aggregation. This comparison is asserted by means of model performance criteria that includes various statistical metrics and utilizes measurement uncertainty associated with the ILM network. Secondly, these observations were integrated in a Bayesian maximum entropy framework to generate prediction maps of PM₁₀ and PM_{2.5} in Eindhoven at hourly and daily temporal resolutions. BME approach allowed incorporation of these observations characterized by their uncertainty.

Results of performance evaluation shows that URBIS predictions were consistent with ILM measurements at daily levels of aggregations. Furthermore, these predictions were found accurate at locations proximal to traffic sources and were inconsistent at city background locations. These inconsistencies were attributed to inadequacy in estimation of background concentration levels of PM in the URBIS. Utilization of mean ILM measurements as background values led to substantial improvement in the prediction performance of URBIS. Spatiotemporal maps from the BME integration were able to show the variability in concentration levels in the city at different locations and time periods. Prediction accuracy of BME was evaluated using leave-one-out cross validation method and were found acceptable for PM_{2.5} maps and moderate for PM₁₀. This research concludes that measurements from ILM can be integrated with URBIS for fine-scale mapping of pollutants in the city.

Keywords: particulate matter, URBIS, ILM, BME

ACKNOWLEDGEMENTS

First and foremost, I would like to thank the omnipotent omniscient and omnipresent God for always lighting up my path and guiding me towards righteousness. I dedicate this research work to my parents for their unconditional love, support and sacrifice. I would like to thank all my teachers for motivating me by their exemplifying ideologies, be it through academics or experiences to help build up my character, morale and thirst for knowledge.

This MSc would not have been possible without the blessings of Dr. Parth Sarathi Roy, Ex-Director, Indian Institute of Remote Sensing, Dehradun whose inspiration motivated me to pursue my career in Geoinformation Sciences. My sincere regards to Dr. C. Udhayakumar, Prof. R. Nagendra, Anna University Chennai and Dr. Gyozo Gidofalvi, Dr. Takeshi Shirabe, KTH Royal Institute of Technology, Sweden for their inspiring lectures that always infused in me a zeal to reason and question everything.

I am deeply indebted to my supervisors, Dr. Nicholas Hamm and Prof. Dr. Ir. Alfred Stein, who have shaped my dream of being a young researcher. Their guidance and encouragement all through the research period has been phenomenal. I feel greatly honoured to have been mentored by them and have learnt a lot from their ideas, suggestions and constructive criticisms. I acknowledge my gratitude to Dr. Hamm for sharing his expertise in the field of air quality modelling and his kind support without which my research would not have been possible. I thank Prof. Stein especially for his introductory lecture in the Spatial Data Quality module on 4th January 2015 which steered my enthusiasm toward this domain of research.

I would like to thank Dr. Jan Duyzer, Mr. Sjoerd van Ratingen from TNO and Drs. Hans Berkhout, from RIVM for their help in obtaining essential datasets needed for the research. I appreciate all the fruitful discussions on air quality modelling with Vera van Zoest, Alfredo Gomez and Noshan Bhattraai which also contributed towards the completion of my thesis. I thank Rahul Raj for his advice and his motivation.

I am blessed to have made a wonderful spectrum of friends during my study at ITC. Their love and affection has really supported me to complete my thesis. I really appreciate mental support of my GFM colleagues and ITC amigos especially Rushikesh, Angela, Andreea, Amos, Noshan, Laura and Mirza during my stay in the Netherlands.

Finally, last but certainly not the least, I would like to thank Sheilla Ayu Ramadhani, for being a friend, philosopher and guide. I really acknowledge her crucial contribution in my life.

“There is no such uncertainty as a sure thing”

Robert Burns (1756-96)

TABLE OF CONTENTS

List of figures	vi
List of tables	vii
List of acronyms	viii
1. Introduction.....	1
1.1. Background and significance.....	1
1.2. Motivation and problem statement	2
1.3. Research identification	4
1.4. Thesis structure	4
2. Literature review	5
2.1. Air quality modelling	5
2.2. Particulate matter in the Netherlands.....	6
2.3. Performance evaluation of air quality models.....	7
2.4. Bayesian maximum entropy method.....	8
3. Study area and data.....	11
3.1. Study area	11
3.2. Datasets description.....	12
4. Methods.....	23
4.1. Evaluation of URBIS predictions against ILM measurements.....	23
4.2. Data integration by Bayesian Maximum Entropy method.....	27
5. Results and analysis	33
5.1. Exploratory analysis.....	33
5.2. Performance evaluation of URBIS Model.....	37
5.3. Spatiotemporal prediction of PM values using BME	47
5.4. Comparison of mean ILM measurements with averaged LML for background PM.....	55
6. Discussion.....	59
7. Conclusions	63
7.1. Answer to research questions.....	63
7.2. Limitations and Recommendations.....	65
List of references	67
Appendices	75

LIST OF FIGURES

Figure 1 Municipality of Eindhoven and its constituent districts	11
Figure 2 Population (left) and landuse (right) categorization in Eindhoven (CBS, 2016a)	11
Figure 3 Spatial representativeness of ILM network in Eindhoven	13
Figure 4 Specifications of PPD42NS Optical sensor (AQICN, 2016).....	13
Figure 5 Schematic representation of HDF storage format of ILM measurement data	14
Figure 6 Schematic representation of URBIS dispersion model and its prediction process	16
Figure 7 Location of LML monitoring stations near Eindhoven.....	19
Figure 8 Boxplots of PM ₁₀ (above); PM _{2.5} concentrations (below) at background LML stations	20
Figure 9 Time series of PM ₁₀ measurements from LML background stations and averaged background ..	21
Figure 10 Time series of PM _{2.5} measurements from LML background stations and averaged background	21
Figure 11 Methodology for performance evaluation of URBIS model against ILM measurements	26
Figure 12 Workflow of integration of URBIS predictions with ILM measurement data in BME	29
Figure 13 Input data and prediction grid for BME analysis.....	30
Figure 14 Airbox locations (ILM network) and corresponding URBIS prediction locations	33
Figure 15 Comparison of PM values from ILM, background LML and URBIS foreground predictions ...	34
Figure 16 Exploratory analysis of PM10 values at airbox locations	34
Figure 17 Exploratory analysis of PM2.5 values at airbox locations	34
Figure 18 Temporal visualization of ILM- PM10 values at 32 airbox locations for June 2015	35
Figure 19 Temporal visualization of ILM- PM2.5 values at 32 airbox locations for June 2015	36
Figure 20 Temporal visualization of URBIS- PM10 values at 32 airbox locations for June 2015.....	36
Figure 21 Temporal visualization of URBIS- PM2.5 values at 32 airbox locations for June 2015.....	37
Figure 22 Principle of equal tolerance plots for hourly aggregations - PM2.5.....	43
Figure 23 Principle of equal tolerance plots for hourly aggregations - PM10.....	44
Figure 24 Principle of equal tolerance plots for daily aggregations - PM2.5	45
Figure 25 Principle of equal tolerance plots for daily aggregations - PM10	46
Figure 26 Covariance analysis for BME predictions of daily PM10.	47
Figure 27 Daily PM10 prediction maps in Eindhoven	48
Figure 28 Covariance analysis for BME predictions of daily PM2.5	49
Figure 29 Daily PM2.5 prediction maps in Eindhoven	50
Figure 30 Covariance analysis for BME predictions of hourly PM10	51
Figure 31 Hourly PM10 prediction maps in Eindhoven	52
Figure 32 Covariance analysis for BME predictions of hourly PM2.5	53
Figure 33 Hourly PM2.5 prediction maps in Eindhoven	54
Figure 34 Timeseries of mean ILM values and averaged background from LML stations	55
Figure 35 Covariance analysis for BME predictions of daily PM2.5 (using ILM as background)	56
Figure 36 Daily PM2.5 prediction maps in Eindhoven (using ILM as background)	57
Figure 37 Principle of equal tolerance - daily aggregated PM2.5 (using ILM as background in URBIS predictions).....	58

LIST OF TABLES

Table 1 PM ₁₀ and PM _{2.5} measurements from airboxes used in research.....	12
Table 2 Brief description of ILM dataset	14
Table 3 Discussions on data quality of ILM measurements.....	15
Table 4 Brief description of URBIS dataset.....	17
Table 5 Discussions on data quality of URBIS model predictions	17
Table 6 Description of LML stations near Eindhoven	19
Table 7 Summary statistics of hourly PM values from LML stations.....	20
Table 8 Model performance criteria based on RMSE values (Thunis et al., 2012a).....	25
Table 9 Model performance criteria matrix for evaluation of URBIS predictions(Thunis et al., 2012a)	25
Table 10 Levels of aggregation of URBIS predictions and ILM measurements.....	26
Table 11 Site specific knowledge base (S-KB) for BME analysis	30
Table 12 Summary statistics of PM values from ILM, background LML and URBIS foreground.....	34
Table 13 Representative airbox locations for analysis	38
Table 14 MPC results at five representative stations for hourly aggregations	38
Table 15 MPC results at five representative stations for 6-hourly aggregations	38
Table 16 MPC results at five representative stations for 12-hourly aggregations	39
Table 17 MPC results at five representative stations for daily aggregations	39
Table 18 Estimates of empirical covariance functions- daily PM10 BME analysis	47
Table 19 Parameters for fitting nested covariance model- daily PM10 BME analysis.....	48
Table 20 Estimates of empirical covariance functions- daily PM2.5 BME analysis	49
Table 21 Parameters for fitting nested covariance model- daily PM2.5 BME analysis.....	49
Table 22 Cross validation results- daily predictions BME.....	50
Table 23 Estimates of empirical covariance functions- hourly PM10 BME analysis.....	51
Table 24 Parameters for fitting nested covariance model– hourly PM10 BME analysis.....	51
Table 25 Estimates of empirical covariance functions- hourly PM2.5 BME analysis	53
Table 26 Parameters for fitting nested covariance model- hourly PM2.5 BME analysis.....	53
Table 27 Cross validation results- hourly predictions BME.....	54
Table 28 Estimates of empirical covariance functions- Daily PM2.5 BME analysis (using ILM as background).....	56
Table 29 Parameters for fitting nested covariance model– Daily PM2.5 BME analysis (using ILM as background).....	56
Table 30 Appendix 1: Measurement uncertainty in the ILM	75
Table 31 Appendix 2: Daily PM10 maps in Eindhoven	77
Table 32 Appendix 3 -Daily PM2.5 maps in Eindhoven	78
Table 33 Appendix 4-Hourly PM10 maps for June 04 in Eindhoven.....	79
Table 34 Appendix 5 - Hourly PM2.5 maps for June 04 in Eindhoven.....	80

LIST OF ACRONYMS

PM	Particulate matter
PM ₁₀	Particulate matter with aerodynamic diameter less than 10 $\mu\text{g m}^{-3}$
PM _{2.5}	Particulate matter with aerodynamic diameter less than 2.5 $\mu\text{g m}^{-3}$
UFPs	Ultrafine particles
ILM	Innovatief luchtmeetstelsel (Innovative air measurement system)
URBIS	Urban information system
MPC	Model performance criteria
BME	Bayesian maximum entropy
RMSE	Root mean square error
NMB	Normalized mean bias
NMSD	Normalized mean standard deviation
R	Correlation coefficient

1. INTRODUCTION

1.1. Background and significance

Clean air is a key requirement for human health. As a consequence of numerous anthropogenic activities and physical processes, various pollutants are introduced in the atmosphere, altering the optimal composition of air. These pollutants in the form of gases and particulates of organic and inorganic origin lead to health effects and environmental deterioration. Epidemiological studies have explained the causality of human morbidity and mortality with exposure to polluted air (Brunekreef & Holgate, 2002). Similarly environmental degradation caused by eutrophication, acid rain, smog and climate change have been linked with air pollution (Colls & Tiwary, 2009; Lazaridis, 2011). This has led to an increased interest in understanding the process behind air pollution and developing strategies for its sustainable mitigation.

Air pollutants of concern for human health can be classified into six classes (EEA, 2015c; EPA, 2015) These are oxides of nitrogen (NO_x) formed as combination of nitrogen dioxide (NO_2) and nitrous oxide (NO), ozone (O_3), particulate matter (PM), carbon monoxide (CO), sulphur dioxide (SO_2) and lead (Pb). Amongst these, health risks associated with exposure to particulate matter (PM) are of significant concern, especially given increases in cardiovascular and respiratory disease (Bernard et al., 2001; Kim et al., 2015; Murad, 2012; Shah et al., 2013). Exposure to PM poses a major immediate threat for pregnant women, resulting in increased chances of autism spectrum disorder in offspring (Raz et al., 2014). It also causes health risks in elderly (Liu et al., 2009) and young children (Yip et al., 2004).

PM varies in chemical composition and size. These are composed of non-organic nitrate and sulphate rich secondary aerosols, organic carbon compounds like polycyclic aromatic hydrocarbons (PAH) and metal traces (WHO, 2013). These are generated primarily from transportation (vehicular exhaust, wear and tear of roads, brakes and tyres) and industrial combustion processes (Visser et al., 2001). Secondary sources of PM include those from agriculture (nitrogenous emissions, tillage operations, fertilizers and pesticides), construction (dust particles, paints) and mining (mineral dust, inorganic particulates) (Araujo et al., 2014; Arslan & Aybek, 2012; Juda-Rezler et al., 2011).

PM it is categorized according to its aerodynamic diameter. This categorization is based on different factors such as correlation of size of PM with its gravimetric mass, ability to transport in the atmosphere and level of penetration into human respiratory system (Kim et al., 2015). Thus different categorizes of PM are coarse particulate matter (PM_{10}) with aerodynamic diameter of less than $10 \mu\text{g m}^{-3}$, fine particulate matter ($\text{PM}_{2.5}$) with aerodynamic diameter of less than $2.5 \mu\text{g m}^{-3}$ and ultra-fine particulate matter (UFPs) with aerodynamic diameter less than $0.1 \mu\text{g m}^{-3}$ (US-EPA, 2015). PM_{10} , depending upon local meteorological conditions tend to stay in the atmosphere from few minutes to hours and has movement of few meters to kilometres from emission source to deposition. $\text{PM}_{2.5}$ generally remain suspended in the atmosphere for few days and have movement in range of few to hundreds of kilometres. UFPs tend to remain in the atmosphere for few days to weeks in and are most susceptible to fluctuations in meteorological conditions (Cheung et al., 2011; Srimuruganandam & Shiva Nagendra, 2012).

In recent years, there has been an increased focus for regulating emission levels to improve air quality. Air quality guidelines mandated by the World Health Organization (WHO, 2006) act as a global standard while these are also set by national bodies such as NAAQS (national ambient air quality standards) for U.S.A.

(EPA, 2015), air quality directives for EU (European Union) member states (EU, 2008). In Europe, annual average for PM₁₀ values should not exceed 40 µg m⁻³ and daily average should not exceed 50 µg m⁻³ with 35 allowable exceedances cases per year. These values are set according to the guidelines of air quality directives and should be obtained by 2005 for all member states (EEA, 2014b; EU, 2008). Similarly, the allowable mean limit values for PM_{2.5} should be less than 25 µg m⁻³ achievable by 2015 (Matthijsen & ten Brink, 2007).

Proper enforcement of these regulations require correct determination of PM (PM₁₀ and PM_{2.5}) values in space and time and are obtained by means of air quality measurements or as predictions from air quality models. Air quality modelling, in general involves combining information of atmospheric behaviour of pollutants with observations to model spatiotemporal characteristics of pollutant and provide predictions in space and time. Predictions from these models can be used to characterize emission sources, quantify their contributions and develop pollution reduction strategies. These models differ at various spatiotemporal scales and also on underlying principles of modelling. City-level air quality models are of particular importance as their predictions have substantial implications on local governance strategies such as monitoring adherence to defined emissions protocols, health studies and sustainable urban planning policies (Chang & Hanna, 2004).

1.2. Motivation and problem statement

The behaviour of PM is dynamic in the atmosphere. The concentration and chemical composition does not remain constant over a particular region at a particular time (Yadav et al., 2014). Concentration levels of PM in space and time are measured at ground based stations mainly by semi-continuous automated methods based on mass measurements (like beta attenuation monitors (BAM), filter based gravimetric samplers or tapered element oscillating microbalance (TEOM) or by continuous method such as optical sensors that correlate particle counts with gravimetric mass (EU, 2010; Williams & Bruckmann, 2002). It is only possible to take measurements at a limited number of locations. In order to obtain values at unmeasured locations, modelling is necessary. Air quality models facilitate low cost assessment of air quality by providing predictions for a continuous geographic region and can augment existing ground based measurement network.

Air quality models simulate the behaviour of pollutants in space and time and thus their predictions may be imperfect (Borrego et al., 2008) and associated with a relevant amount of uncertainty. Uncertainties associated in modelling can be due to inadequate representation of sources, errors in modelling procedures, errors associated with input data such as instrument errors and the spatiotemporal variability of PM₁₀ in atmosphere (Riccio et al., 2006) might lead to incorrect representation of pollutant. A near-ideal model would be that which represents adequately the spatiotemporal variability of a pollutant and predicts with a minimal amount of quantifiable uncertainty. Furthermore, formulation of air quality models are dependent on input data, their spatial resolution and temporal frequency. Models designed for predicting air quality such as at city-level require input data at a finer spatiotemporal scale and thus needs to overcome input data scarcity.

Following developments in micro-electrical mechanical systems (MEMs), the availability of cost effective and reliable sensors have become increasingly popular in urban air quality monitoring (Kumar et al., 2015). These distributed system of sensor networks, relying on the state-of-the-art wireless transmission infrastructure can be used for pollutant measurements in near-real time and overcome the observational data scarcity. These measurements can be utilized to support real time assessment of exceedance levels and can be used as input data in air quality models for predicting concentration levels at unmeasured locations (Knox et al., 2013). In Eindhoven, AiREAS initiative (AiREAS, 2014; Close et al., 2016) has set up a low-cost sensor network ILM (Innovatief Luchtmeetstelsel) since 2013. This network measures pollutants like

PM, UFPs, O₃, oxides of nitrogen and meteorological information like temperature and relative humidity at 35 locations (airboxes) spread across the city for every 10 minute interval and are made available in real-time in an online repository (Hamm et al., 2016).

In the Netherlands, to predict pollutant levels in a city, an urban-scale air quality model- Urban Information System (URBIS) (Beelen et al., 2010; Duyzer et al., 2015; Fritz & Borst, 1999) is also used. It is developed and maintained by Nederlandse Organisatie voor Toegepast Natuurwetenschappelijk Onderzoek (TNO) translated as (Netherlands organisation for applied scientific research) (TNO, 2015). URBIS takes into account emissions from various stationary sources (like industries, residential areas and construction sites), non-stationary sources (like traffic in highways and street canyons) and uses an ensemble of dispersion models to provide mean predictions of pollutants like PM (PM₁₀, PM_{2.5}), O₃, NO_x at a yearly basis. In order to use these predictions for augmenting pollution reduction strategies through continuous monitoring, URBIS predictions are downscaled to finer temporal scales such as hourly values.

Integration of predictions from downscaled URBIS model and continuous measurements from ILM network can facilitate an improved understanding of spatiotemporal variability of PM (PM₁₀ and PM_{2.5}) in Eindhoven. However, to use predictions from URBIS model with confidence, it is important to evaluate its performance accuracy. Measurements from the ILM network can be used to evaluate accuracy of URBIS model predictions and can give an overview its performance by employing a number of statistical indicators. Statistical evaluation of air quality models is considered as one of the key methods to assess the accuracy of predictions relative to measured values. Multiple statistical indicators such as root mean square error (RMSE), bias, standard deviation, correlation coefficient have been recommended for evaluation of air quality models. (Borrego et al., 2008). Nonetheless, it is also imperative to consider the uncertainty associated with the PM measurements in the ILM network as the first step for an unbiased evaluation of model accuracy. Limits of measurement uncertainties of pollutants by instruments are generally standardized in the air quality directives with adherence to specific data quality objectives. (Pernigotti et al., 2013). For instance in Europe, relative uncertainty associated with PM is set at 25% around the mean daily values of measurement, whilst that for O₃ is 15% around mean 8-hourly values and NO₂ remains 15% for hourly values (EU, 2010; Thunis et al., 2012a). These are representative standards and actual values depends upon instrument used and on reference time period. Thus URBIS predictions can be evaluated against ILM measurements taking into consideration different statistical indicators standardized by measurement uncertainty of ILM network before its integration.

Modern geostatistical methods like spatiotemporal kriging, can predict concentration levels in with associated prediction error variance that quantifies its uncertainty (Gräler et al., 2012; Knotters et al., 2010). Bayesian maximum entropy (BME) is one such hybrid approach which can be used to model pollutants in a stochastic space-time framework (Christakos & Serre, 2000; Christakos, 1990; Serre & Christakos, 1999). BME formulates on an epistemic knowledge synthesis, taking into account available information to characterize the space-time dependence structure of pollutant and integrates with data from multiple sources to predict concentration levels. It has the ability to incorporate soft data (data with quantified uncertainty in its value) with hard data (data with negligible amount of uncertainty associated with its values) as input and estimates the concentration levels for requisite geographical area and temporal range. Prediction at each location is associated with a probability distribution function which leads to better quantification of estimation uncertainty, in terms of error variances, occurrence probabilities, confidence levels (Pang et al., 2009). Quantification of uncertainty in pollutant concentration estimates is of particular importance for decision makers for applications while assessing exceedance levels and human exposure. Predictions from URBIS can be integrated with ILM measurements in a BME framework to produce spatiotemporal maps of PM levels (PM₁₀ and PM_{2.5}) in Eindhoven that can facilitate continuous monitoring of air quality.

1.3. Research identification

There are two aspects to this research. Firstly, to evaluate PM predictions (PM_{10} and $PM_{2.5}$) of URBIS, by using a set of quantitative statistical indicators, against ILM measurements. Uncertainty associated with ILM measurements is utilized in these statistical indicators. This is to determine, given a threshold uncertainty level in ILM measurements how efficient is the URBIS model in constraining this uncertainty in its predictions.

Secondly, to utilize BME to integrate ILM measurements and predictions from URBIS dispersion model to map spatiotemporal variability of PM in Eindhoven region. The motivation is to compare the prediction of the integrated model against independent measurements and assess the feasibility of using low cost sensor network to augment prediction.

1.3.1. Research objectives

Based on the domain of research identified, the following are the objectives of this research:

1. Statistical evaluation of PM predictions (PM_{10} and $PM_{2.5}$) from the URBIS model against PM measurements from the ILM network using allowable limits of measurement uncertainty.
2. Integration of data from ILM network and URBIS model predictions in a BME framework to map spatiotemporal variability of PM (PM_{10} and $PM_{2.5}$) in Eindhoven.

1.3.2. Research questions

Questions related to objective 1:

- a) What are the key statistical indicators that are needed to evaluate URBIS model?
- b) How to formulate and interpret model performance criteria (MPC) to evaluate URBIS model based on statistical indicators and measurement uncertainty of ILM network?
- c) What are suitable space-time scales for representing PM concentration levels?

Questions related to objective 2:

- a) Which data should be considered as soft (data with uncertainty) and hard (certain data)?
- b) How to model the space-time dependence of PM?
- c) How to integrate space-time dependence of PM with available data from URBIS model and ILM measurements to generate prediction maps?
- d) How can the accuracy of BME process be assessed?

1.3.3. Innovations aimed at

1. Defining model evaluation criteria of PM predictions from the URBIS model against measurements from the ILM network at different temporal scales.
2. Integration of ILM measurements with URBIS model predictions in a BME framework for spatiotemporal mapping of PM in Eindhoven.

1.4. Thesis structure

Chapter 1 gives the rationale of the study and details the research objectives and underlining research questions that are intended to be addressed in the thesis. **Chapter 2** gives a detailed review of the literature pertaining to air quality model evaluation and application of BME in air quality modelling. **Chapter 3** describes the study area and the datasets used in the research and **Chapter 4** gives a conceptual framework and workflow of methods involved. Results and analysis are presented in **Chapter 5**. **Chapter 6** includes discussions of the results. **Chapter 7** summarizes the study and deals with conclusions, limitations and recommendations.

2. LITERATURE REVIEW

2.1. Air quality modelling

Jerrett et al., (2005) reviewed and categorized six different classes of air quality models based on their underlining modelling procedure and assessed their credibility in measuring exposure levels in Hamilton, Canada. These were: proximity models, dispersion models, spatial interpolation models, land use regression models and integrated meteorological-emission models. Proximity based models generally predict concentration levels based on nearness to emission source. These predictions are reliable near pollution sources but tend to be uncertain at non-proximal locations. Land use regression models require an optimal selection of predictor variables for plausible predictions. Spatial interpolation models can be affected by sparse input observations and may produce erroneous results. Regional chemical transport models (CTMs), which take into consideration various meteorological factors and chemical composition of pollutants in atmosphere, tend to deliver predictions at rather coarser resolution that limits its credibility to predict subtle spatial variations such as in a city. Their studies concluded that improvisation in input data and combination of more than one modelling methods tend to increase accuracy of predictions

Daly & Zannetti, (2007) discussed the effectiveness of dispersion models and photochemical models in simulating the behaviour of pollutants in the atmosphere. They explained the behaviour of a pollutant after its emissions in atmosphere is governed by processes of dispersion, transportation, chemical alteration and finally ground deposition. Dispersion models, which tend to model emissions to deposition of pollutant are categorized as Lagrangian models which and Eulerian models based on their interpretation of atmospheric interaction. Whilst Eulerian model divides atmosphere into grids and simulate the behaviour of pollutant at each grid, Lagrangian model consider trajectory of pollutant as an air parcel and simulate its behaviour in space and time.(Nielinger et al., 2004). Photochemical models take into consideration the physical and chemical transformation of a pollutant in the atmosphere and simulate its behaviour. Facilitating low-cost assessment of air quality, these models are preferred for larger geographical regions like national or global level. Nguyen, (2014) reviewed dispersion models, photochemical models and receptor models on the basis of their input data, modelling procedures and probable applications. Receptor models employ series of statistical and mathematical processes to elucidate contributions of different sources of pollution at receptor locations.

Landuse regression models (LUR) have been used to link air quality modelling with human exposures. Ryan & LeMasters, (2007) mentioned four classes of predictor variables that were mostly influential for concentration levels. These were, type of road, traffic counts, elevation and land cover of which traffic count. Beelen et al., (2010) compared the performances of LUR to that of URBIS model in yearly predictions of NO₂ in Rijnmond area in Rotterdam, the Netherlands. They concluded that predictions from URBIS model explained intra-urban small-scale variability better than that of LUR. Studies by de Hoogh et al., (2013); Hoek et al., (2008) gives an understanding about developments of LUR models and its applications in human exposure studies in European cities. Alam & McNabola, (2015) studied the usage of multiple linear regression models in predicting daily levels of PM₁₀ at Vienna and Dublin and were able to demonstrate the effectiveness of LUR in providing consistency in model predictions over time. Wang et al., (2014) developed LURs for NO₂ and PM at continental and regional scales and reported that these LURs provided reasonably good predictions where monitoring stations were absent.

Spatiotemporal interpolation methods used widely in environmental modelling purposes (Li & Heap, 2011, 2014) have also been implemented for air quality studies. Geostatistical methods such as spatiotemporal

kriging, take into account the correlation in space and time of pollutant observation and use it to model predictions at unknown locations. It relies on similarity in air pollutant characteristics governed by its spatiotemporal structure and can be explained by Tobler's law of geography "*everything is related to everything else, but near things are more related than distant things*" (Miller, 2004; Tobler, 1970). Wong et al., (2004) utilized four different methods such as spatial averaging, nearest neighbourhood, IDW and spatial interpolation method of ordinary kriging to predict PM₁₀ and O₃ concentrations in the U.S. and explained the effectiveness of these methods in air quality predictions. Authors reported that kriging provided optimal results with relatively scarce monitoring data. Real-time modelling of air quality was done by Janssen et al., (2008) using measurements and landuse information from CORINE dataset by means of a de-trended kriging model for prediction of pollutants such as O₃, PM₁₀ and NO₂ in Belgium. Jha et al., (2011) appraised various interpolation techniques for predicting suspended particulate matter (SPM), sulphur dioxide (SO₂) and nitrogen dioxide (NO₂) in Port Blair, India and reported that these methods are suitable for prediction when a scarce amount of input data is available.

Hybrid models employ an integrated approach of using two or more modelling frameworks to improvise the prediction abilities by overcoming weakness of individual modelling techniques (Hamm et al 2015). Akita et al.,(2014) demonstrated the effectiveness of discerning intra-urban exposure variability by integrating results of land use regression model and output of chemical transport model in a BME framework. The overall accuracy was higher as compared to individual accuracies of land use regression model or that of chemical transport model. Similar works by Beckerman et al., (2013); Li et al., (2013) also demonstrates the capability of hybrid air quality models for estimating concentration of pollutants with improved accuracy. Works by van de Kassteele et al., (2009); van de Kassteele & Stein, (2006) combined air quality measurements and output from dispersion model by means of external drift kriging (KED) in an Bayesian framework to predict NO₂ in the Netherlands. They were successful in demonstrating the use of KED as a suitable interpolation method and ability to combine different data sources in improvising the predictions. Hamm et al., (2015) utilized a spatially varying coefficient geostatistical (SVC) model to map PM₁₀ in central, south and eastern Europe using measurement data from Airbase network (EEA, 2014c) and regional CTM LOTOS-EUROS (Schaap et al., 2008). Authors concluded that SVC model predictions could be used for mapping exceedance levels of PM₁₀ and also to evaluate the performance of LOTOS-EUROS model.

2.2. Particulate matter in the Netherlands

Matthijssen & Koelemeijer, (2010) showed that anthropogenic sources contributing to PM₁₀ and PM_{2.5} in the Netherlands compose of secondary aerosol formation (including sulphates, nitrates, ammonia, volatile organic compounds, and mineral dust). By implementation of proper policy measures of reducing emissions of secondary aerosols into the atmosphere, considerable amount of reduction in PM levels is expected. Additionally, contribution of sea salt to PM₁₀ and PM_{2.5} levels are 12% and 5% respectively. Emissions from road traffic also account towards contribution to PM_{2.5} and elemental carbon (EC), however PM is majorly dominated by background concentrations. According to Matthijssen & ten Brink, (2007) current annual regional background concentrations of PM_{2.5} range between 12-16 µg m⁻³ while urban background concentration are in range of 16-18 µg m⁻³. Additional increments from the streets predominantly due to traffic lies between 2-6 µg m⁻³ while that for highways lies in range of 7-14 µg m⁻³. VROM, (2008) also reported that major contributions of PM₁₀ in the Netherlands were results from non-anthropogenic sources and from transboundary anthropogenic emissions that dominated local level contributions to PM₁₀.

Even though with stringent European Union policy of using low exhaust vehicles (Euro Standards: light-duty vehicles are Euro V/Euro VI and heavy-duty vehicles are Euro IV (EEA, 2015b)) has led to decrease in PM levels from exhaust emissions, but with increase in traffic count, contribution from non-exhaust

sources like brake wear and tear, tyres, road wears still contribute to the levels of PM. This has also been concluded by studies of Boogaard et al., (2011) wherein high contrasts were found in concentration levels of coarse PM components (Chromium, Copper and Iron), particle number concentrations (PNCs) and black carbon while comparing eight major roadways and nine sub-urban background stations. Keuken et al., (2011) conducted a health impact assessment of PM_{10} and elemental carbon (EC) in Rotterdam by studying the trends in concentration levels and life expectancies for 1985-2008 and concluded that increasing traffic count with efficient vehicular combustion have led to overall decrease emissions. Furthermore, decrease in industrial emissions by stricter regulations and stringent urban planning policies, air quality has improved with decrease of averaged urban PM_{10} background concentration from $43 \mu\text{g m}^{-3}$ (1985) to $25 \mu\text{g m}^{-3}$ (2008) and has resulted in considerable gain life expectancy (for PM_{10}).

Hoogerbrugge et al., (2010) reported that average annual concentration of PM_{10} resulting from anthropogenic sources have reduced considerably since 1990-2000. Approximately two thirds of the decrease was due to reduction in emissions of sulphates and nitrates from anthropogenic sources and remaining from primary vehicle exhausts and secondary aerosols. European Environmental Agency (EEA, 2014a, 2015a) reported that there has been a reduction in the yearly average levels of PM_{10} and $PM_{2.5}$ for the Netherlands. Estimate exposure levels to daily limiting values of PM_{10} (as set by European Union Air Quality Directives (EU, 2008) of $50 \mu\text{g m}^{-3}$) was 0.5% approximately for urban population in 2010 which had increased to 2.9% in 2011 and reduced to 0% by 2012.

2.3. Performance evaluation of air quality models

A detailed discussion on quantitative methods for assessing performance of model predictions to measurements was presented by Bencala & Seinfeld, (1979). Performance of an air quality model can be described broadly in terms of model validity, which refers to the ability of a model to replicate behaviour of a pollutant in atmosphere and model accuracy, which refers to the correctness of model outcome. These methods were based on analysis of residuals (difference in measured concentration and predicted concentration at a particular location and time), analysis of model-measurement agreements including correlation coefficient and linear least square fit and were part of a FORTRAN based performance assessment package called "AQMAAP".

Three major sources of uncertainties can be accounted while evaluating predictions of an air quality model to that of measurements. They are namely, comparison of volume average predictions, generally given by an air quality model to that of point measurements; instrument errors associated with measurements, wrong input parameters and incorrect modelling techniques. MacKay & Bornstein, (1982) presented both quantitative and qualitative methods of evaluating air quality simulation models. The quantitative methods were basic statistical indicators like model bias, gross errors, noise and correlation coefficient defined around pairs of model predictions and observations. Qualitatively, histograms and cumulative frequency plots were favoured by the authors to depict the residuals while isopleths and time-series plots were argued suitable for spatial correlation and temporal correlation respectively. Evaluating two or more air quality models by a composite performance indicator based on aggregating fractional bias and absolute fractional bias was recommended by Cox & Tikvart, (1990).

Chang & Hanna, (2004), reviewed various qualitative and quantitative methods for model evaluation. The authors urge the use of multiple evaluation methods to assess the performance. Apart from discussing about statistical parameters like root mean square error, fractional bias, geometric mean bias, normalized mean square error, geometric variance, correlation coefficient and fraction of predictions within a factor of two of observations, they discussed on qualitative performance indices like Taylor's nomogram method (which

combines normalized standard deviation, normalized root mean square error and correlation coefficient in a single plot), figure of merit in space (ratio of prediction and observation contour area based on a certain threshold) and cumulative distribution function method.

Boylan & Russell, (2006) considered evaluation of air quality models by using model bias (measure of model's over or under-prediction) and model error (measure of deviance of a model's predictions to observations). Similar works have been carried out in Tessum et al., (2015); Thi et al., (2012) wherein evaluation of chemical transport model (CTM) predictions and dispersion model output against measurements based on statistical parameters has been done. Bennett et al., (2013) characterised environmental model performance and also explained various statistical, graphical and qualitative methods for evaluating model output which can be utilized in air quality domain. Borrego et al., (2008), studied different aspects of estimating uncertainty of model predictions and discussed several statistical metrics that can be used for evaluation of performance of air quality model predictions against measurement data.

Air quality model evaluation can be differentiated into multiple components involving scientific evaluation (ability of model to incorporate different emission sources and behaviour of a pollutant in atmosphere), code verification (interpretation of processes as sound mathematical and physical expressions), model accuracy (ability of model to predict concentration levels which coincides with observations) and sensitivity analysis (checking the sub-models for their effectiveness) (Borrego et al., 2008; Chang & Hanna, 2004). Statistical evaluation plays an important role in concluding whether a model is able to replicate the concentration levels based on observed data. It can be considered as a crucial step to determine the effectiveness of a model for a particular application.

Evaluating model predictions against reference data can give credible results if the reference data are error-free. However, both model predictions and measurement data are associated with some degree of uncertainty. These uncertainties in modelling and measurements can be attributed to different sources, such as model might be wrongly formulated or has incorrect input parameters, while measurements may be uncertain due to instrument errors (Borrego et al., 2008; Chang & Hanna, 2004). Thus prior to statistical evaluation of model predictions against measurements, it is important to ascertain the uncertainty in measurement data. This can help in determining how well modelled predictions are against given measurement data and how accurately the model predicts pollutant value, whose actual value might lie between the intervals of measurement data uncertainty. Thunis et al., (2012), proposed a model performance criteria (MPC) that utilizes measurement data uncertainty in these statistical parameters for evaluating air quality model performance. Furthermore, by utilization of various graphical tools like target diagrams, a better insight into model performance can be achieved which can be used by decision makers to see explicitly in which geographical area and time period the model performed well or badly. In works of Pernigotti et al., (2013); Thunis et al., (2013) these aspects of model evaluation were addressed specifically for pollutants like ozone (O_3), particulate matter (PM) and nitrogen dioxide (NO_2). Riccio et al., (2006); Romanowicz et al., (2000) successfully demonstrated uncertainty evaluation for air quality models using a stochastic perspective in a Bayesian framework.

2.4. Bayesian maximum entropy method

Bayesian maximum entropy (BME), detailed by Christakos, (1998) is a spatiotemporal interpolation method that incorporates holistic information about any environmental phenomena (regarded as knowledge base) by considering all available information about it, be it from its physical or chemical behaviour, variations in space and time (regarded as general-knowledge base) and from available data from different sources such as

observations or modelled predictions (regarded as site specific-knowledge base). Author especially highlighted its applicability in cases where limited credible data (termed as hard data) is available, BME facilitates usage of quantified uncertain data (or soft data) in augmenting process of interpolation. In limiting cases BME can be considered similar to spatiotemporal kriging and is also flexible to operate in space-only/time-only domains. Explanation about BME process is presented in details in works of Christakos, Bogaert, & Serre, (2002); Kanevski, (2010). Serre & Christakos, (1999) applied the context of BME to study the water-level elevations of “eqqus bed” aquifers in Kansas and concluded that incorporation of uncertain (soft) data as input with measurement observation (hard data) leads to better accuracy in estimation.

Christakos & Serre, (2000) studied the spatiotemporal distribution of PM₁₀ across North Carolina, United States using BME analysis and concluded that kriging can be considered as a limiting case of BME, and that BME framework facilitates increased flexibility in parameter estimation leading to improved characterization of spatiotemporal variability. Nazelle et al., (2010) used BME approach to predict the concentration of 8-hour O₃ in North Carolina with improved accuracy and precision. They also demonstrated the flexibility of BME method over other modern geostatistical interpolation methods like Bayesian melding. Similar results were presented by Lee et al., (2008) as a synthetic case study, wherein proportion of increased soft data input led to decrease in mean square error of the model predictions. The authors, by using BME were able to improve accuracy in mapping minimum temperature of an urban heat island and demonstrated ability of BME to incorporate soft data. Beckerman et al., (2013) utilized a hybrid model taking into consideration remote sensing data, LUR and Bayesian maximum entropy (BME) methodology to study the spatiotemporal variability of PM_{2.5} in the U.S. The employed BME interpolated predictions were more accurate than the LUR method or remote sensing predictions alone. Similar work by Akita et al., (2014) involved usage of a BME framework to integrate outputs from a dispersion model, LUR model and observation data for intra-city exposure variability of NO₂ half yearly concentration predictions and was able to evaluate that the hybrid model performs better than any individual methods alone. Study done by Adam-poupart et al., (2014) on spatiotemporal modelling of O₃ in Quebec, Canada investigated three methods of predictions namely, LUR modelling, kriging and integrated the output of LUR and kriging in a BME framework and reported that the predictions from the integrated method were the most accurate.

3. STUDY AREA AND DATA

3.1. Study area

The study area is the city of Eindhoven (Figure 1). It spans from (51.40° N, 5.40° E) to (51.49° N, 5.53° E) and is one of the major cities in the Netherlands. Figure 2 (left) is a bar chart showing the population distribution according to different age groups and Figure 2 (right) shows landuse categories in Eindhoven and their proportions (CBS, 2016b).

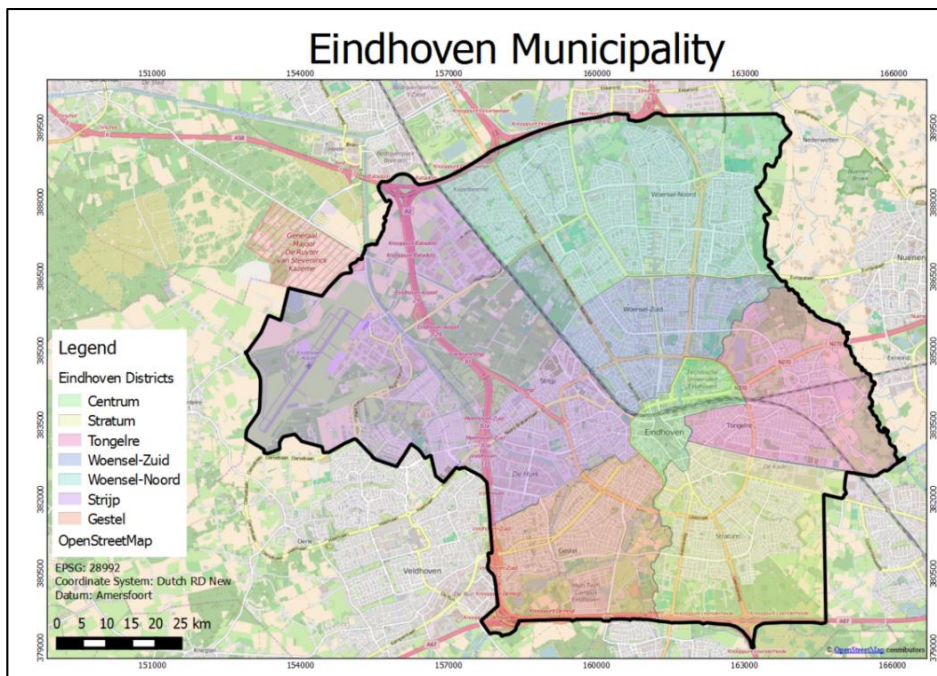


Figure 1 Municipality of Eindhoven and its constituent districts

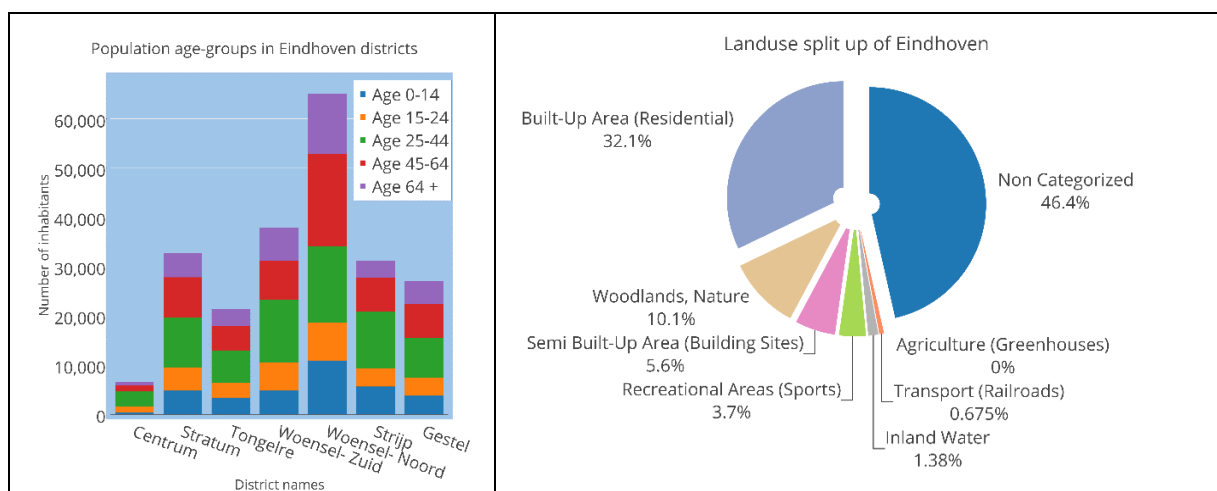


Figure 2 Population (left) and landuse (right) categorization in Eindhoven (CBS, 2016a)

Eindhoven houses 224,855 residents (November 2015) with average population density of 2.5 per km². It consists of 7 districts and has total surface area of 8,887 hectares. Approximately one third area of Eindhoven comprises of residential units and other built up regions and has relatively lower area of greenery. Majority of population resides in district Wessel-Noord (64,405 inhabitants) and least number of inhabitants reside in Centrum district (6565 inhabitants). A distinct share of population belongs to age group of 25-44 and 15-24 and can be attributed to majorly students and working professionals. Majority of industries in Eindhoven are located in districts of Gestel and Strijp, with some of the industries located in northern regions of district Woensel-Noord.

The A2 motorway passes through Eindhoven across the district of Strijp and along district Gestel. Furthermore, road N2 (randweg) forms a beltways around the western border of Eindhoven and consists of motorways A50 and A2. Motorway A270/N270, connects Helmond area with Tongelre district of Eindhoven. These three motorways have potential influence on the PM emissions. Eindhoven airport and aviation base are located in the western part of the municipality (district Strijp), and also contribute to the emission of PM.

3.2. Datasets description

3.2.1. AiREAS initiative- ILM

During recent years, as a strive for clean air and healthy city, a low cost sensor network for measuring air quality has been set up called- ILM (Innovatief Luchtmeetstelsel) translated as “Innovative air measurement system” and operational (AiREAS, 2014; Close et al., 2016). It is a joint initiative of municipality of Eindhoven with University of Utrecht and University of Twente, ECN, Philips and Axians/Imtech ICT. There are currently 35 airboxes operating in and around Eindhoven which give information about local air quality (particulate matter- PM₁₀, PM_{2.5}, PM₁, UFPs, O₃, and NO₂) and meteorology (relative humidity, temperature). This is the basis of ILM network. These data are obtained by respective pollutant sensors installed in the airboxes; transmitted to a central repository via GPRS/GSM. They are then processed and made available for use via an online portal with temporal resolution of 10 minutes.

3.2.1.1. Spatial representativeness of ILM network

Hamm et al., (2016) distinguished four spatial representative classes of locations of the ILM based on two factors. First, it should properly address the emission sources spread across the city of Eindhoven. It should not only include major sources like industrial regions or major highways, but also other sources like street canyons, building sites, residential areas to name a few. Secondly, airbox locations should take into account regions where population is most vulnerable to pollutant exposure, like city centre, busy streets near residential area, schools and hospitals. This is of particular importance in linking studying the effects of air quality on human health. They are busy road which have high density traffic, city background which have least amount of traffic, residential areas including street canyons, regions around city centre, and public hospital. (Figure 3) and (Table 1).

Table 1 PM₁₀ and PM_{2.5} measurements from airboxes used in research

Spatial representativeness of airboxes (Hamm et al., 2016)	Airbox number used in the research
Busy road	3, 4, 7, 11, 23, 25, 26, 34, 35, 36, 37, 39
City background	1, 9, 13, 30, 31
Residential area	2, 5, 6, 12, 14, 16, 17, 19, 20, 24, 27, 28, 32
Public hospital	29

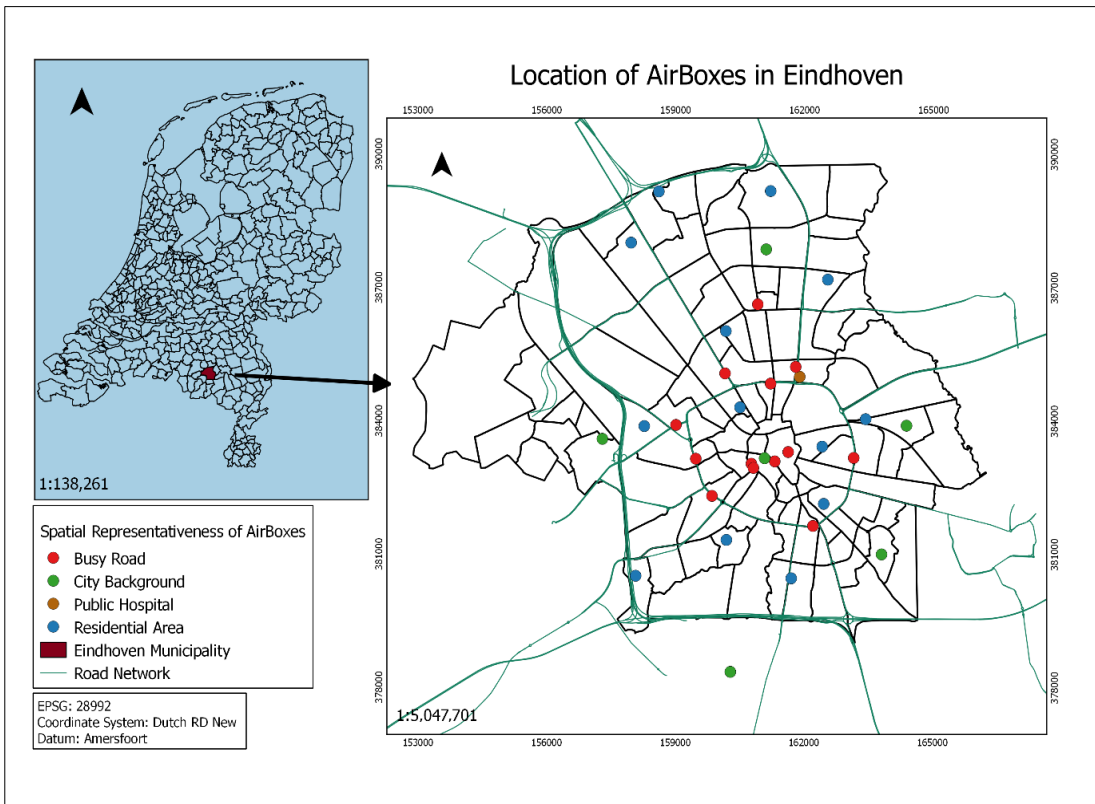


Figure 3 Spatial representativeness of ILM network in Eindhoven

3.2.1.2. PM measurement sensor

All the airboxes in the ILM network are installed with Shinyei PPD42 sensor (Shinyei Technologies, 2010) which is a low cost optical sensor for measuring particulate matter (Figure 4). It consists of a simple arrangement of infrared LED and a photo-transistor detector and air is allowed to pass through the arrangement. Based on light scattering method, the device counts the number of particles based on its aerodynamic diameter. These are classified into 3 types, PM₁₀, PM_{2.5} and PM₁. These values are then transferred to the central microcontroller present in the airboxes which are sent to the central repository.

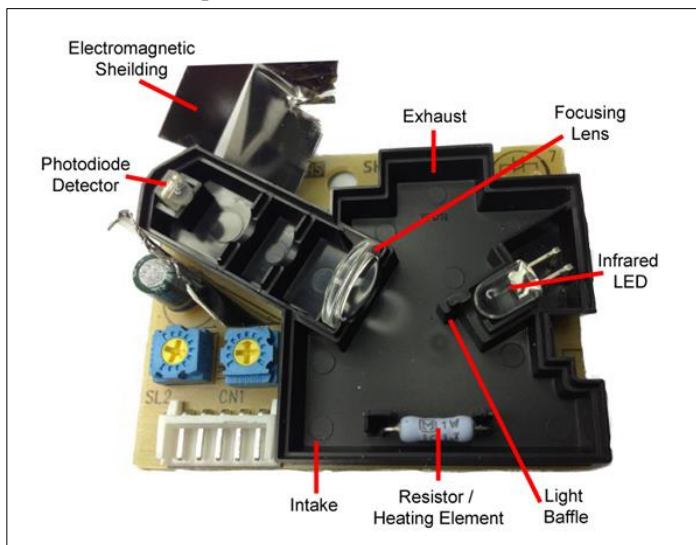


Figure 4 Specifications of PPD42NS Optical sensor (AQICN, 2016)

3.2.1.3. ILM dataset

Measurements at the airboxes are stored in an online repository that can be accessed by the universal resource locator (URL) <http://82.201.127.232:80/>. These are available as both real time data in form of java script object notation (JSON) via URL <http://82.201.127.232:80/api/v1/?airboxid=#.cal> (where # can be replaced by sensor number) while historic data is available in both hierarchical data format (HDF) and comma separated value format (CSV) via URL <http://90.145.62.12:8080/>. Whilst HDF format is indexed by date, that of CSV format is indexed by sensor locations.

A single HDF file consists of all the observations for a particular date. It consists of 3 levels of data indexing (Figure 5). The preliminary indexing level is the date, and the second level is the airbox number and the third level consists of list of attributes for a particular airbox number. Pertaining to each airbox number are 10 observation columns of which 9 are active and contain information about spatial position (latitude and longitude); pollutants measurements (O_3 , PM_{10} , PM_1 , $PM_{2.5}$); meteorological information (relative humidity, temperature) and time. The “Not Used” column contains UFP measurements and is currently available for some airboxes (airbox 10, 18, 38, 25, 36 and 15) where UFP sensor is functional.

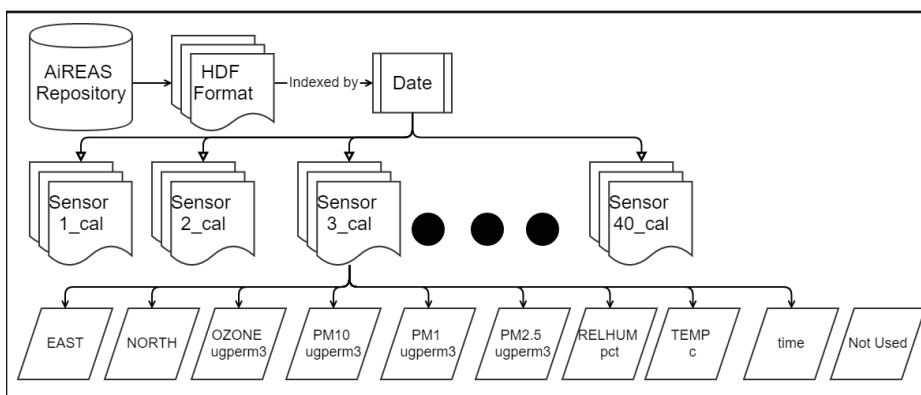


Figure 5 Schematic representation of HDF storage format of ILM measurement data

For this research, data from June, 2015 were used. It was because, downscaled URBIS predictions at hourly interval were available for June 2015. HDF files containing PM_{10} and $PM_{2.5}$ measurement data were available for 1st- 4th June and from 8th- 30th June and were missing for 5th – 7th June in the online repository. These were made available in CSV formats after personal communications with AiREAS officials. Measurements were available for every 10 minutes for each airbox resulting in 144 observations for a single date. Utilizing R environment for statistical computing (v3.2.3) (R Core Team, 2014) it was imported and structured using library h5 (v 0.9.4) (Annau, 2015). 32 airboxes were considered for this research as these were present in the HDF files, corresponding to the above mentioned dates. Using the rollapply function used in zoo package (v 1.7-12) in R (Shah et al., 2005) temporal aggregation of 10 minute observation to hourly values were computed for all the observations at the airbox locations to match the temporal resolution of downscaled URBIS model. Thus utilizing data from both the sources, a completed dataset for June 2015 was created for analysis (Table 2)

Table 2 Brief description of ILM dataset

ILM dataset description	
Pollutant	PM_{10} and $PM_{2.5}$
Locations	32 airboxes
Timeperiod	June 2015 (30 days)
Temporal Resolution	10 minutes

3.2.1.4. Quality of ILM dataset

Before proceeding with the research, the dataset was evaluated qualitatively based on different aspects of geographic data quality presented in ISO/FDIS 19157 report on geographic data quality (ISO, 2013). These are completeness, logical consistency, positional accuracy, thematic accuracy, temporal quality and usability. Qualitative discussions on data quality aspects of ILM are tabulated in

Table 3

Table 3 Discussions on data quality of ILM measurements

Data quality parameter	Results for the ILM dataset (both PM10 and PM2.5)
Completeness of data	<p>Observations were missing for prolonged timeperiods in airbox 6 (8th June 06:00 to 30th June 23:59), airbox 17 (7th June 12:43 to 8th June 12:33), airbox 23 (4th June 13:49 to 11th June 12:37), airbox 25 (6th June 07:39 to 11th June 10:53), airbox 36 (6th June 01:16 to 11th June 12:20) and airbox 39 (5th June 22:37 to 11th June 11:55).</p> <p>Coordinates of airboxes were present for all observations at all timestamps which were redundant as airboxes are stationary.</p>
Logical consistency	Data stored in HDF and CSV formats were suitable to retrieve and structure for processing.
Positional accuracy	<p>Coordinates of airboxes obtained from the dataset were checked against postcodes and locations provided in (Hamm et al., 2016)</p> <p>These were also matched with airbox location description from http://aireas.scapeler.com/index.php/Airbox_Open_Data and were found to be matching.</p>
Thematic accuracy	Due to absence of reference data, this quality parameter could not be evaluated.
Temporal quality	
Usability	Timestamp of data collection in each sensor of ILM network was different which made it difficult to analyse the data at 10 minute interval. Aggregation to hourly values, however solved the purpose and was usable.

3.2.2. URBIS

URBIS (URBAN Information System) (Figure 6) is a city level air quality model developed by TNO(Beelen et al., 2010; Keuken et al., 2011; TNO, 2015). It takes into account different categorizes of emission sources and predicts the concentrations of pollutants like (PM, O₃, NO₂) for user defined locations. Generic URBIS model is an ensemble of three sub-dispersion models which cater specific to the type of emissions (Beelen et al., 2010; TNO, 2015). These are namely, contribution from traffic in the highways (modelled as line sources); contribution from traffic in street canyons (modelled as line sources) and contribution from industries, shipping yards and households (modelled as point and area sources).

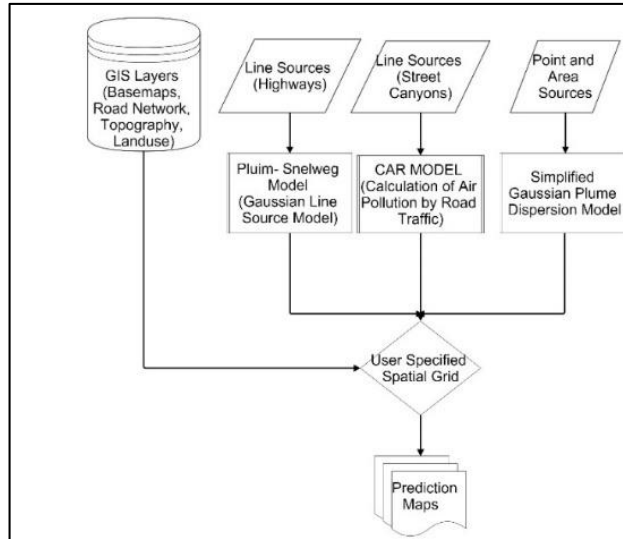


Figure 6 Schematic representation of URBIS dispersion model and its prediction process

Emissions from highway are modelled by a Gaussian line source model (Pluim-Snelweig model) which is a standard dispersion model for line sources (Vardoulakis et al., 2003; Wesseling et al., 1996). It takes buffer region up to 5000 meters across the highways as limit for modelling emissions (Beelen et al., 2010). In a similar manner, the CAR dispersion model (Calculation of Air pollution by Road traffic) (Den Boeft et al., 1996; Eerens et al., 1993; Vardoulakis et al., 2003) is employed for modelling the contribution from road traffic in urban areas, especially city canyons. It takes into account the interaction of built-up area with exhausts and wind, which causes leeside waves. For the CAR model, a buffer up to 30 meters across road pavements is used. Finally to model point and area sources, like emissions from industries, households and other secondary sources, it employs a simplified Gaussian plume dispersion model. Based on user defined spatiotemporal grid, it predicts the concentration of pollutants.

For PM, the calculation of predictions can be represented as, (Amato et al., 2015)

$$C_{slc} = C_{background} + C_{foreground} \quad (1)$$

$$C_{foreground} = \Delta C_{Snelweig} + \Delta C_{Street} + \Delta C_{point\ and\ area\ sources} \quad (2)$$

$$C_{slc} = C_{background} + \Delta C_{Snelweig} + \Delta C_{Street} + \Delta C_{point\ and\ area\ sources} \quad (3)$$

Where, C_{slc} is the total predicted PM concentration, ($\mu\text{g m}^{-3}$)

$C_{background}$ is the contribution of background PM concentration ($\mu\text{g m}^{-3}$)

$\Delta C_{Snelweig}$ is the highways traffic contribution given by Gaussian pluim-snelweig line model ($\mu\text{g m}^{-3}$)

ΔC_{Street} is the contribution from road traffic in street canyons given by the CAR model ($\mu\text{g m}^{-3}$)

$\Delta C_{point\ and\ area\ sources}$ is the contribution from point and area sources modelled by the simplified Gaussian plume model. ($\mu\text{g m}^{-3}$)

The Gaussian pluim-snelweig model and CAR model are given by the following mathematical formula (Amato et al., 2015).

$$\Delta C_{Snelweig} = \frac{E \cdot d_w}{\sqrt{2\pi} \cdot \sigma_z \cdot C \cdot u} \cdot \frac{1}{\pi \cdot \frac{R_B}{n}} \cdot e^{\frac{-(z-h)^2}{2\sigma_z^2}} \quad (4)$$

$$\Delta C_{Street} = E \cdot \theta \cdot F_b \cdot \frac{U}{u_{avg}} \quad (5)$$

Where, E is emission strength per unit length ($\mu\text{g m}^{-1} \text{s}^{-1}$)

d_w is length of road segment (m)

R_B is distance from source to receptor (m)

- σ_z is vertical diffusion coefficient (m)
 z is receptor height (m)
 C is roughness length depended correction factor
 u is wind speed ($m s^{-2}$)
 h is source height (m)
 θ is dispersion equation depending on street type ($s m^{-2}$)
 F_b is correction for trees in the street
 U is annual average reference wind speed ($m s^{-1}$)
 u_{avg} is annual averaged wind speed at specific height ($m s^{-1}$)

For this research a subset URBIS data was made available by TNO for the month of June 2015 (Table 4). This contained hourly particulate matter foreground predictions (PM_{10} and $PM_{2.5}$) at 1226 locations in and around Eindhoven. 32 of these prediction locations corresponds to that of airbox locations (ILM measurement sites) and were used for its performance evaluation against ILM measurements while remaining 1194 locations were used along with ILM observations for integrating in a BME framework to produce spatiotemporal maps of PM in Eindhoven.

Table 4 Brief description of URBIS dataset

URBIS dataset description	
Pollutant	PM_{10} and $PM_{2.5}$ (foreground predictions)
Locations	1226 Locations: (includes 32 airbox locations)
Time period	June 2015 (30 days)
Temporal Resolution	1 hour

3.2.2.1. Quality of URBIS dataset

A qualitative check of data quality of URBIS dataset are tabulated in Table 5. These data quality parameters based on ISO definitions for geographic data quality (ISO, 2013).

Table 5 Discussions on data quality of URBIS model predictions

Data quality parameter	Results for the URBIS dataset (both PM_{10} and $PM_{2.5}$)
Completeness of data	There were no missing observations in the dataset.
Logical consistency	Data stored in CSV formats were suitable to retrieve and structure for processing. However, URBIS foreground predictions contained contributions from Gaussian plume-snelweig model and CAR model. Contributions from point and area sources (simplified Gaussian plume model) were not accounted in these predictions. Background values of PM were also not accounted for in the predictions.
Positional accuracy	Coordinates of URBIS foreground predictions were plotted against airboxes (32 locations). Other prediction locations were plotted which were found to be in and around Eindhoven
Thematic accuracy	PM_{10} and $PM_{2.5}$ values of URBIS foreground predictions were very low (in ranges of few $\mu g m^{-3}$). This was consistent with reports by (Matthijzen & ten Brink, 2007; VROM, 2008) that suggested that traffic contribution to PM levels are generally lower in the Netherlands..
Temporal quality	Due to absence of reference data, this quality parameter could not be evaluated
Usability	Availability of data at hourly values were suitable for the purpose of research

3.2.3. PM background estimation

PM is the combination of contributions from local emission sources and also from the background values (Amato et al., 2015; Lenschow, 2001). As discussed in Section 2.2 PM levels are often dominated by background concentrations as compared to the foreground values(Hoogerbrugge et al., 2010; VROM, 2008). Background concentration levels of PM at a location arises from a number of anthropogenic and natural sources which may not be present in the immediate vicinity of the location. Furthermore, owing to transboundary movement and atmospheric mixing, PM from these sources remain stabilized in the atmosphere for a longer period and their movement depends on meteorological conditions. To account for background concentration of PM in the URBIS model predictions, (Equation 3), PM₁₀ and PM_{2.5} hourly measurements were used from the nearby LML stations.

3.2.3.1. LML monitoring network

Landelijk Meetnet Luchtkwaliteit (LML) translated as Rural Air Quality Monitoring Network is the national air quality measurement network in the Netherlands and are maintained by Rijksinstituut voor Volksgezondheid en Milieu translated as Netherlands national institute for public health and the environment (RIVM) (RIVM, 2015). These stations provide air quality measurements for pollutants like PM₁₀, PM_{2.5}, O₃ and NO₂ to name a few. These values are validated and published on the LML website (<http://www.lml.rivm.nl/gevalideerd/index.php>) as CSV files and infographic maps. PM₁₀ measurements are available as daily averaged values whilst PM_{2.5} measurements are available as hourly values. Since URBIS foreground predictions were hourly values, measurements from LML stations should correspond to hourly values for entire month of June 2015. Hourly PM_{2.5} measurements were obtained from the website and hourly PM₁₀ measurements were obtained after personal communication with RIVM officials.

3.2.3.2. LML stations near Eindhoven

LML stations are distributed all over the Netherlands and five of these are located in and around Eindhoven (Figure 7). Table 6 tabulates the location and characteristics of these LML stations .Two of these stations are located inside the city (Eindhoven- Genovevalaan and Eindhoven- Noordbrabantlaan) are classified as street stations. Air quality at these stations are mostly dominated by road traffic emissions. Another LML stations, Veldhoven-Europalaan is located in the immediate vicinity of Eindhoven and is a designated urban background station. Air quality at this station is majorly influenced by emissions from street canyons, residential areas and other built up areas. To get a better estimation of background values of PM, two more LML stations (which are designated background stations), Vredepeel- Vredeweg and Biest Houtakker-Biestsestraat are also considered in the study. These are located approximately 20-30 kms away from Eindhoven. Thus in order to calculate background values of PM in Eindhoven, measurements from Station 131, Station 230 and Station 247 were considered. These are classified as background stations and measurements from these stations are not influenced by road traffic emissions or emissions from industrial areas or other major sources.

Background values for PM₁₀ and PM_{2.5} are calculated as,

$$C_{background_i} = \frac{C_{i_{station\ 131}} + C_{i_{station\ 230}} + C_{i_{station\ 247}}}{3} \quad (6)$$

Where, i refers to the species of pollutant- PM₁₀ or PM_{2.5}.

$C_{background_i}$ is the hourly averaged background values of PM₁₀ or PM_{2.5}.

$C_{i_{station\ 131}}$ is the hourly measurements from LML station 131.

$C_{i_{station\ 230}}$ is the hourly measurements from LML station 230.

$C_{i_{station\ 247}}$ is the hourly measurements from LML station 247.

Table 6 Description of LML stations near Eindhoven

LML Stations near Eindhoven (centre assumed at 51.43 N, 5.48 E)				
Name	Latitude (degrees)	Longitude (degrees)	Distance to Eindhoven approx(km)	Classification
Station 131 Vredepeel- Vredeweg	51.54N	5.85E	28	Background Station
Station 236 Eindhoven- Genevievolaan	51.47N	5.47E	4	Street Station (inside city)
Station 237 Eindhoven- Noordbrabantlaan	51.44N	5.44E	3	Street Station (inside city)
Station 247 Veldhoven- Europalaan	51.41 N	5.39E	7	City Background Station
Station 230 Biest Houtakker- Biestsestraat	51.52N	5.15E	25	Background Station

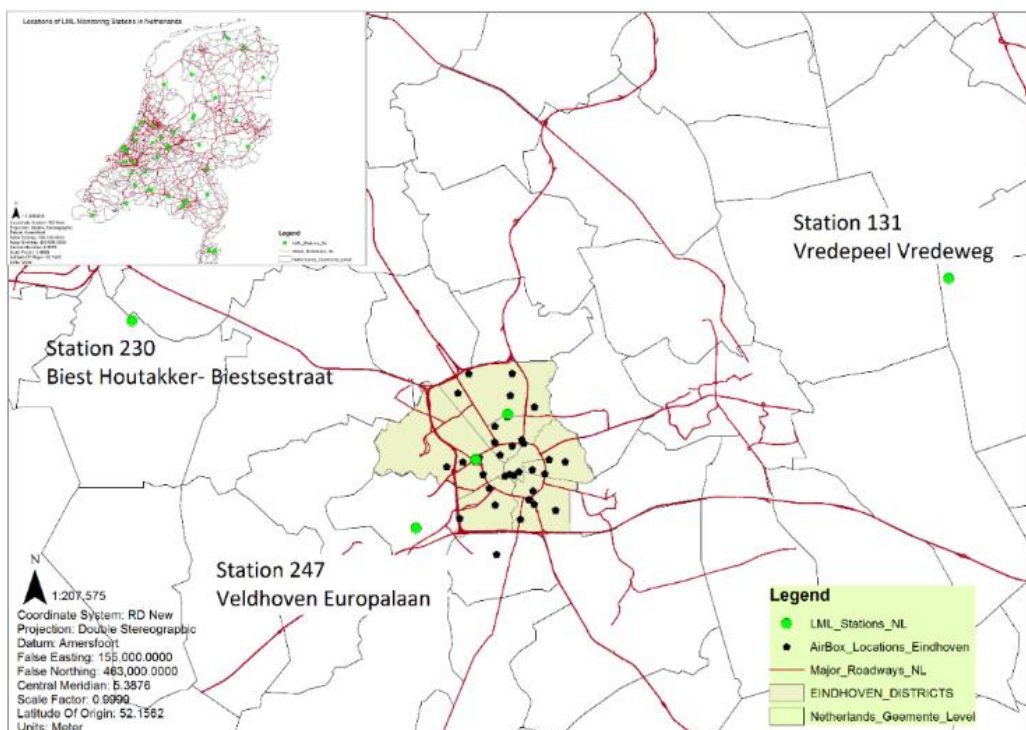


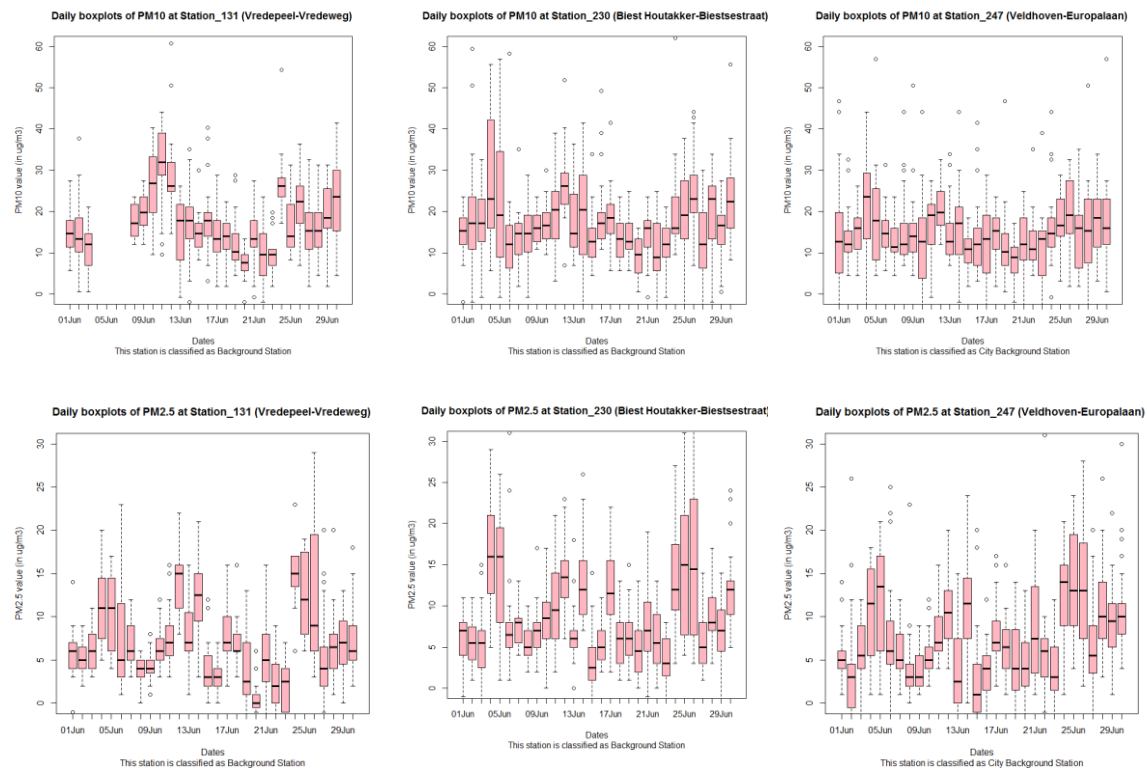
Figure 7 Location of LML monitoring stations near Eindhoven

The summary statistics of these background stations and the corresponding averaged PM concentrations are shown in tabular format in Table 7. The analysis is done for both PM₁₀ and PM_{2.5}. Prior to averaging these concentration values from background stations, there were some issues with the values. Some hourly measurements were negative values. These values might occur in the data due to calibration problems or sensor malfunction. Negative values of PM were replaced with NA. Furthermore, there were some missing observations in all stations and these were also taken into consideration before calculating the average.

Table 7 Summary statistics of hourly PM values from LML stations

	PM ₁₀ ($\mu\text{g m}^{-3}$)				PM _{2.5} ($\mu\text{g m}^{-3}$)			
	Station 131	Station 230	Station 247	Averaged Background	Station 131	Station 230	Station 247	Averaged Background
Mean	18.04	17.95	15.85	17.10	7.16	8.82	8.04	8.06
NA values	167	29	38	0	56	13	51	0

From Table 7 it can be seen that the mean values of PM₁₀ and PM_{2.5} at the three background stations tends to be similar. The difference of averaged value to that of the mean measurement of PM10 was largest for Station 247 and least for Station 131. Similarly, this difference was largest for Station 131 for PM2.5. To study the trend in concentration levels at these stations, boxplots of PM₁₀ and PM_{2.5} measurements at these stations for June 2015 (Figure 8). From these boxplots, it can be seen that these measurements at these stations show similar trends in values averaged value can be considered as the background values of PM in Eindhoven.

Figure 8 Boxplots of PM₁₀ (above); PM_{2.5} concentrations (below) at background LML stations

To further emphasize on the similar trends in particulate matter concentrations at these stations, timeseries plots were drawn for both PM₁₀ (Figure 9) and PM_{2.5} (Figure 10). It was done using timeProp function in “openair” library (v 1.6.7) in R (Carslaw & Ropkins, 2012). These were plotted along with averaged background values that was calculated from these three stations. It can be seen that averaged background values (shown in violet) resembles approximately the trends of individual background stations in time. Smoothing line represented in each time series is lowess smooth line and uses locally weighted linear regression to smooth the data with 95% confidence interval. There were some time periods where there were missing observations and abrupt increases in concentration levels at individual stations, that might affect the averaging.

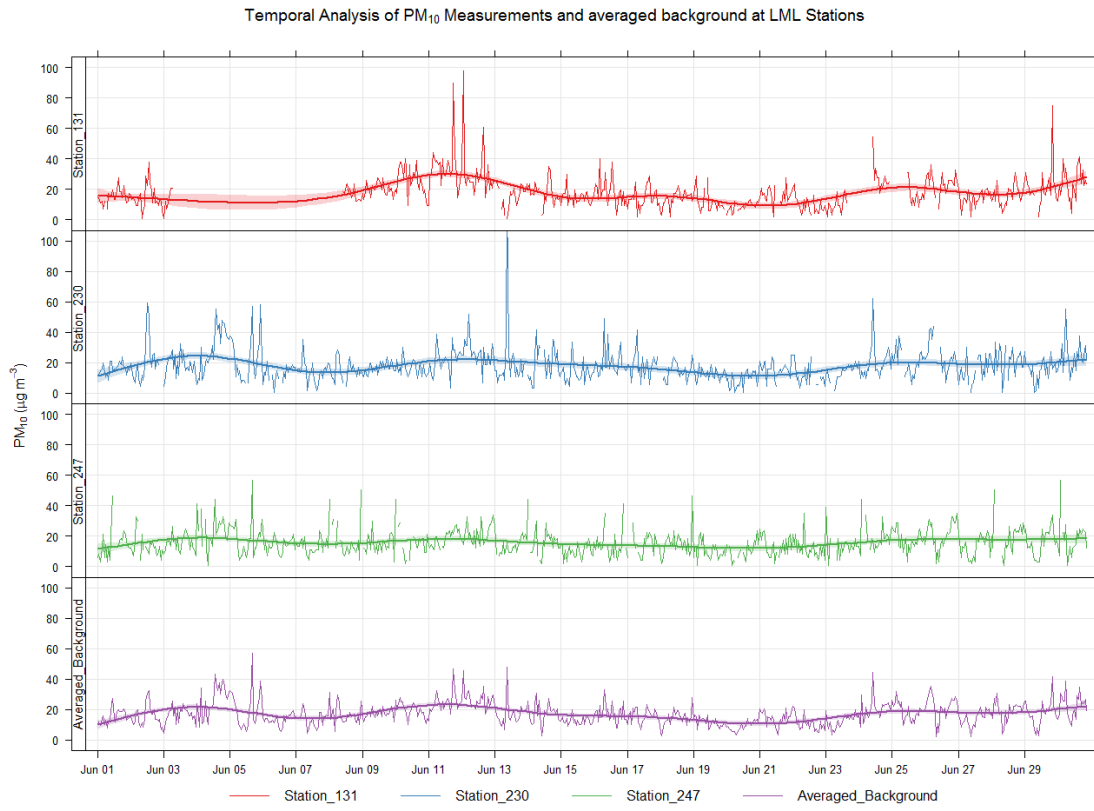


Figure 9 Time series of PM₁₀ measurements from LML background stations and averaged background

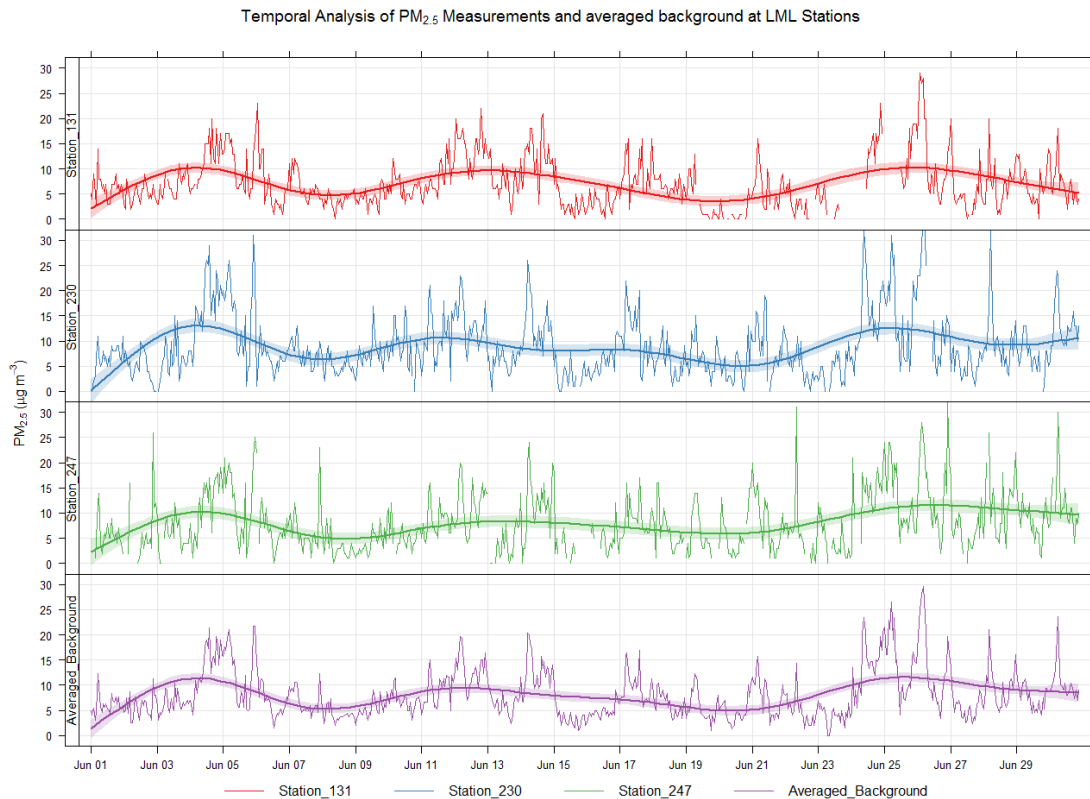


Figure 10 Time series of PM_{2.5} measurements from LML background stations and averaged background

Thus average concentration levels from these three stations were added to URBIS foreground predictions (contribution from traffic in highways and street canyons) to yield PM₁₀ and PM_{2.5} concentration levels at URBIS prediction locations. The sum of URBIS foreground and averaged background concentration from LML stations are considered as URBIS predictions as a naming convention in the research.

4. METHODS

4.1. Evaluation of URBIS predictions against ILM measurements

4.1.1. Conceptual description

Thunis et al., (2012) describes the usage of measurement uncertainty (U) in evaluating model predictions against measurements. Uncertainty of measurement data depends on relative uncertainty associated with measurement of a pollutant species as per air quality directives (EU, 2010), dataset, reference time for averaging, measurement techniques and instrument used. It is generally estimated by experimental methods (Pernigotti et al., 2013; Thunis et al., 2013). Utilization of measurement uncertainty interval $\pm U$ in the measurements leads to a range of values where actual concentration value is assumed to lie. The process assumes that the model predictions, in order to perform accurately, should also lie in the same interval thereby concluding how well model predictions are against the measurement data around these limits. This can thus be utilized in comparing modelled predictions for an unbiased evaluation. Furthermore, by using statistical indicators around these uncertainty margins $\pm U$ a definitive model performance criteria (MPC) can be generated which describes the minimum level of quality that is sufficient for the modelling application with respect to measurement data.

4.1.1.1. Measurement uncertainty

Measurement uncertainty (U) is defined as (Thunis et al., 2012a):

$$U = \sqrt{\frac{1}{N} \sum_{i=1}^N (U_r(O_i) * O_i)^2} \quad (7)$$

Where, $U_r(O_i)$ refers to the total uncertainty in the measurement instrument for a particular pollutant,

U_r refers to the relative uncertainty of a given pollutant,

O_i refers to the measurement values for time i and

N refers to the total number of observation instances.

Based on European Union Air Quality directives (EU, 2008), the value of U_r is set to 25% for mean daily values of PM₁₀ and PM_{2.5} and should be noted that this 25% is a guideline that should not be exceeded. Since actual value of measurement uncertainty $U_r(O_i)$ was not available for the PM sensor in ILM network, the standardised value of 25% was used. Furthermore, this value is assigned for daily values of PM10 and PM2.5 as measurement uncertainty tends to increasingly fluctuate for lower temporal resolutions. Absence of information on these values for hourly, 6-hourly and 12-hourly scales lead to assumption of constant value of 25% of measurement uncertainty in this research. Similarly, predictions from the URBIS model, which are heavily dominated by background concentration obtained by averaging measurements from the LML stations, the model uncertainty for PM₁₀ and PM_{2.5} was also assumed to be 25 %. Uncertainty associated with PM measurements at LML stations have been reported to be 16 % for daily values and tend to increase drastically for increased temporal resolutions (Hoogerbrugge et al., 2010) Furthermore, uncertainties due to averaging of measurements from LML stations and those associated with URBIS model

formulations whose exact values could not be obtained also contribute to model uncertainty .Thus model uncertainty was also assumed to be 25% for all temporal resolutions.

Measurement uncertainty is utilized to normalize key statistical indicators like root mean square error (RMSE), normalized mean bias (NMB), normalized mean standard deviation (NMSD) and correlation coefficient (R) to portray how effective model predictions are against measurements. Although literature review suggests several other statistical parameters that can be utilized for performance evaluation(Section 2.3), based on recommendations of forum for air quality modelling in Europe (FAIRMODE) JRC, (2015); Thunis et al., (2015); Thunis et al., (2012b) Borrego et al., (2008) the following statistical parameters are considered for definition of model performance criteria (MPC).

Root mean square error is defined as (Chang & Hanna, 2004; Thunis et al., 2012a):

$$RMSE = \sqrt{\frac{1}{N} \sum_{i=1}^N (O_i - M_i)^2} \quad (8)$$

Where, O_i refers to measurement for time i

M_i refers to model predictions at time i and

N refers to the total number of observation instances.

Normalized mean bias is defined as (Thunis et al., 2012a):

$$NMB = \frac{\bar{M} - \bar{O}}{\bar{O}} = \frac{Bias}{\bar{O}} \quad (9)$$

Where, \bar{M} refers to the mean of the predictions for a single location at all observation instances

\bar{O} refers to the mean of the measurements for a single location at all observation instances.

Normalized mean standard deviation is defined as (Thunis et al., 2012a):

$$NMSD = \frac{\sigma_M - \sigma_O}{\sigma_O} \quad (10)$$

Where, σ_M is the standard deviation of model predictions at a single location at all observation instances

σ_O refers to standard deviation of the measurements at a single location at all observation instances.

Correlation coefficient is defined as (Thunis et al., 2012a):

$$R = \frac{\sigma_M^2 + \sigma_O^2 - \sqrt{RMSE^2 + bias^2}}{2\sigma_M\sigma_O} \quad (11)$$

4.1.1.2. Derivation of model performance criteria for URBIS model

Model performance criteria (MPC) for URBIS model predictions based on measurement uncertainty of PM values in ILM network were based on the method proposed by Thunis et al., (2012a) These criteria were defined for four statistical metrics, $RMSE$, NMB , $NMSD$ and R .

For equal tolerance levels of uncertainty in model and measurement($\pm U$), $RMSE$ is divided by $2U$, and hence the MPC for $RMSE$ is:

$$RMSE_U = \frac{RMSE}{2U} = \frac{\sqrt{\frac{1}{N} \sum_{i=1}^N (O_i - M_i)^2}}{2U} < 1 \quad (12)$$

Three cases can be concluded for the values of $RMSE_U$ for a single location concerning all temporal episodes (Table 8):

Table 8 Model performance criteria based on RMSE values (Thunis et al., 2012a)

$RMSE_U$	Conclusion
>1	Model predictions do not coincide with observations. The uncertainty levels ($\pm U$) of model predictions and observations do not overlap.
(0.5,1]	Uncertainty levels ($\pm U$) of model predictions and observations overlap partially and model predictions are in acceptable range to observations.
< 0.5	Model predictions coincide with observations and the uncertainty levels ($\pm U$) of model predictions and observations overlap.

Similarly, the MPC for NMB as described in (Thunis et al., 2012a) is:

$$|NMB| < \frac{2U}{\bar{o}} \quad (13)$$

MPC for $NMSD$ as described in (Thunis et al., 2012a) is:,

$$|NMSD| < \frac{2U}{\sigma_o} \quad (14)$$

MPC is derived for R as described in (Thunis et al., 2012a)

$$R > 1 - 2 \left(\frac{U}{\sigma_o} \right)^2 \quad (15)$$

Table 9 summarizes four definitions of MPC that are utilized to evaluate PM_{10} and $PM_{2.5}$ predictions from URBIS model against ILM measurements. This evaluation is performed at different temporal scales so as to determine in which temporal resolution (hourly, 6-hourly, 12-hourly or daily) URBIS model predictions correspond optimum to those of ILM measurements.

Table 9 Model performance criteria matrix for evaluation of URBIS predictions(Thunis et al., 2012a)

MPC definitions for URBIS model evaluation		
Statistical Metric	Model Performance Criteria	Comments
Root mean square error	$RMSE_U < 1$	
Normalized mean bias	$ NMB < \frac{2U}{\bar{o}}$	$\frac{2U}{\bar{o}}$ is considered as MPC NMB
Normalized mean standard deviation	$ NMSD < \frac{2U}{\sigma_o}$	$\frac{2U}{\sigma_o}$ is considered as MPC NMSD
Correlation coefficient	$1 - R < 2(U/\sigma_o)^2$	$2(U/\sigma_o)^2$ is considered as MPC R

4.1.2. Workflow

The workflow for evaluating URBIS predictions against ILM measurements is depicted in Figure 11. ILM measurements (PM_{10} and $PM_{2.5}$) obtained at 10 minute resolution at 32 airboxes for June 2015 are aggregated to different temporal resolutions. Similarly, hourly PM_{10} and $PM_{2.5}$ predictions from URBIS model, available at these 32 airbox locations for June 2015 were also aggregated (Table 10). Evaluation were done at four different temporal scales. Whilst for URBIS model predictions, hourly values were aggregated to 6-hours, 12- hours and 24 hours; for ILM measurements, data obtained at 10 minute interval were aggregated to hourly, 6-hour, 12- hours and 24 hours.

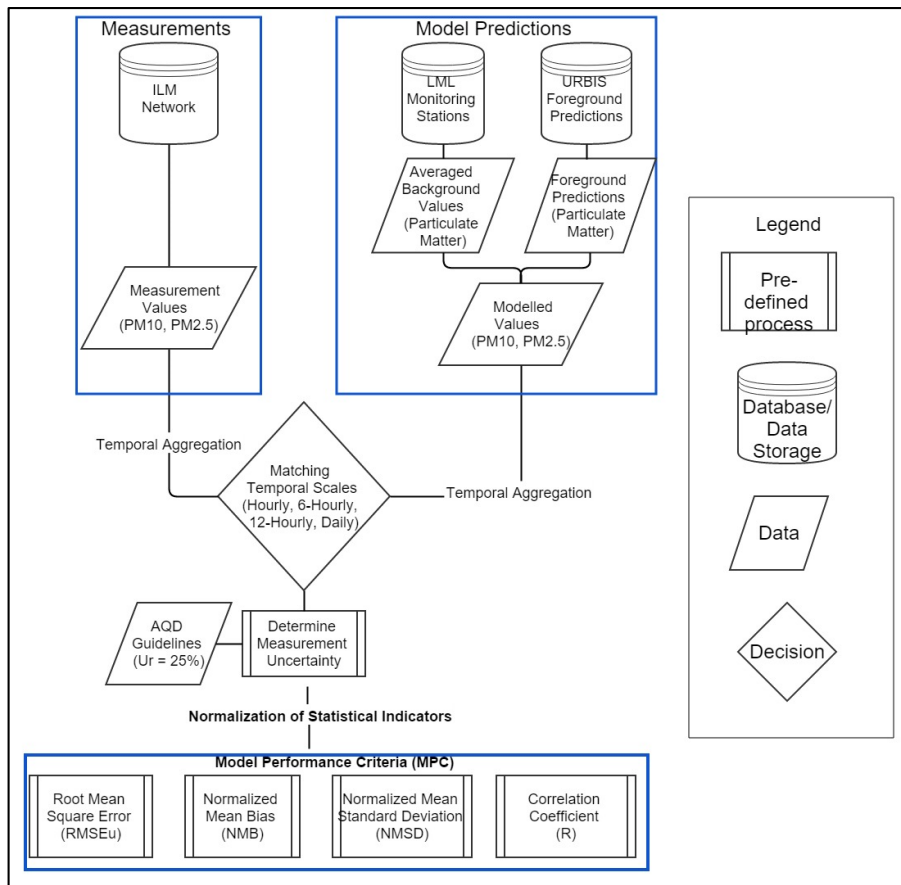


Figure 11 Methodology for performance evaluation of URBIS model against ILM measurements

Table 10 Levels of aggregation of URBIS predictions and ILM measurements

Temporal Aggregation	Spatial locations	Temporal Instances	Comment on URBIS data (Model)	Comments on ILM data (Measurement)	
Hourly	32	720	Default temporal resolution, no aggregation needed	Measurements obtained at 10 minute interval were aggregated to requisite levels.	
6-Hourly		120	Hourly observations were aggregated		
12-Hourly		60			
Daily (24-Hourly)		30			

Since the exact value of measurement uncertainty for PM sensor in ILM network was unknown, measurement uncertainty (U) for the performance evaluation framework was considered to be 25% (for PM_{10} and $\text{PM}_{2.5}$) based on EU- AQD (Denby & Larssen, 2010; EU, 2008). This value corresponds to the maximum allowable uncertainty of particulate matter for daily values and was assumed constant for all temporal aggregation levels. Based on the formula mentioned in Section 4.1.1.2, measurement uncertainty (U) was calculated for different aggregation levels of ILM measurements and URBIS model values. This was used to generate MPC metrics for PM_{10} and $\text{PM}_{2.5}$ for different temporal aggregations to assess at which optimal resolution URBIS predictions are similar to ILM measurements. .

4.2. Data integration by Bayesian Maximum Entropy method

4.2.1. Conceptual description

Bayesian Maximum Entropy uses an epistemic knowledge synthesis framework and considers spatiotemporal behaviour of a pollutant can be asserted by possessing knowledge about two concepts which are analogous as subjective (concepts and belief about any phenomenon) and objective (measured or actual evidence) paradigms of philosophy (Christakos et al., 2002; Yu et al., 2015).

Available information about a pollutant in space and time corresponds to **Total knowledge base (T)** comprising of the following components:

- **General knowledge base (G-KB):** This consists of information that describes the spatiotemporal dependence structure of a pollutant in space and time. It includes physical interaction laws, conceptual models, spatiotemporal mean trend and spatiotemporal covariance functions. This information can be ascertained from various sources such as previous knowledge about pollutant behaviour, experiments, statistical modelling to name a few.
- **Site-specific knowledge base (S-KB):** It is a database containing observations of pollutant, their coordinates in space and time and associated uncertainty in their values. These observations can be obtained from various sources such as from measurement networks, model predictions. Observations are categorized based on their uncertainty levels in two categories. These are hard data and soft data.
 - Hard Data corresponds to observations that are obtained at satisfactory level of accuracy. Since their values are certain, these are represented as numerical values in the database.
 - Soft Data comprises of observations which have inherent uncertainty associated with their values. These observations are represented in probabilistic form or in intervals in the database.

PM values in Eindhoven can be considered as a spatiotemporal random field model (S/TRF). A S/TRF is a spatiotemporal data structure comprising of locations in time and space (denoted as nodes) and its attributes (Christakos, 2000; Serre & Christakos, 1999). In this study, these correspond to PM values at spatial coordinates (locations) in Eindhoven for entire month of June 2015. This S/TRF is denoted as $X(p)$. where, $p = (s, t)$ represents its location in space and time. $s = (x, y)$, where s refers to the location in two-dimensional space and t is time point.

$X(p)$ refers to nodes where observations (hard and soft data) are present and also to nodes where interpolation is to be performed (locations without any attribute value). Locations of hard data are denoted as p_{hard} , locations of soft data points are denoted as p_{soft} and locations where predictions are to be done can be considered as p_k . Similarly, $X_{map}(p)$ consists of attribute values and includes $X_{hard}(p)$, $X_{soft}(p)$ and $X_k(p)$.

Thus attribute of the S/TRF can be considered as:

$$X_{map}(p) = [X_{hard}(p), X_{soft}(p), X_k(p)] \quad (16)$$

Where, $X_{data}(p) = X_{hard}(p) \cup X_{soft}(p)$ and $X_{data}(p) \subset X_{map}(p)$

The total spatiotemporal range of S/TRF p_{map} is represented as:

$$p_{map} = [p_{hard}, p_{soft}, p_k] \quad (17)$$

Let, χ_{map} is a realization at points p_{map} of the given S/TRF and is represented by the multivariate probability distribution function (PDF) given by:

$$f_X(\chi_{map})d\chi_{map} = Prob[\chi_{map} < X_{p_{map}} < \chi_{map} + d\chi_{map}] \quad (18)$$

It consists of attributes of soft and hard data which are represented as:

$$\text{Hard Data: } Prob[X_{hard}(p) = \chi_{hard}] = 1$$

$$\text{Soft Data: } Prob[X_{soft}(p) < q] = \int_{-\infty}^q d\chi_{soft} f_{S-KB}(\chi_{soft})$$

BME integrates G-KB (spatiotemporal dependence structure) and S-KB (attributes values) in three steps to model the spatiotemporal characteristics of PM (Hwa-Lung & Chih-Hsin, 2010; Lee et al., 2009; Rajasegaran et al., 2014).

The steps can be described as:

1. Prior Stage: The expected information contained in the S/TRF for X_{map} is computed by the entropy function as

$$E[Info_{G-KB}(X_{map}(p))] = - \int f_{G-KB}(X_{map}(p)) \log[f_{G-KB}(X_{map}(p))] dX_{map}(p) \quad (19)$$

Where, f_{G-KB} constitutes a multivariate PDF model whose shape is determined by maximizing the expected prior information available based on G-KB (such as spatial covariance structure and temporal covariance structure, spatiotemporal mean)

$$E[g_\alpha(X_{map}(p))] = \int g_\alpha(X_{map}(p)) f_{G-KB}(X_{map}(p)) dX_{map}(p) \text{ for } \alpha = 0, 1, 2 \quad (20)$$

- a) $\alpha = 0, g_0 = 1$;
- b) $\alpha = 1, g_1 = E[(X_{map})]$ refers to mean trend describing spatiotemporal structure.
- c) $\alpha = 2, g_2 = E[\{(X_{map}(p)) - E[(X_{map}(p))]\} \{(X_{map}(p')) - E[(X_{map}(p'))]\}]$
which refers to the covariance function that denotes spatiotemporal dependencies.

By using Lagrange's multiplier, optimization of g_α is done and prior PDF is determined. The prior PDF can be written as:

$$f_{G-KB}(X_{map}(p)) = J^{-1} e^{-\psi_{G-KB}(X_{map}(p))} \quad (21)$$

Where, values of J and $\psi_{G-KB}(X_{map}(p))$ are derived by equations below and μ_0, μ_α refer to Lagrange multipliers.

$$J = e^{-\mu_0} \quad (22)$$

$$\psi_{G-KB}(X_{map}(p)) = \sum_{\alpha=1}^2 \mu_\alpha g_\alpha(X_{map}(p)) \quad (23)$$

2. Meta-prior Stage: Site specific knowledge, in terms of hard and soft data are considered and the prior PDF is optimized by Bayesian conditionalization (Christakos, 2000).

3. Integration Stage: The posterior PDF is generated based on the integration of G-KB and S-KB. After incorporating the site-specific knowledge base (S-KB) in form of soft and hard data in the prior PDF (Equation 30), posterior PDF can be written as:

$$\psi_{S-KB}(X_{map}(p)) = A^{-1} \int_1^{p_{map}} e^{\psi_{G-KB}(X_{map}(p))} df_{S-KB}(X_{map}(p)) \quad (24)$$

Where, $f_{S-KB}(X_{map}(p))$ refers to the cumulative distribution function (CDF) containing soft and hard data in S-KB. A is the normalization constant and is given by the following equation (Rajasegaran et al., 2014):

$$A = \int_1^{p_{map}} df_{S-KB}(X_{soft}(p)) f_{G-KB}(X_{map}(p)) \quad (25)$$

4.2.2. Workflow and processing

The flowchart for integration of URBIS model predictions and ILM measurement data in the BME framework is depicted in Figure 12. BME processing was implemented in STAR-BME plugin (Yu et al., 2015; Yu et al., 2012; Yu, 2014) in QGIS (v 2.10.1 Pisa) (QGIS Development Team, 2015).

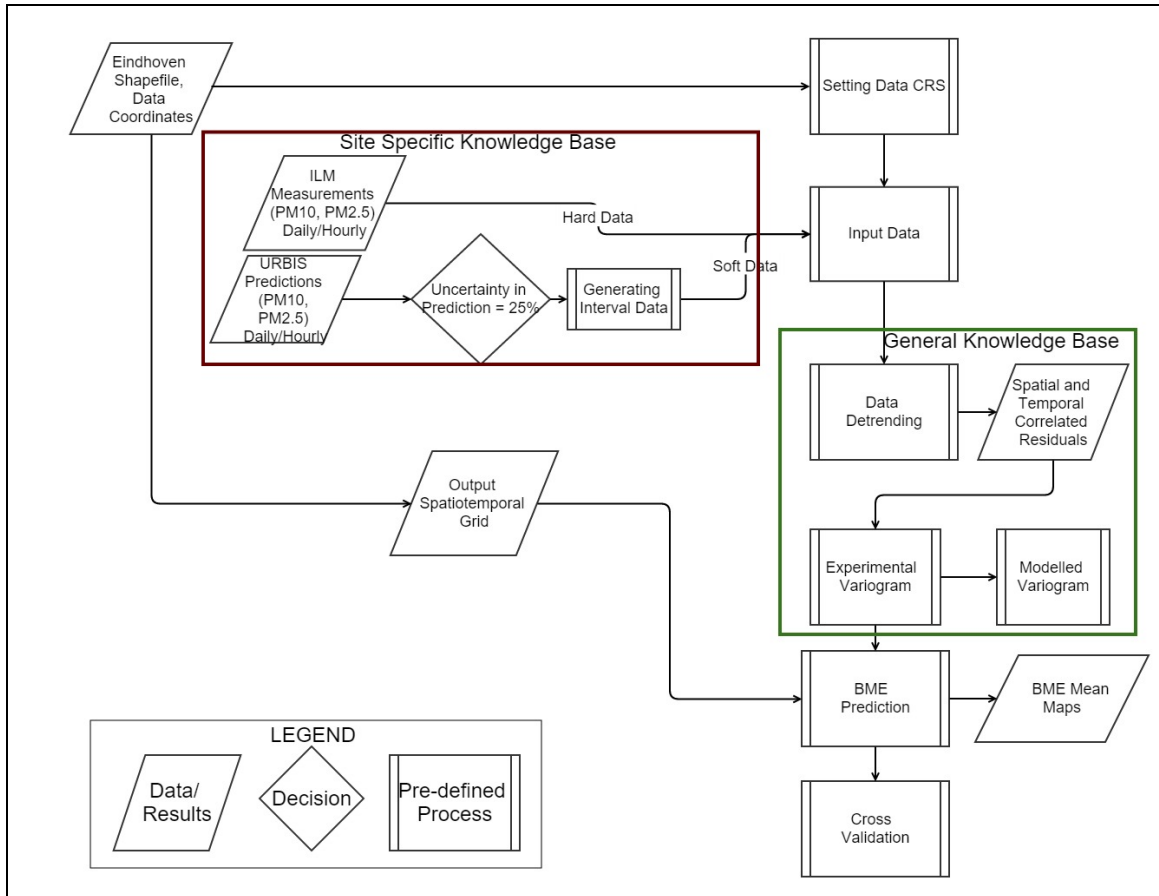


Figure 12 Workflow of integration of URBIS predictions with ILM measurement data in BME

4.2.2.1. Categorization of soft and hard data

Data pertaining to BME analysis consisted of hourly PM measurements from 32 ILM stations (airboxes) and a set of 500 URBIS prediction locations. The locations were randomly sampled from the URBIS dataset containing 1226 locations. These data were then categorized on their uncertainty levels as hard and soft data. By definition, soft data consists of those datum whose values are uncertain and are generally characterized stochastically. These can be represented by a probability distribution function (PDF). Hard data are data which can be considered as certain or have relatively low uncertainty associated with their values.

Based on the guidelines of measurement uncertainty by European air quality directives (EU, 2008), uncertainty associated with PM measurements in the ILM network were assumed to be 25% for mean daily values. This was the focal point in carrying out the first objective of this research (evaluating PM predictions from the URBIS model against ILM measurements). Similarly, PM values of URBIS predictions were also considered to have at least 25% uncertainty in their daily values. This attributes to two reasons, firstly since predictions from URBIS model consists of simulated output from an ensemble of dispersion models, inherent uncertainties associated with individual dispersion models also account as uncertainties in predictions of URBIS model. Furthermore, as mentioned in Section 4.1.1.1 URBIS predictions are affected by uncertainties in the background PM levels. In this research, background values of PM₁₀ and PM_{2.5} were

averaged measurements from the LML stations. , uncertainty associated with PM measurements from LML stations is attributed to 16% for daily values and tend to increase drastically for hourly values. This uncertainty contributes to total uncertainty in PM predictions of URBIS model. Thus pertaining to this research PM values from URBIS predictions are considered as soft data as compared to ILM measurements. For this research, hard data, or ILM measurements were characterized by their numerical attribute, and their spatiotemporal location, whilst PM values of soft data or URBIS predictions were considered as interval data based on uncertainty range of 25%. Thus it was considered that, actual PM value any spatiotemporal location of URBIS prediction could be any value set by the bounds of $\pm 25\%$ of the prediction made by the URBIS model. Thus, the input data characterized by the S-KB (site-specific knowledge base) in the BME process can be summarized in Table 11.

Table 11 Site specific knowledge base (S-KB) for BME analysis

	Attributes	Spatial Range	Temporal Range
Input Data S-KB			
Hard Data	PM ₁₀ and PM _{2.5} values from ILM measurements	32 coordinates	Hourly values for June 2015 (720 time points)
Soft Data	$\pm 25\%$ PM ₁₀ and $\pm 25\%$ PM _{2.5} values from URBIS predictions	500 coordinates	Hourly values for June 2015 (720 time points)

4.2.2.2. BME prediction grid

Prediction maps of PM values (PM₁₀ and PM_{2.5}) in Eindhoven were generated at two temporal scales, daily and hourly predictions. Whilst daily predictions maps corresponded to full month of June, 2015 (30 maps for each pollutant), hourly predictions were obtained for one day – 4th of June (Wednesday), 2015 to reduce the computational efforts. The choice of choosing the date June 4th was based on time series analysis of PM values, as described in Section 5.1. PM values were relatively high during June 4th and showed abrupt changes in concentrations and motivated to obtain PM prediction maps at hourly time periods to study in detail the spatiotemporal variability. Output grid for prediction consisted on 100x100 spatial locations spread around Eindhoven and temporal extent was dependant on the temporal scale of prediction (daily or hourly).

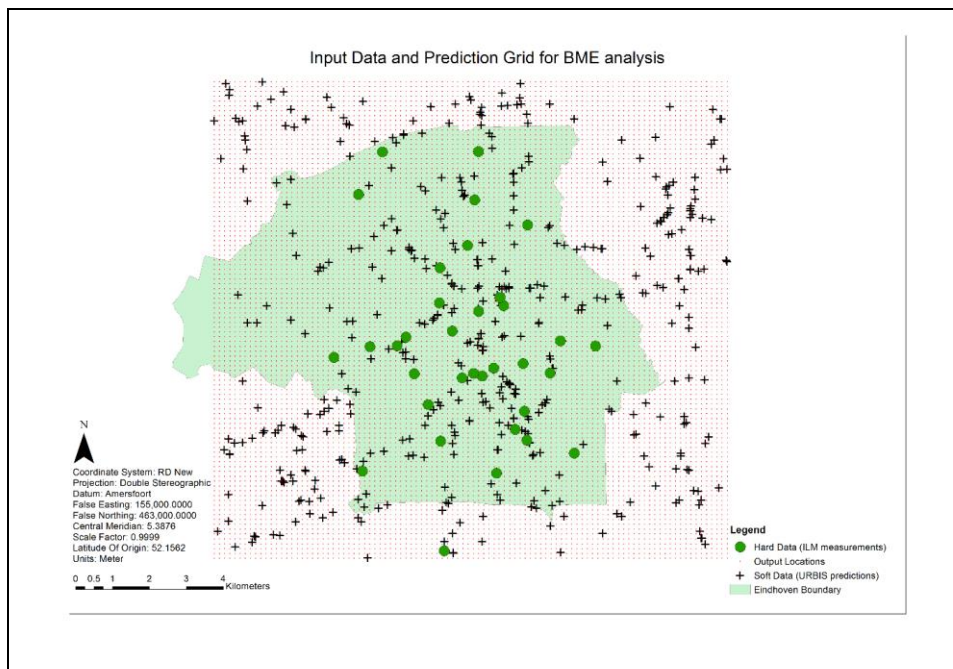


Figure 13 Input data and prediction grid for BME analysis

Spatial extent of the grid was constrained according to the bounding box of the data coordinates and temporal extent of the grid was constrained to temporal range of the data. These were 24 time points for hourly temporal scale, corresponding to each hour from 00:00 hours to 23:59 hours of 4th June, 2015. Prediction scale for daily level comprised of 30 time points, each corresponding to a day of June 2015.

4.2.2.3. Modelling spatiotemporal dependence structure

G-KB (General Knowledge Base) involves modelling the stochastic behaviour of PM values in space and time. This includes characterizing the spatiotemporal dependence structure of PM values in Eindhoven for June 2015. It involves estimation of spatiotemporal mean trend and spatiotemporal covariance function. PM value at a space-time node in Eindhoven can be decomposed into two aspects,

$$\hat{X}(p) = m(p) + \varepsilon(p) \quad (26)$$

Where,

$\hat{X}(p)$ refers to value of PM at any given space-time node p , and $p = (s, t)$

$m(s, t)$ refers to the spatiotemporal mean trend and

$\varepsilon(s, t)$ refers to the auto correlated residuals in space-time.

Spatiotemporal mean trend $m(p)$ are long range variations in the PM values and spatiotemporal auto correlated residuals $\varepsilon(p)$ characterize the actual space-time structure of PM. In order to estimate the autocorrelation in spatial and temporal domain accurately, it is imperative to remove any mean trends in the dataset. Data de-trending prior to the characterization of spatiotemporal autocorrelation is important as it removes spatial inhomogeneity and temporal non-stationarity in the observations (hard and soft data) (Lee et al., 2008).

Data de-trending in STAR-BME is achieved by means of a smoothing kernel filter. Based on explanations provided in (Yu et al., 2009; Yu et al., 2015), mean trend $m(p)$ is estimated by the following equation,

$$m(p_{est}) = \frac{\sum_{i=1}^N K(p_{est}, p_{obs}) \hat{X}_{obs}}{\sum_{i=1}^N K(p_{est}, p_{obs})} = \sum_{i=1}^N w(p_{est}, p_{obs}) \hat{X}_{obs} \quad (27)$$

Where,

p_{est}, p_{obs} correspond to estimation node and observation node; $p = (s, t)$

$m(p_{est})$ is the mean spatiotemporal trend at an estimation location p_{est}

\hat{X}_{obs} refers to the attribute value at p_{obs} (in this case, PM values from hard and soft data)

$K(p_{est}, p_{obs})$ is the kernel function that depends on spatiotemporal distance between p_{est}, p_{obs}

N refers to the number of nodes.

Kernel function $K(p_{est}, p_{obs})$ is expressed as,

$$K(p_{est}, p_{obs}) = e^{\left(\frac{-(s_{est}-s_{obs})^2}{2\lambda_s^2}\right) + \left(\frac{-(t_{est}-t_{obs})^2}{2\lambda_t^2}\right)} \quad (28)$$

Where,

$p_{est} = (s_{est}, t_{est})$ and $p_{obs} = (s_{obs}, t_{obs})$ refers to estimation node and observation node,

λ_t refers to the temporal bandwidth of the kernel and

λ_s refers to the spatial bandwidth of the kernel

Optimal values of λ_s and λ_t are obtained using adjusted generalized cross validation (GCV) method (Altman, (1990) cited in Yu et al., 2009) which takes into account correlation among residuals. Adjusted GCV around a given number of nodes n is computed by the following equation,

$$GCV_{adj} = n \left(\frac{\sum_{i=1}^n (\hat{X}_i - m(p_i))^2}{n - \text{trace}(W_i C_n)} \right) \quad (29)$$

Where,

n refers to the number of nodes of data

\hat{X}_i is the attribute value at node i

C_n is the correlation among the data present in n nodes of data

W_i is the kernel function matrix $w(p_{est}, p_{obs})$ where (p_{est}, p_{obs}) are any two nodes among n .

After the step of data-detrending, estimation of empirical covariance functions in spatial and temporal domains were done. Residuals after removal of mean trend from the available data (hard and soft) were used for the process. Separate covariance functions autocorrelation in spatial and temporal domain were estimated using the following parameters. Spatial and temporal distance limits, which refer to the maximum range in spatial and temporal domains where correlation among data is assumed. Lag tolerance refers to the distance (spatial and temporal) at which covariance is calculated for data points and number of spatial and temporal lags refer to division of spatial and temporal distance limit based on lag tolerance. Based on different combination of values, empirical covariance function is estimated.

Suitable separable space-time covariance model was then fitted to the empirical covariance function to characterize the spatiotemporal characteristics of PM values. STAR-BME facilitates the use of nested separable space-time covariance models (Yu et al., 2015, 2012).

Nested separable covariance models in space and time can be defined by (Yu et al., 2009; Yu et al., 2012)

$$\text{cov}_{st}(h, \tau; \Theta_{st}) = \sum_{l=1}^L b_l \text{cov}_s(h; \Theta_s) \text{cov}_t(\tau; \Theta_t) \quad (30)$$

Where,

h, τ refer to the spatial lag and temporal lag respectively;

L refers to total number of separable covariance function in space and time

cov_{st} refers to the covariance model in space and time with Θ_{st} its parameters (sill, ranges)

cov_s refers to covariance model in spatial domain with Θ_s its parameters (sill, ranges)

cov_t is the covariance model in temporal domain with Θ_t its parameters (sill, ranges)

b_l is the joint sill (contribution of variance of an individual separable space-time covariance model to the variance of the nested separable covariance model)

Fitting the empirical covariance model with a nested separable covariance model in STAR-BME was carried out using automated methods involving PSO (particle swarm optimization) (Yu et al., 2009) which is used to initialize parameters for b_l , Θ_s and Θ_t and subsequently by using iterative method of BOBYQA (bound optimization by quadratic approximation), optimal values of parameters are determined by using a weighted least squares optimization of theoretical and empirical covariance (Cressie, (1985) cited in Yu et al., 2009; Yu et al., 2015). Assessment of these model fitting were done by comparing the AIC (Akaike Information Criteria) values. Then BME predictions were made at given spatiotemporal output grid and included mean value of a prediction and were associated with a distribution function characterised by its mean and variance. STAR-BME includes a leave-one-out cross validation tool and this was used to assess the prediction accuracy of BME. These results are described in Section 5.3

5. RESULTS AND ANALYSIS

5.1. Exploratory analysis

Prior proceeding with the research objectives, exploratory analysis of the data was performed. As described in Chapter 3, data used in this research can be categorized as modelled data and measurement values of PM₁₀ and PM_{2.5} pertaining to June 2015. Measurement data consisted of hourly measurements at 32 airboxes of the ILM network and modelled data were hourly predictions from the URBIS model at 1226 locations. Modelled dataset included predictions at 32 airbox sites and 1189 other locations. Figure 14 shows the locations of ILM measurements and URBIS predictions. It can be seen that most of the URBIS predictions were located in the vicinity of roadways and street canyons as it tries to model PM values based on emissions from traffic sources (described in Section 3.2.2.).

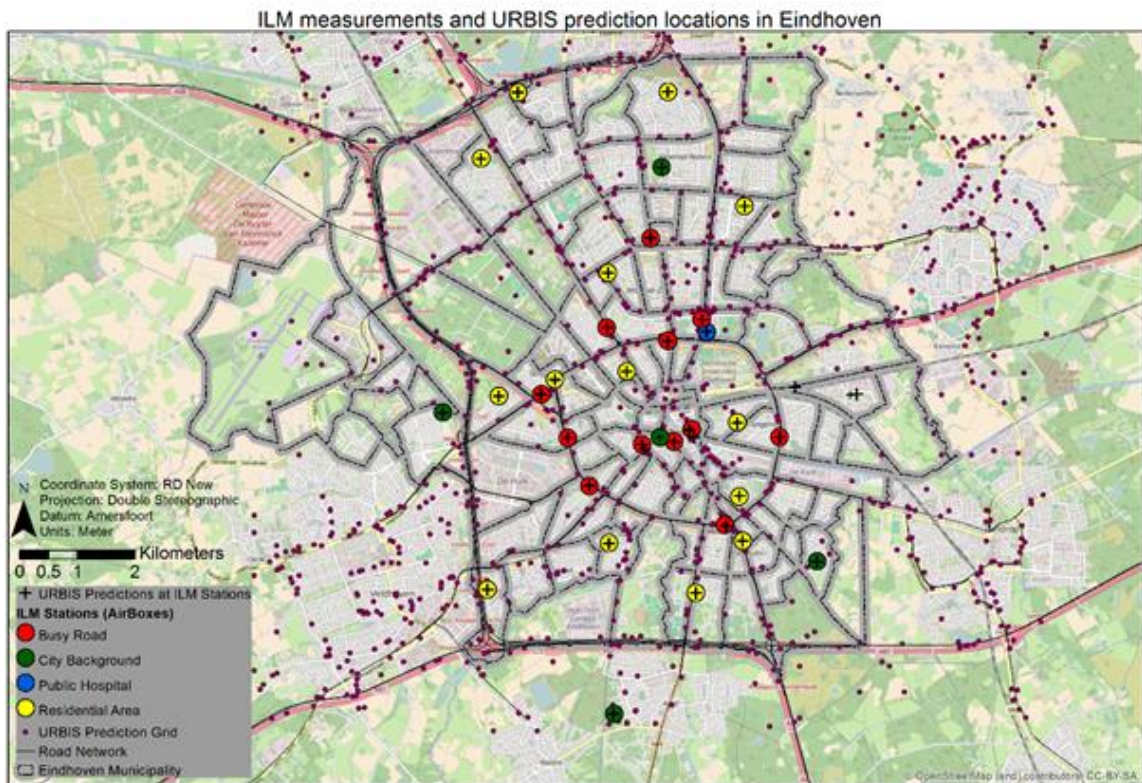


Figure 14 Airbox locations (ILM network) and corresponding URBIS prediction locations

From Table 12 and Figure 15, it can be seen that mean values of PM₁₀ and PM_{2.5} of URBIS predictions (URBIS total) are slightly higher than those for ILM measurements. Additionally, it can be seen that PM values for URBIS foreground predictions are quite small as compared to averaged LML background values (substantiated by boxplots in Figure 15). Matthijsen & ten Brink, (2007) that stated the averaged background values of PM_{2.5} in the Netherlands generally lie in the range of 12-16 $\mu\text{g m}^{-3}$ for rural background, 16-18 $\mu\text{g m}^{-3}$ for urban background while contribution of emissions from traffic in the streets lie in range of 2-6 $\mu\text{g m}^{-3}$. Mean values of ILM measurements were lower than that of mean values of LML background. This is consistent for both PM₁₀ and PM_{2.5} values. The distribution of the ILM data and URBIS total predictions

were right skewed as the difference of mean and maximum value is very high compared to difference of mean to minimum value as confirmed from the histogram of data (Figure 16and Figure 17).

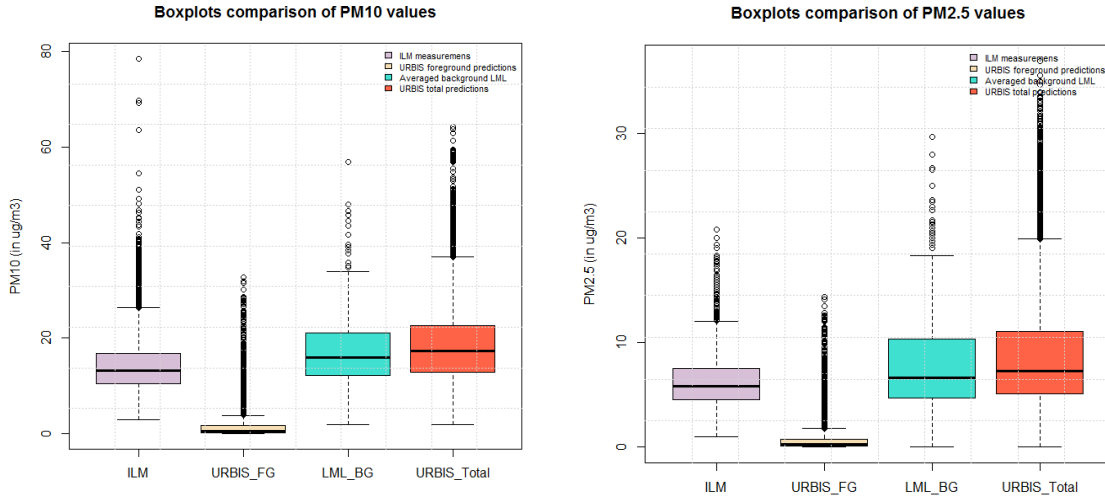


Figure 15 Comparison of PM values from ILM, background LML and URBIS foreground predictions

Table 12 Summary statistics of PM values from ILM, background LML and URBIS foreground

	PM10 ($\mu\text{g m}^{-3}$)			URBIS total	PM2.5 ($\mu\text{g m}^{-3}$)			URBIS total
	ILM	URBIS Foreground	Averaged background LML		ILM	URBIS Foreground	Averaged background LML	
Median	13.24	0.52	15.95	17.32	5.83	0.24	6.67	7.3
Mean	14.16	1.25	17.10	18.39	6.23	0.57	8.06	8.64

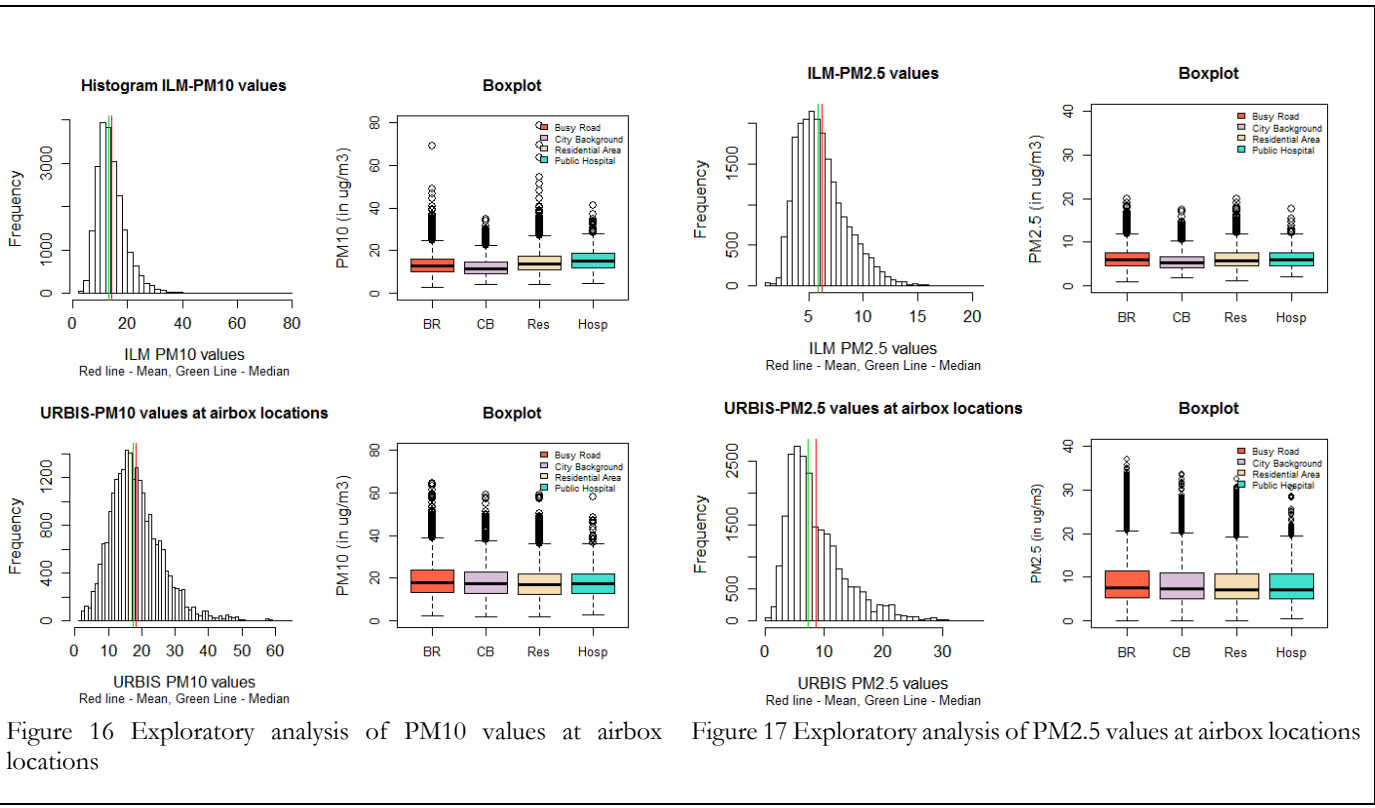


Figure 16 Exploratory analysis of PM10 values at airbox locations

Figure 17 Exploratory analysis of PM2.5 values at airbox locations

Airbox locations were categorized based on its spatial representativeness (Table 1) and boxplots of PM₁₀ and PM_{2.5} values of measurements and modelled data were plotted (Figure 16 and Figure 17). From these plots, it can be seen that concentration levels are almost similar and there is no variability in the categories. It can be inferred that since mean values of PM tend to remain constant at these categories of airbox locations, mean ILM measurements can also be used as an alternative for estimating the background concentrations in Eindhoven.

5.1.1. Temporal variability of PM_{2.5} and PM₁₀ in June 2015

Using mvtsplot library in R (v 1.0-1) (Peng, 2008), the temporal visualization of hourly PM₁₀ (Figure 18 for ILM measurements and Figure 20 for URBIS predictions) and hourly PM_{2.5} (Figure 19 for ILM measurements and Figure 21 for URBIS predictions) values were plotted. This consisted of three sub-plots, the left plot shows the hourly concentration values of pollutant (at each airbox location). The values are categorized as tertiles (high values= red, medium values= orange, low values= yellow and white= no data). The right plot shows box plot distribution of concentration at each airbox location. The bottom plot shows the time series of averaged concentration values at all airbox locations for a particular time instance.

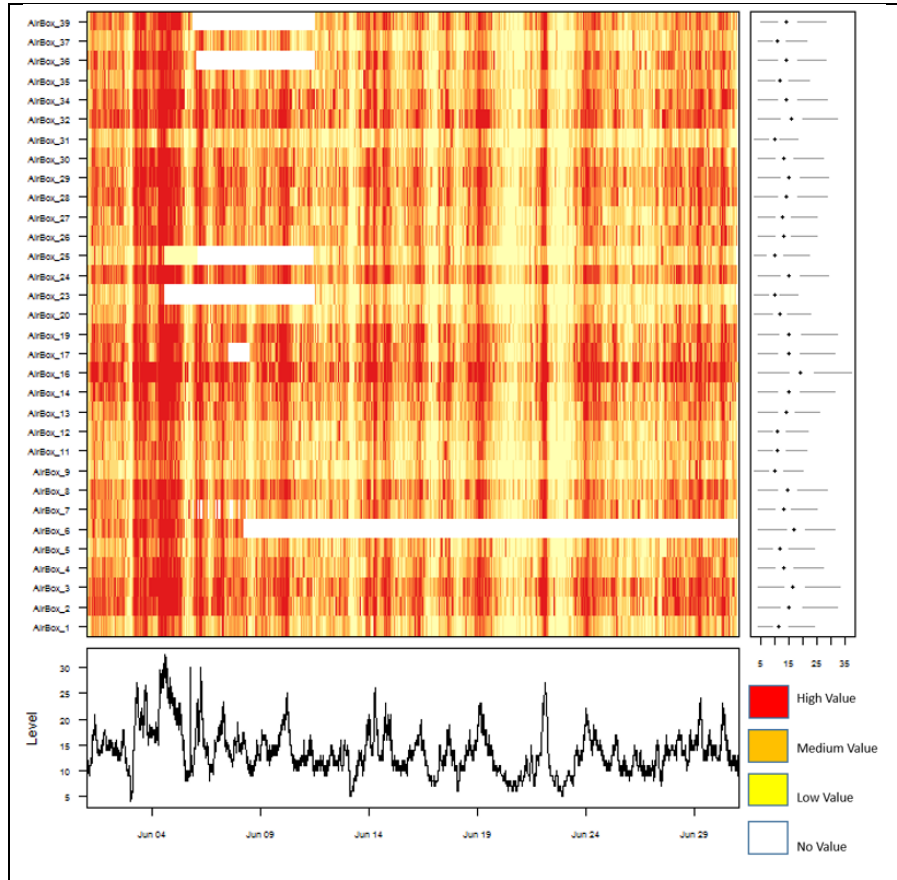


Figure 18 Temporal visualization of ILM- PM10 values at 32 airbox locations for June 2015

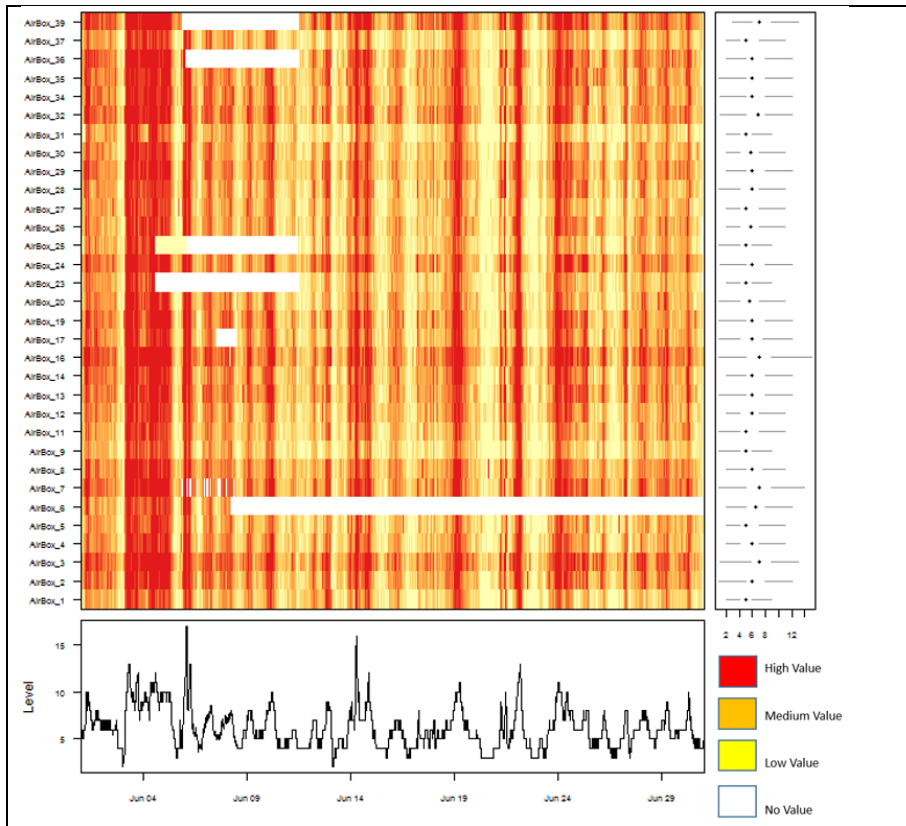


Figure 19 Temporal visualization of ILM- PM2.5 values at 32 airbox locations for June 2015

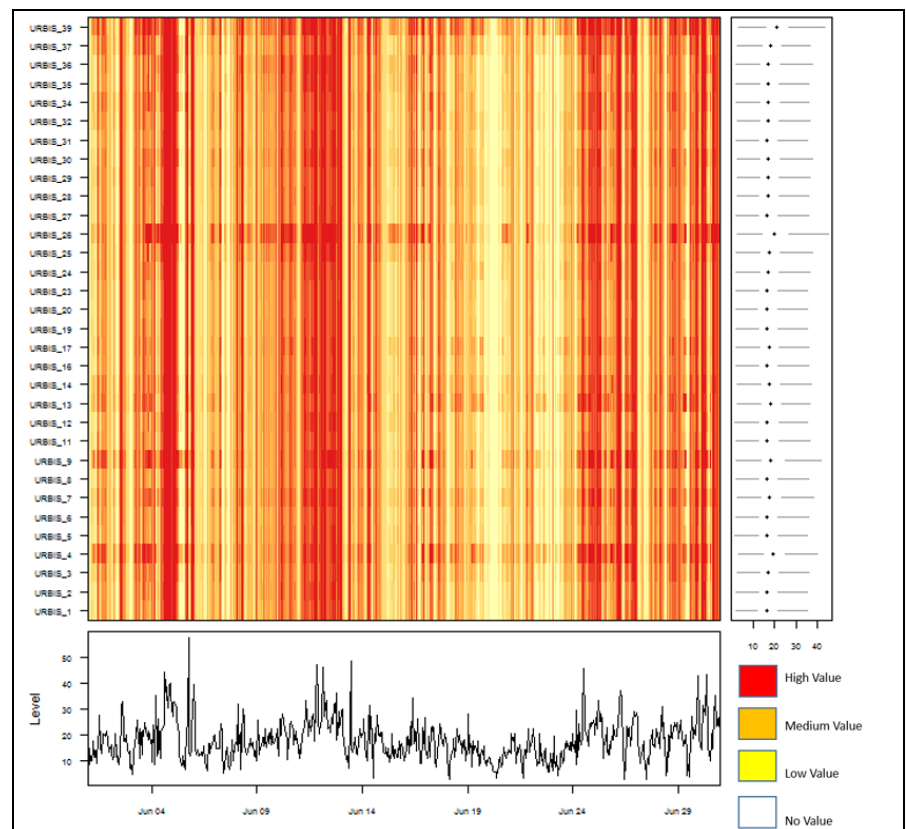


Figure 20 Temporal visualization of URBIS- PM10 values at 32 airbox locations for June 2015

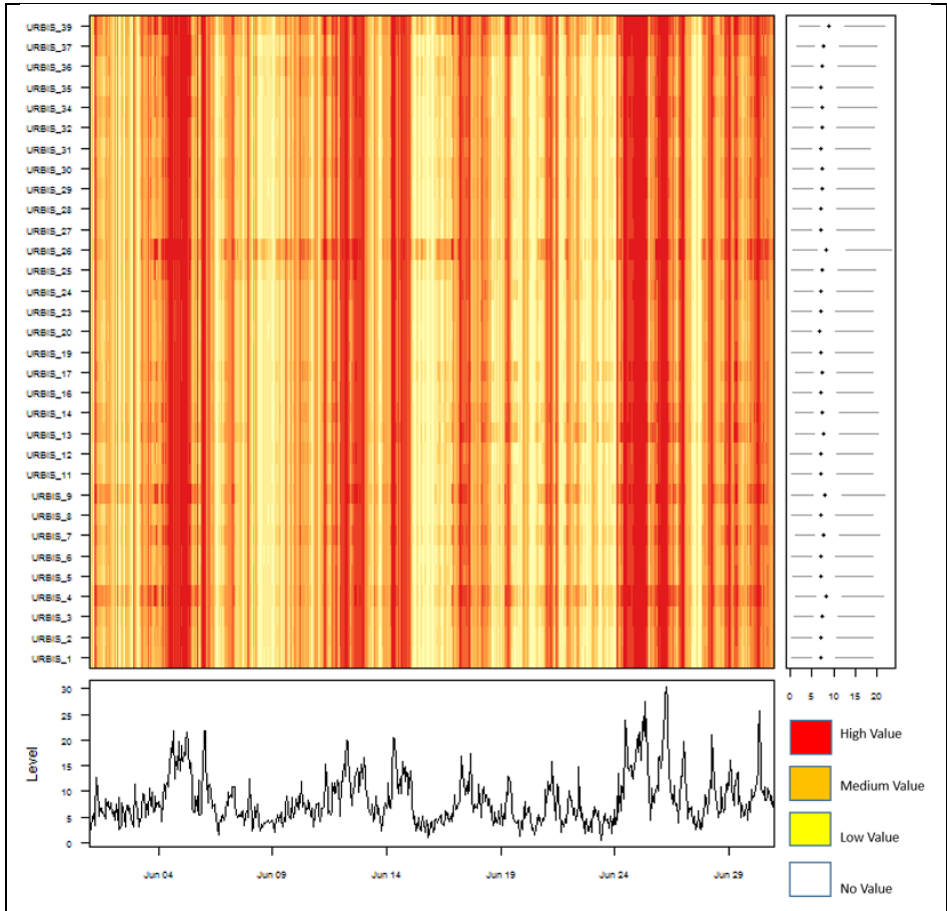


Figure 21 Temporal visualization of URBIS- PM2.5 values at 32 airbox locations for June 2015

From Figure 18 and Figure 19 it can be seen that data gaps in ILM dataset are present in airboxes 6, 17, 23, 25, 36 and 39. From the time series (bottom plot), it can be noticed that PM values show clear temporal variability (values increase and decrease in pattern. PM values are relatively high around June 4th, 14th and 24th. Comparing visualizations of PM values from URBIS model and ILM network, it can be seen that URBIS predictions shows smoother temporal variability than compared to ILM measurements. This is because URBIS model predictions are affected by heavier dominance of background values from three LML monitoring stations as compared to URBIS foreground predictions as discussed previously (Figure 15 and Table 12).

5.2. Performance evaluation of URBIS Model

Based on the methods described in Section 4.1, measurement uncertainty (U) were derived for PM10 and PM2.5 at all airbox locations. These values are presented in the appendix (Table 30). These were then used to calculate MPC for four different temporal aggregations (hourly, 6-hourly, 12-hourly and daily). Metrics for MPC are described in Table 9.

For the purpose of representation of results, five representative airbox locations were chosen. These correspond to a different category of spatial representativeness and by comparison of MPC values at these locations, it can be evaluated at which locations, URBIS predictions conform to the ILM measurements. Furthermore, this can also be used to analyse at which temporal resolution these predictions are consistent with measurements. These were chosen according to their classification presented in (Close et al., 2016; Hamm et al., 2016)

Table 13 Representative airbox locations for analysis

Airbox Location	Spatial Representativeness	Address (Hamm et al., 2016)
1	City background	Eij-erven 41, 5646 JM
31	City background (outside Eindhoven)	Vincent Cleeradinlaan Waalre 5582 EJ
2	Residential area	Lijmbeekstraat 190 5612 NJ
3	Busy Road	Keizersgracht 28 5611GD
29	Public Hospital	Ds. Fleidnerstaat 5631 BN

5.2.1. MPC results for hourly aggregation

Table 14 MPC results at five representative stations for hourly aggregations

Spatial Representativeness	AirBox location	U	RMSE	NMB		NMSD		R	
			RMSEu	NMB	MPC NMB	NMSD	MPC NMSD	1-R	MPC R
Hourly PM ₁₀									
City Background	1	3.21	1.39	0.42	0.52	3.54	1.65	0.70	1.35
	31	2.73	1.90	0.68	0.53	3.68	1.23	0.82	0.76
Residential Area	2	4.32	0.91	0.08	0.80	5.41	2.74	0.68	3.76
Busy Road	3	4.60	0.85	0.04	0.89	4.34	3.02	0.67	4.55
Public Hospital	29	4.18	0.95	0.14	0.69	3.84	2.35	0.67	2.76
Hourly PM _{2.5}									
City Background	1	1.43	1.86	0.52	0.53	2.90	1.49	0.66	1.11
	31	1.37	2.08	0.60	0.54	2.86	1.29	0.82	0.83
Residential Area	2	1.74	1.38	0.26	0.69	3.73	1.98	0.61	1.96
Busy Road	3	1.94	1.20	0.16	0.72	2.94	2.11	0.61	2.23
Public Hospital	29	1.70	1.47	0.33	0.58	2.69	1.62	0.63	1.31

5.2.2. MPC results for 6-hourly aggregations

Table 15 MPC results at five representative stations for 6-hourly aggregations

Spatial Representativeness	AirBox location	U	MPC RMSE	NMB	MPC NMB	NMSD	MPC NMSD	1-R	MPC R
			RMSE		NMB		NMSD		MPC R
6-Hourly PM ₁₀									
City Background	1	3.17	1.15	0.42	0.52	1.99	1.90	0.65	1.80
	31	2.70	1.66	0.68	0.52	2.29	1.46	0.79	1.07
Residential Area	2	4.26	0.69	0.08	0.79	3.72	3.15	0.62	4.97
Busy Road	3	4.54	0.62	0.04	0.87	2.51	3.30	0.61	5.44
Public Hospital	29	4.13	0.70	0.14	0.68	2.23	2.70	0.58	3.66
6-Hourly PM _{2.5}									
City Background	1	1.42	1.70	0.52	0.52	3.13	1.66	0.66	1.37
	31	1.36	1.91	0.60	0.53	3.79	1.43	0.83	1.02
Residential Area	2	1.72	1.22	0.26	0.68	3.24	2.15	0.59	2.32
Busy Road	3	1.92	1.05	0.16	0.71	3.12	2.23	0.59	2.49
Public Hospital	29	1.68	1.32	0.33	0.57	2.88	1.76	0.63	1.56

5.2.3. MPC results for 12-hourly aggregations

Table 16 MPC results at five representative stations for 12-hourly aggregations

Spatial Representativeness	AirBox location	U	MPC RMSE	NMB	MPC NMB	NMSD	MPC NMSD	1-R	MPC R
12-Hourly PM ₁₀									
City Background	1	3.15	1.09	0.42	0.51	1.79	2.16	0.65	2.33
	31	2.67	1.58	0.68	0.52	2.16	1.69	0.74	1.43
Residential Area	2	4.23	0.62	0.08	0.79	3.46	3.49	0.63	6.10
Busy Road	3	4.52	0.57	0.04	0.86	1.96	3.40	0.63	5.76
Public Hospital	29	4.10	0.64	0.14	0.68	2.00	3.10	0.58	4.80
12-Hourly PM _{2.5}									
City Background	1	1.40	1.65	0.52	0.52	2.45	1.87	0.66	1.74
	31	1.35	1.86	0.60	0.53	2.29	1.53	0.86	1.17
Residential Area	2	1.70	1.15	0.26	0.67	3.07	2.38	0.56	2.83
Busy Road	3	1.91	0.99	0.16	0.70	2.25	2.31	0.57	2.67
Public Hospital	29	1.66	1.26	0.33	0.57	2.22	1.96	0.61	1.93

5.2.4. MPC results for daily aggregations (24 Hour)

Table 17 MPC results at five representative stations for daily aggregations

Spatial Representativeness	AirBox location	U	MPC RMSE	NMB	MPC NMB	NMSD	MPC NMSD	1-R	MPC R
24-Hourly PM ₁₀									
City Background	1	3.11	1.04	0.42	0.51	1.81	2.72	0.67	3.69
	31	2.65	1.54	0.68	0.52	2.39	2.24	0.78	2.52
Residential Area	2	4.18	0.53	0.08	0.78	3.34	4.29	0.63	9.22
Busy Road	3	4.46	0.48	0.04	0.86	2.13	4.73	0.61	11.20
Public Hospital	29	4.05	0.56	0.14	0.67	2.00	3.97	0.57	7.90
24-Hourly PM _{2.5}									
City Background	1	1.38	1.52	0.52	0.51	2.08	2.37	0.76	2.80
	31	1.33	1.73	0.60	0.53	1.90	1.79	1.01	1.60
Residential Area	2	1.68	1.03	0.26	0.66	2.71	2.92	0.63	4.27
Busy Road	3	1.89	0.86	0.16	0.70	1.88	2.84	0.61	4.02
Public Hospital	29	1.64	1.14	0.33	0.56	1.86	2.44	0.68	2.99

From the results, it can be seen that measurement uncertainty denoted by U (Equation 7) is lower in case of PM_{2.5} as compared to PM₁₀, owing to difference in concentration levels. There is almost no change in the value of U for different temporal aggregations. However a contrasting feature that can be noticed is the difference in values of U at airbox location 1 and airbox location 31 even though both are considered as city background locations. In case of busy road (airbox location 3), the value of U is highest for both PM₁₀ and PM_{2.5} and at all temporal aggregation levels. This can be attributed to the fact that URBIS prediction values are relatively high in busy roads. However, the heavier dominance of background values (from averaged LML stations) may have resulted in increased values of U at all the representative airbox locations.

MPC for RMSE denoted by RMSE_u (Equation 12) is generally lower for PM₁₀ values as compared to PM_{2.5}. For URBIS predictions to conform with ILM measurements, RMSE_u should be less than 1. The lowest values in each case is associated with airbox located at Busy Road (Airbox location 3) and the highest values in each case are associated with airbox location 31 and airbox location 1, which is a city background station. MPC for RMSE_u is not adhered in almost all cases of PM_{2.5}, except for 12-hourly and daily aggregation values at airbox location 3. RMSE_u is always higher than 1 for city background station.

The MPC for NMB (Equation 13) generally remained violated at city background location 31 for PM₁₀ and PM_{2.5} and remains fulfilled in all other cases. Considering the MPC for R (Equation 15), in all the cases the MPC is fulfilled. The MPC for NMSD (Equation 14) are violated in all cases for hourly and 6-hourly aggregations for both PM_{2.5} and PM₁₀ at all airbox locations. However, for 12-hour aggregations, this is adhered only for airbox located at busy road (for PM_{2.5}) and for busy road and public hospital (for PM₁₀). In case of daily aggregations, these are only violated for city background (airbox location 31) for PM₁₀ and airbox location 2 (residential area) for PM_{2.5}.

Comparison of these RMSE_u values at different temporal aggregations suggest that predictions from URBIS model were poorly consistent with ILM measurements at hourly levels and were moderately consistent at daily values. Specifically for URBIS predictions at airbox 2, which is a spatial representative of busy roads showed the consistent results of adhering to all MPC. whilst prediction at airbox location 1 showed least consistent results. Thus, it can be said that URBIS predictions are generally suited for locations which have busy roads in its vicinity, and since URBIS model is an ensemble of dispersion models it is justifiable. Furthermore, dominance of background values play a key role in the adherence of URBIS predictions to that of ILM measurements and consequently affect MPC metrics.

5.2.5. Equal tolerance graphs (PM10) and (PM2.5)

The following plots depict the principle for equal tolerance, i.e. uncertainty levels for both model and measurements are kept constant at 25% which is in accordance to EU Air Quality Directives (EU, 2008). The plots depict the comparison of modelled and measured concentration levels of hourly PM₁₀ ($\mu\text{g m}^{-3}$) and PM_{2.5} ($\mu\text{g m}^{-3}$) for air boxes 1, 2, 3 and 31 (airbox 1 represent city background; airbox 3 represents busy road ,airbox 2 represents residential area and airbox 31 represents city background, but is located outside Eindhoven) those were taken as spatial representatives (Table 13). The tolerance limits of modelled and measured concentrations are fixed at $\pm U$. These graphs are plotted at two different temporal aggregations-daily values and hourly values for PM₁₀ (Figure 23 and Figure 25) and PM_{2.5} (Figure 22 and Figure 24). Equal tolerance graphs (Thunis et al., 2012a) infers how well model predictions overlap measurements within the interval of measurement uncertainty. Overlap time periods are those when RMSE_u values are less than 1 and model adheres to MPC for RMSE (Table 8). Analysis of these plots with RMSE_u values can lead to assessment on which temporal periods and locations, model predictions conformed to those of measurements. The analysis of these plots are depicted in subsequent sections.

5.2.5.1. Equal tolerance graphs for hourly values

Figure 22 and Figure 23 represents the equal tolerance graphs of hourly aggregated ILM measurements and URBIS predictions at airbox locations 1, 2, 3 and 31 for PM_{2.5} and PM₁₀ respectively. It can be seen that hourly values tend to fluctuate and these fluctuations are prominent in case of PM_{2.5} than that of PM₁₀. URBIS prediction values tend to be more than ILM measurements at all representative stations. Abrupt increase in URBIS prediction values can be seen on dates around June 04, June 25 and on these days amongst other, the MPC for RMSE is violated. On dates around June 07, June 19, predictions tend to overlap measurements.

Considering airbox location 31, which is a city background station, it can be noticed that the trends in PM₁₀ and PM_{2.5} values are not the same for URBIS predictions and ILM measurements, and thus has led to increase value of RMSE violating MPCs (Table 14). Airbox locations 2 and 3 show prominent overlaps in the URBIS predictions and ILM measurements. Airbox location 3, (busy road) in particular shows relatively high temporal episodes of overlap and this is also seen from the MPC metrics, which is adhered to by this location. (Table 14).

5.2.5.2. Equal tolerance graphs for daily values

Figure 24 and Figure 25 represents the equal tolerance graphs of daily aggregated ILM measurements and URBIS predictions at airbox locations 1, 2, 3 and 31 for PM_{2.5} and PM₁₀ respectively. It can be seen that there is a similar trend in URBIS prediction values at all locations. Similarly, there is also a similar trend in ILM measurements at all locations. These trends overlap for some specific time periods, and this overlap is greater for PM₁₀ values than PM_{2.5} values. Airbox locations 2 and location 3 show increased temporal periods of overlapping for PM₁₀ while airbox locations 1 and 31 show fewer time periods of overlap. Particularly for airbox location 31, least overlap is seen for PM₁₀. In general, there is no significant overlap of URBIS predictions and ILM measurements for PM_{2.5}, signifying the violation of MPC at all airbox locations except location 3 (busy road) (Table 17).

An interesting pattern can be seen from the trends of PM₁₀ and PM_{2.5} at these airbox locations. For ILM measurements, all the airbox locations have a similar temporal trend. Similarly, URBIS predictions at all airbox locations have a similar temporal trend. This can lead to two conclusions. Firstly, URBIS predictions as seen are high as compared to ILM measurement, Due to heavier dominance of background concentration from averaged LML measurement stations and comparatively lower values of URBIS foreground predictions, it can be said that there is a difference in values of ILM measurements and that of averaged background concentration calculated from LML stations. Secondly, since ILM measurements at all these airbox locations show similar temporal trend, mean value of ILM measurements can be an alternative for considering background value of PM and can be used in URBIS predictions.

5.2.5.3. Hourly aggregations

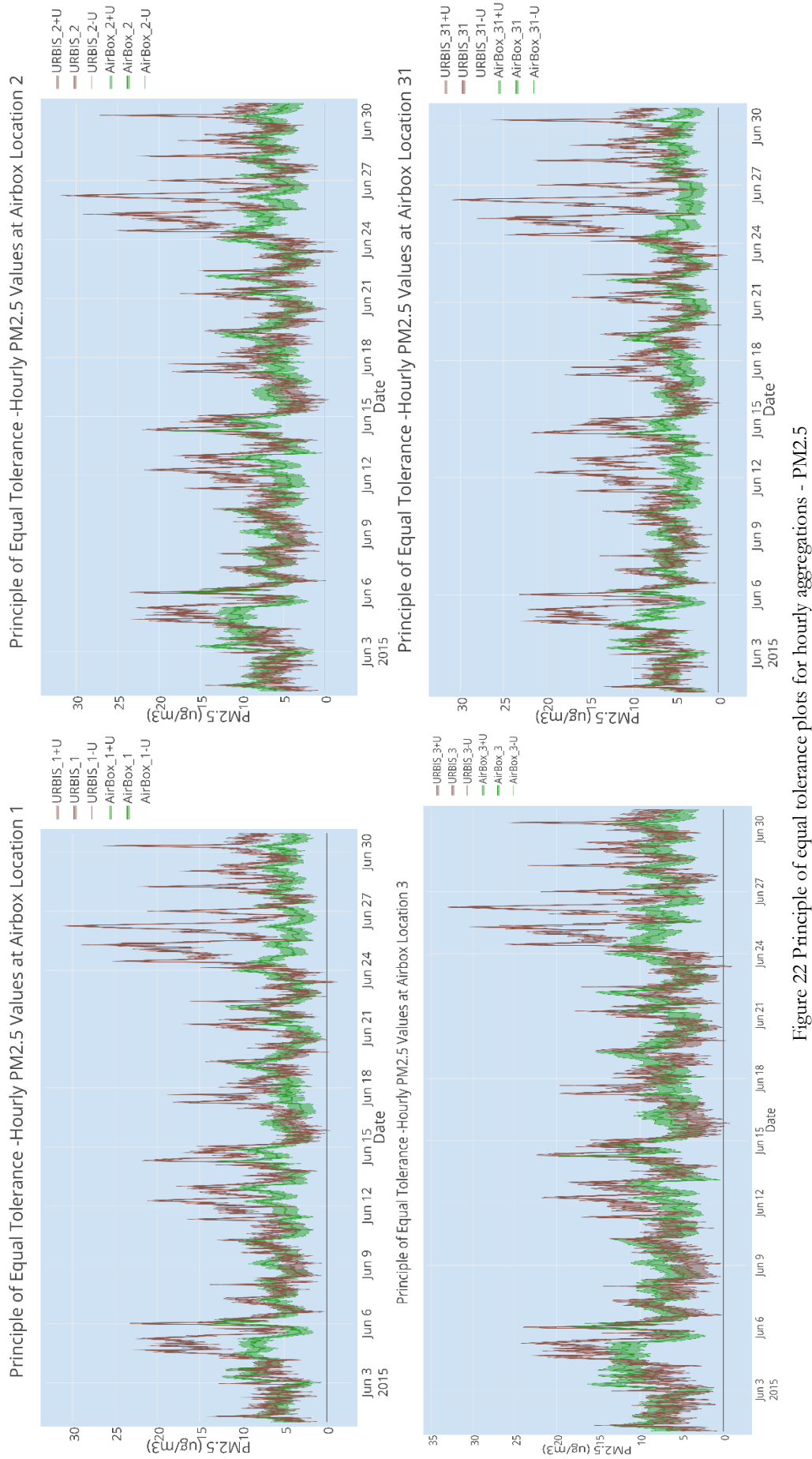


Figure 22 Principle of equal tolerance plots for hourly aggregations - PM2.5

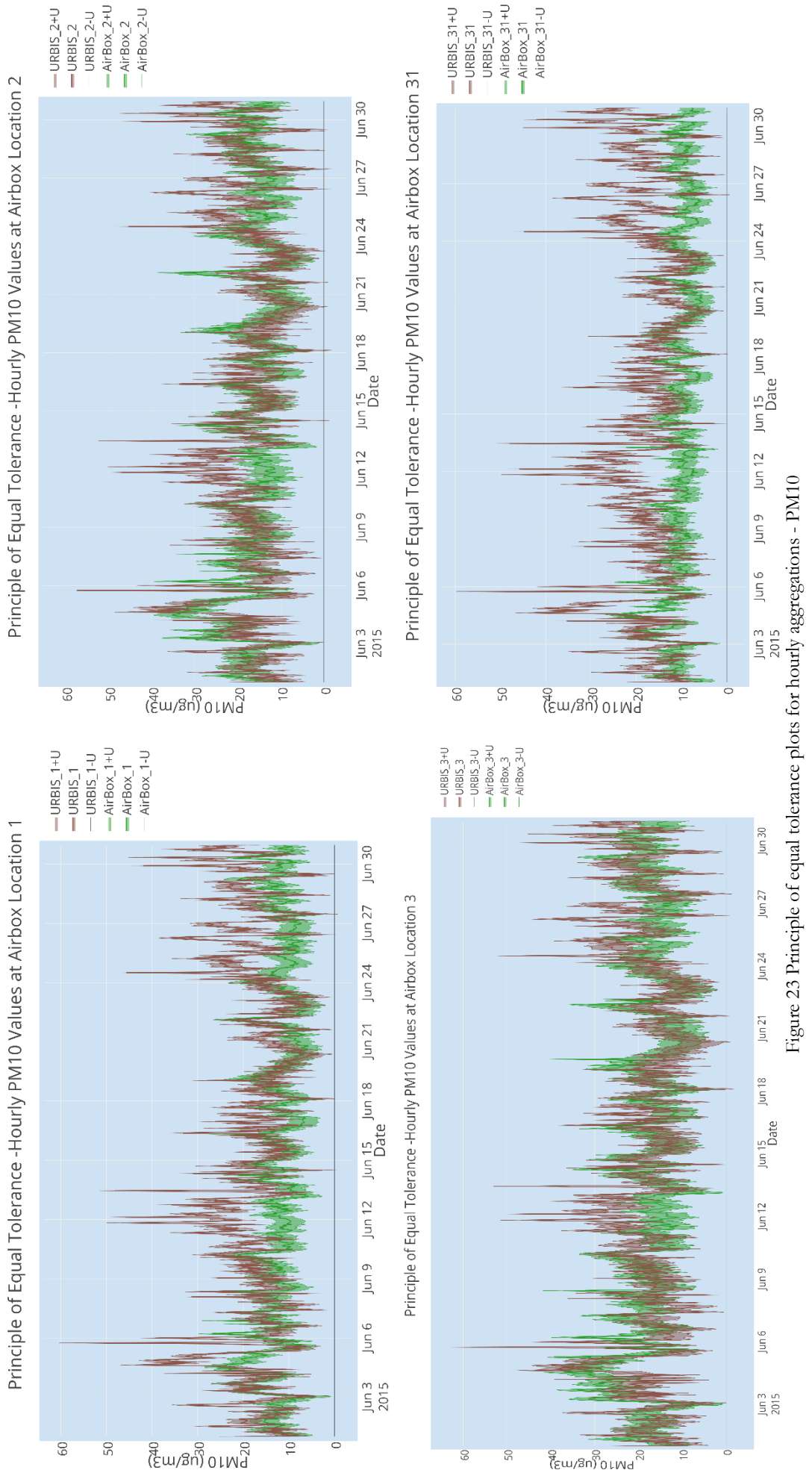
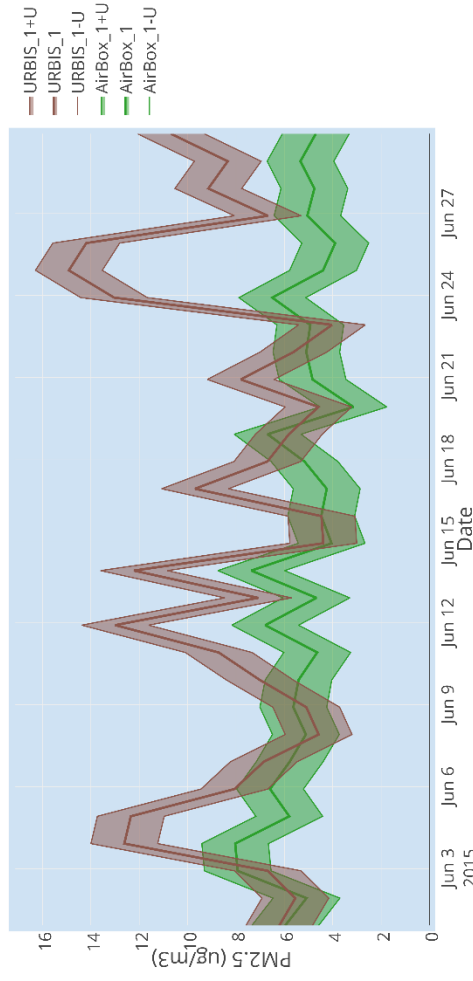


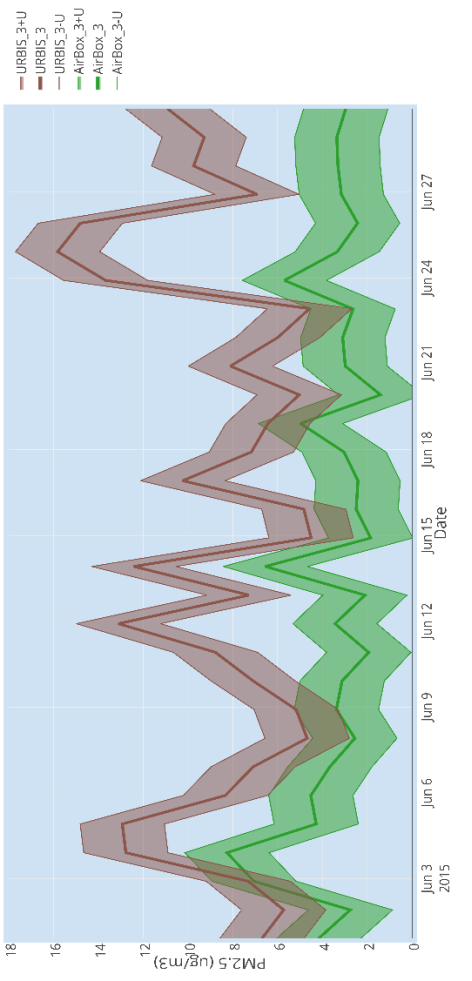
Figure 23 Principle of equal tolerance aggregations - PM10

5.2.5.4. Daily aggregations

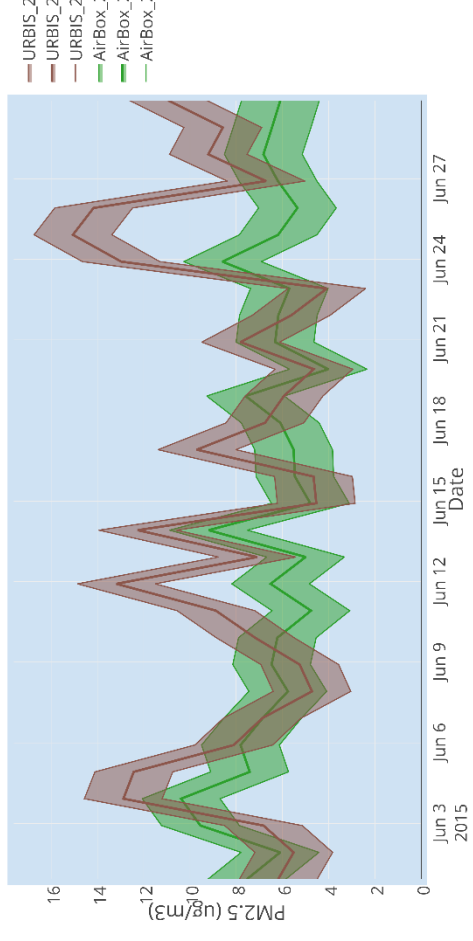
Principle of Equal Tolerance - Daily Aggregated PM2.5 Values at Airbox Location 1



Principle of Equal Tolerance - Daily aggregated PM2.5 Values at Airbox Location 3



Principle of Equal Tolerance - Daily Aggregated PM2.5 Values at Airbox Location 2



Principle of Equal Tolerance - Daily Aggregated PM2.5 Values at Airbox Location 31

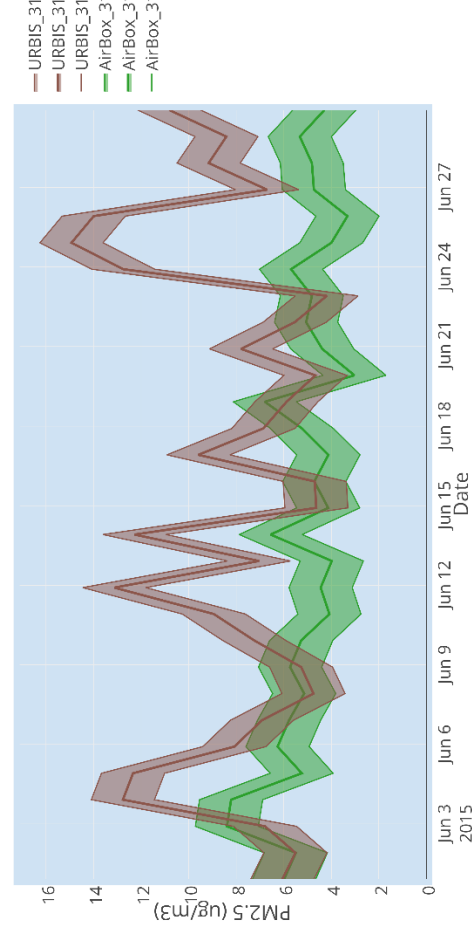
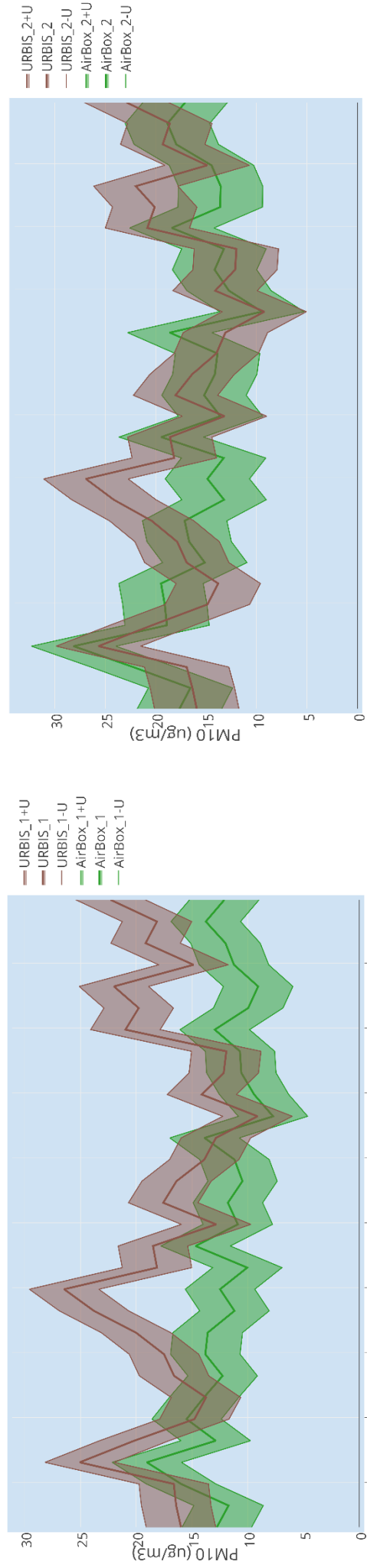


Figure 24 Principle of equal tolerance plots for daily aggregations - PM2.5

Principle of Equal Tolerance -Daily Aggregated PM10 Values at Airbox Location 1



Principle of Equal Tolerance -Daily Aggregated PM10 Values at Airbox Location 2

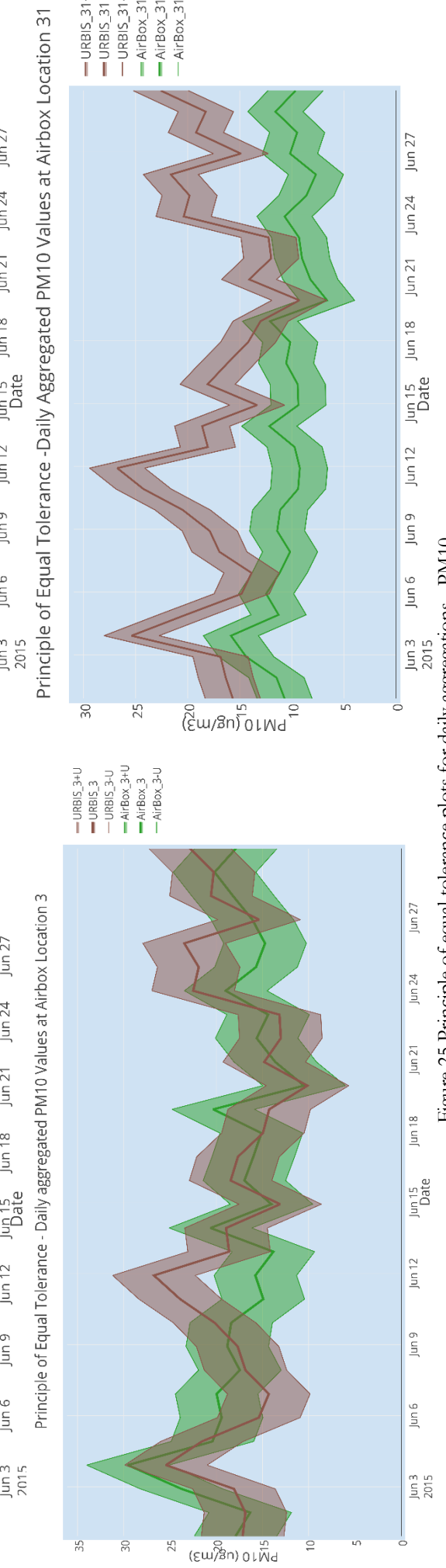


Figure 25 Principle of equal tolerance plots for daily aggregations - PM10

5.3. Spatiotemporal prediction of PM values using BME

This section describes the intermediary steps and results of integration of PM predictions from URBIS model and ILM measurements that corresponds to second objective of the research. Conceptual description of BME framework and the methodology followed to generate spatiotemporal maps of PM values in Eindhoven for June 2015 are discussed in details in Section 4.2.

5.3.1. Spatiotemporal Maps for daily predictions

Soft and hard data which were initially available as hourly values were aggregated to daily levels. This was used in the BME prediction analysis. Results pertaining to PM₁₀ predictions and PM_{2.5} predictions are presented in the subsequent section.

5.3.1.1. Predictions for PM10

After de-trending of the data, empirical marginal covariance functions in spatial (time lag =0) and temporal domain (distance lag = 0) were plotted (Figure 26 (left)). The units of empirical marginal covariance function in spatial domain was in meters and that of temporal domain was in days. Probable values of parameters of empirical covariance functions are tabulated in Table 18.

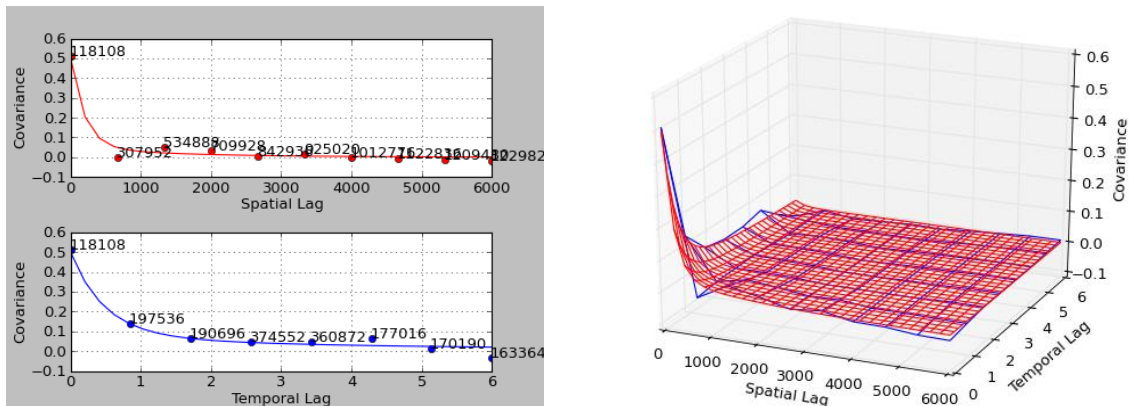


Figure 26 Covariance analysis for BME predictions of daily PM10.

Table 18 Estimates of empirical covariance functions- daily PM10 BME analysis

Estimates for Empirical covariance function	
Spatial distance limit: 6000	Temporal distance limit: 6
Number of spatial lags: 10	Number of temporal lags: 8
Spatial lag tolerance: 606	Temporal lag tolerance: 0.6

Covariance in spatial domain decreases to zero around 1000 meters while covariance in time domain reduces to zero approximately at 6 temporal units. The change in covariance is rather abrupt in spatial domain than in the temporal domain implying the large spatial variability as compared to temporal variability. Based on Equation (30), nested covariance model consisted of three space-time separable covariance models. After iterating with different combinations of nested separable covariance models the following nested covariance model was used for fitting the empirical variogram (Figure 26 (right)).

$$\begin{aligned} cov_{st}(h, \tau; \Theta_{st}) = & C_1 cov_{s1}(h; \Theta_{s1}) cov_{t1}(\tau; \Theta_{t1}) + C_2 cov_{s2}(h; \Theta_{s2}) cov_{t2}(\tau; \Theta_{t2}) \\ & + C_3 cov_{s3}(h; \Theta_{s3}) cov_{t3}(\tau; \Theta_{t3}) \end{aligned} \quad (31)$$

Table 19 Parameters for fitting nested covariance model- daily PM10 BME analysis

$C_1=0.05$	cov_{s1} = Exponential	$\Theta_{s1}=4544.16$	cov_{t1} =Exponential	$\Theta_{t1}=4.32$
$C_2=0.05$	cov_{s2} = Exponential	$\Theta_{s2}=600$	cov_{t2} =Exponential	$\Theta_{t2}=18.8$ 4
$C_3=0.4$	cov_{s3} = Exponential	$\Theta_{s3}=600$	cov_{t3} =Exponential	$\Theta_{t3}=1.41$

BME prediction process then resulted in integration of G-KB (defined by the mean spatiotemporal trend and nested separable spatiotemporal covariance function) and S-KB (hard and soft data) to produce daily PM₁₀ values in Eindhoven. Maps for four different days of the week are plotted to see the variability of PM₁₀ (Figure 27). This included June 01, 2015 (Monday), June 04, 2015 (Thursday), June 20, 2015 (Saturday) and June 30, 2015 (Tuesday). June 4th was chosen as there was a sudden increase in PM values as compared to adjacent dates (as discussed in Section 5.1.1). Concentration maps for dates in June 2015 are presented in the appendix (Table 31). It can be seen that PM₁₀ levels are comparatively high for June 04, 2015 as compared to other days. Additionally, PM₁₀ levels are the lowest on June 20th. Locations where ILM measurements are present have relatively low values of PM₁₀. This may be due to the difference in the PM₁₀ values of ILM network and that of URBIS predictions. Since URBIS predictions are dominated by background values (averaged LML measurements), the difference in ILM measurements and LML background might be a probable cause. This difference is most prominent in June 30th.

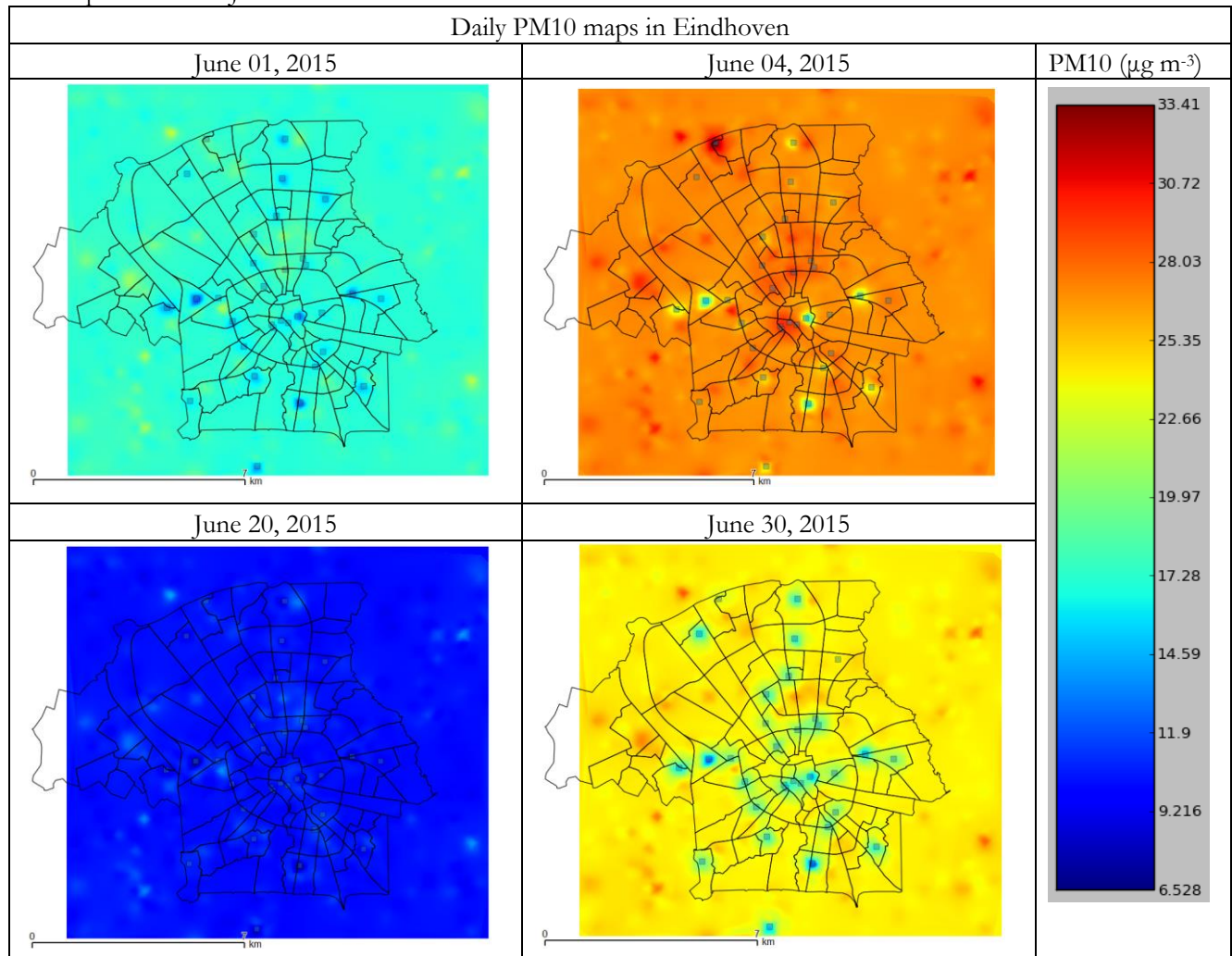


Figure 27 Daily PM10 prediction maps in Eindhoven

5.3.1.2. Predictions for PM_{2.5}

Similarly, BME analysis to generate spatiotemporal maps for daily values of PM_{2.5} were carried out. The empirical covariance functions in space and time domain were generated (Table 20) and by means of nested space-time separable covariance function (Equation 30), model fitting was done. Figure 28 represents the empirical covariance functions in space and time (left) and the fitted covariance model (right). The units for spatial lag is meters and temporal lag is days. It can be noticed that the effective range for the covariance in spatial domain is approximately 4000 meters whilst that for temporal domain is approximately 6 days. It can be noticed that the slope of both spatial and temporal covariance functions are smooth and give an indication that there is no sudden change in spatiotemporal variability.

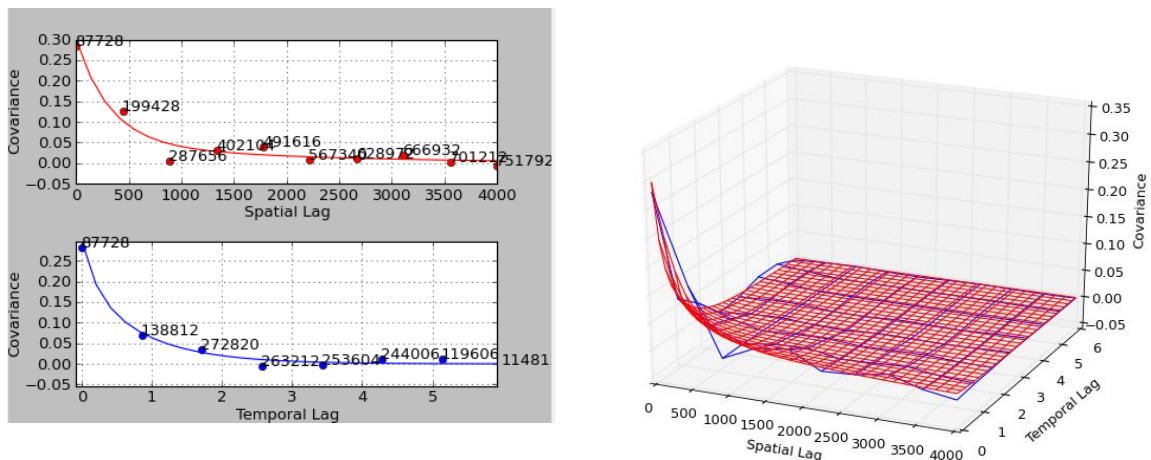


Figure 28 Covariance analysis for BME predictions of daily PM_{2.5}

Table 20 Estimates of empirical covariance functions- daily PM_{2.5} BME analysis

Estimates for Empirical covariance function	
Spatial distance limit: 4000	Temporal distance limit: 6
Number of spatial lags: 10	Number of temporal lags: 8
Spatial lag tolerance: 450	Temporal lag tolerance: 0.8

The modelled space-time covariance function consisted of three space time separable covariance functions and its parameters are depicted in Table 21. This was used to generate spatiotemporal maps of PM_{2.5} for daily values.

$$\begin{aligned} cov_{st}(h, \tau; \Theta_{st}) = & C_1 cov_{s1}(h; \Theta_{s1}) cov_{t1}(\tau; \Theta_{t1}) + C_2 cov_{s2}(h; \Theta_{s2}) cov_{t2}(\tau; \Theta_{t2}) \\ & + C_3 cov_{s3}(h; \Theta_{s3}) cov_{t3}(\tau; \Theta_{t3}) \end{aligned} \quad (32)$$

Table 21 Parameters for fitting nested covariance model- daily PM_{2.5} BME analysis

$C_1=0.05$	cov_{s1} = Exponential	$\Theta_{s1}=5509.58$	cov_{t1} =Exponential	$\Theta_{t1}=2.28$
$C_2=0.15$	cov_{s2} = Exponential	$\Theta_{s2}=975.63$	cov_{t2} =Exponential	$\Theta_{t2}=2.7$
$C_3=0.1$	cov_{s3} = Exponential	$\Theta_{s3}=943.42$	cov_{t3} =Exponential	$\Theta_{t3}=0.6$

PM_{2.5} prediction maps are shown for four days of June 2015 (Figure 29). Concentration maps for dates in June 2015 are presented in the appendix (Table 32). The pattern corresponds in a similar manner to that of PM₁₀ predictions (Figure 27). PM_{2.5} values tend to be high on June 04 and lowest for June 20. There is a decrease in PM_{2.5} level at locations near to ILM measurements and can be asserted to difference in URBIS predictions and ILM measurements.

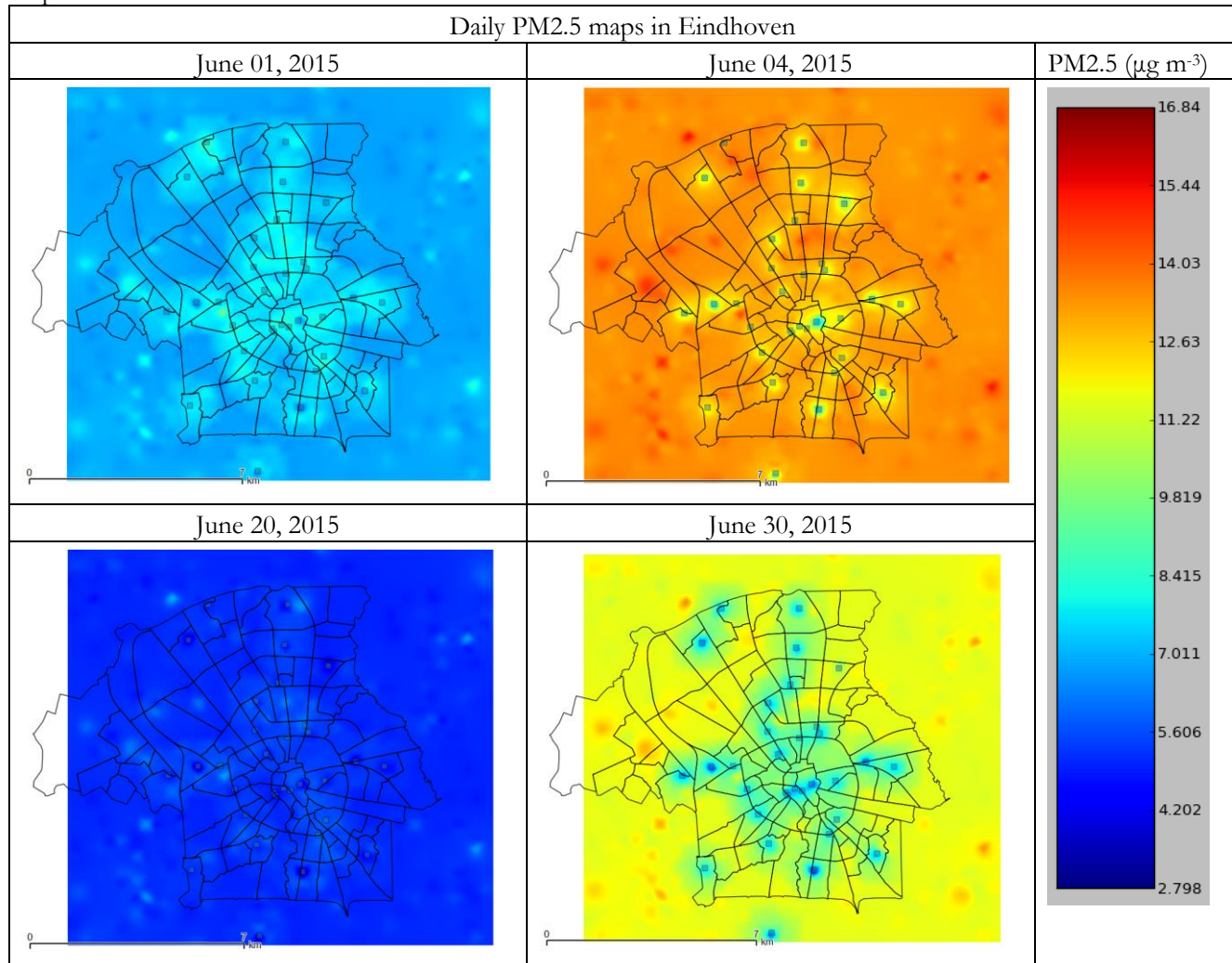


Figure 29 Daily PM_{2.5} prediction maps in Eindhoven

5.3.1.3. Cross validation

Cross validation of BME predictions were assessed by means of leave-one-out method employed in STAR-BME. 2000 soft and hard data were chosen in random and predictions were obtained at those locations. RMSE value was low for PM_{2.5} predictions as compared to PM₁₀. It might be due to the fact the spatial variability is high in PM₁₀ as compared to PM_{2.5} (as seen from the empirical covariance function for spatial domain (Figure 26, Figure 28).

Table 22 Cross validation results- daily predictions BME

BME Prediction	Data	RMSE	Residual Mean	Residual Standard Deviation
PM ₁₀ Daily	200 soft and hard	1.48	0.24	1.46
PM _{2.5} Daily	2000 soft and hard	0.85	0.05	0.85

5.3.2. Spatiotemporal Maps for hourly predictions

To understand about spatiotemporal variability of PM in a day, hourly prediction maps were generated. These were done for June 04, 2015, which showed an abrupt increase in PM values (as discussed in Section 5.1.1). Hourly soft and hard data pertaining to June 4th were used in the BME analysis. Spatiotemporal maps of hourly values of PM₁₀ predictions and PM_{2.5} predictions are presented in the subsequent section.

5.3.2.1. Predictions for PM10

Empirical space-time covariance functions were estimated from the given data (Table 23). Marginal covariance functions in space and time domain were plotted in Figure 30 Covariance analysis for BME predictions of hourly PM The unit for spatial lag is in meters and that for temporal lag is in hour. From the empirical covariance functions, it can be seen that the covariance value is relatively high as compared to daily values (Figure 26). There us a smooth decrease in the spatial and temporal covariance of PM₁₀ values.

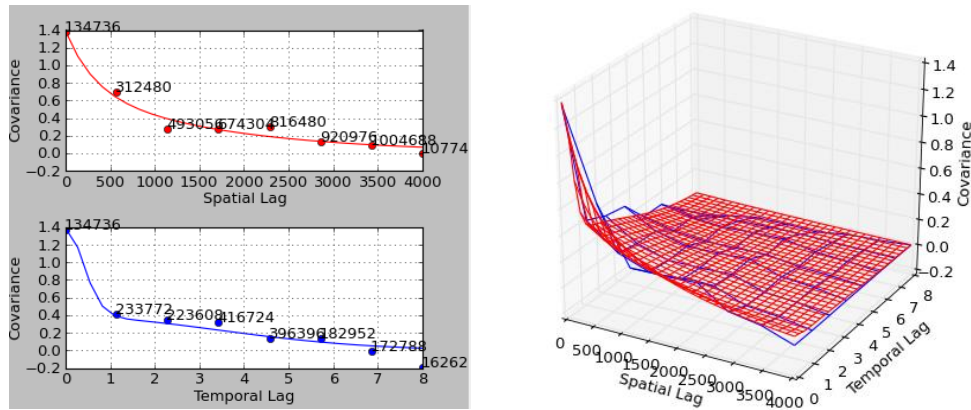


Figure 30 Covariance analysis for BME predictions of hourly PM10

Table 23 Estimates of empirical covariance functions- hourly PM10 BME analysis

Estimates for Empirical covariance function	
Spatial distance limit: 4000	Temporal distance limit: 8.
Number of spatial lags: 8	Number of temporal lags: 8
Spatial lag tolerance: 800	Temporal lag tolerance: 0.6

The modelled space-time covariance function consisted of three space time separable covariance functions and its parameters are depicted in Table 23. This was used to generate spatiotemporal maps of PM₁₀ for hourly values.

$$\begin{aligned} cov_{st}(h, \tau; \Theta_{st}) = & C_1 cov_{s1}(h; \Theta_{s1}) cov_{t1}(\tau; \Theta_{t1}) + C_2 cov_{s2}(h; \Theta_{s2}) cov_{t2}(\tau; \Theta_{t2}) \\ & + C_3 cov_{s3}(h; \Theta_{s3}) cov_{t3}(\tau; \Theta_{t3}) \end{aligned} \quad (33)$$

Table 24 Parameters for fitting nested covariance model– hourly PM10 BME analysis

$C_1=0.65$	cov_{s1} = Exponential	$\Theta_{s1}=953.85$	cov_{t1} =Gaussian	$\Theta_{t1}=1.1$
$C_2=0.38$	cov_{s2} = Exponential	$\Theta_{s2}=5444.88$	cov_{t2} = Gaussian	$\Theta_{t2}=8.38$
$C_3=0.36$	cov_{s3} = Exponential	$\Theta_{s3}=4599.87$	cov_{t3} = Gaussian	$\Theta_{t3}=0.8$

In June 04, 2015, four time periods were chosen at 6 hour intervals for representation purposes. Concentration maps for all hourly time periods in June 04 2015 are presented in the appendix (Table 33). These were 03:00 to 04:00, 09:00 to 10:00, 15:00 to 16:00 and 21:00-22:00 hours and corresponded to late night, post-morning rush hour, afternoon rush hours and before midnight. PM₁₀ values tends to gradually increase through the day till afternoon rush hour after which it tends to recede. However, these values (21:00-22:00 hours) tend to remain high as compared to morning rush hour. Regions around ILM measurement stations have lower value of PM₁₀ as compared to other locations and is prominent at all the cases.

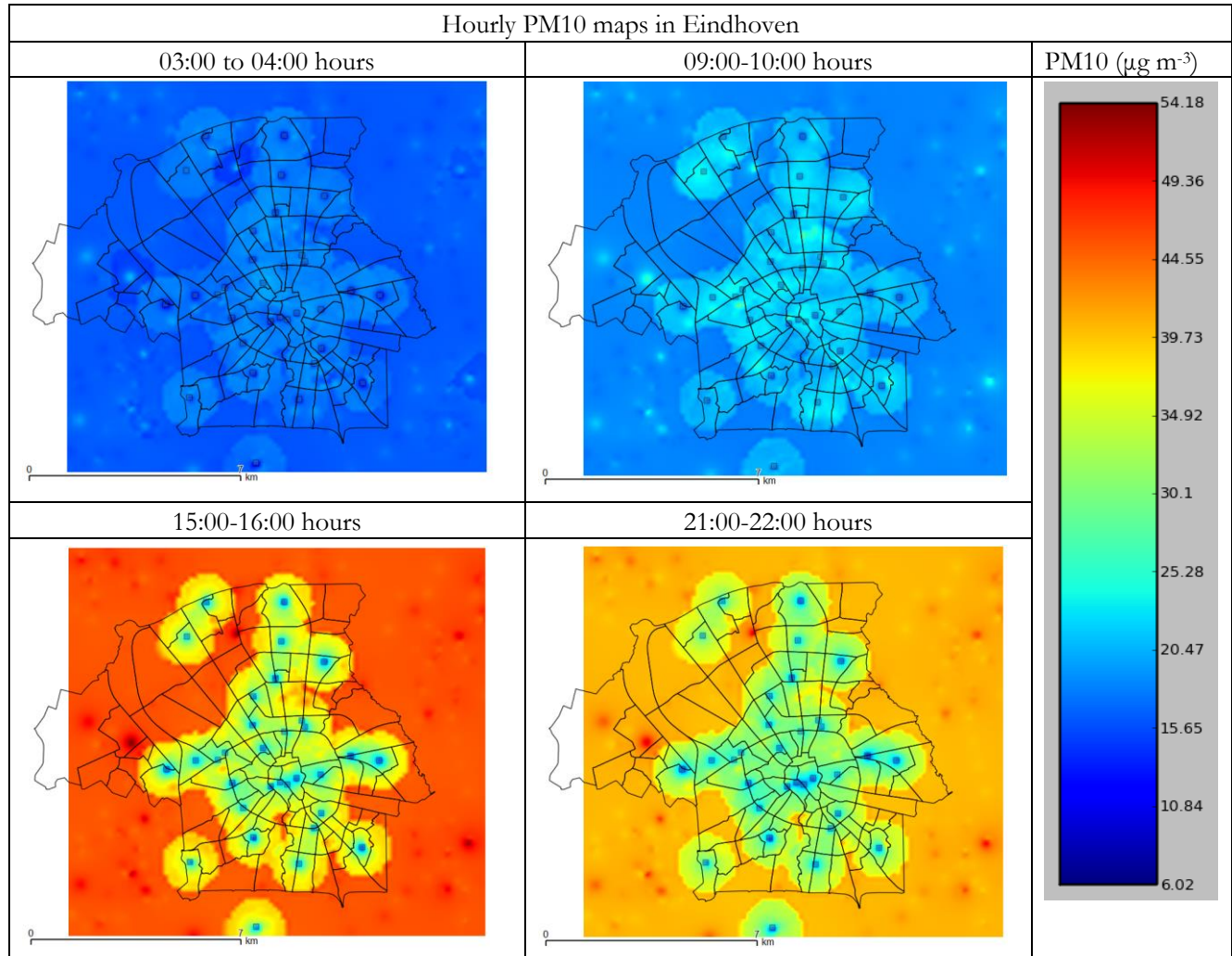


Figure 31 Hourly PM10 prediction maps in Eindhoven

5.3.2.2. Predictions for PM2.5

BME analysis using hourly PM_{2.5} values of ILM measurement and URBIS predictions for June 04, 2015 were done to generate hourly spatiotemporal maps. The empirical covariance functions in spatial and temporal domains are plotted (Figure 32) using estimates from the data (Table 25). The unit of empirical covariance functions in spatial domain is meters and temporal domain is hour. The spatial covariance function has an effective range of 4000 meters, beyond which it is considered that there is no correlation among the values. Similarly, the temporal covariance function has an effective range of approximately 6 days. The decrease in covariance values are gradual in case of temporal covariance function while spatial covariance decreases abruptly up to 1000 meters.

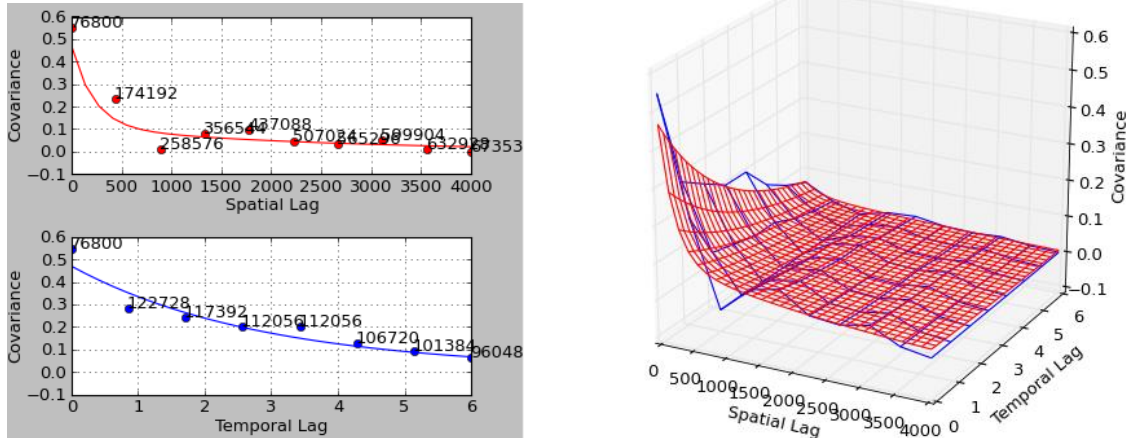


Figure 32 Covariance analysis for BME predictions of hourly PM2.5

Table 25 Estimates of empirical covariance functions- hourly PM2.5 BME analysis

Estimates for Empirical covariance function	
Spatial distance limit: 4000	Temporal distance limit: 6
Number of spatial lags: 10	Number of temporal lags: 8
Spatial lag tolerance: 500	Temporal lag tolerance: 0.5

The modelled space-time covariance function consisted of three space time separable covariance functions and its parameters are depicted in (Table 26). This was used to generate spatiotemporal maps of PM_{2.5} for hourly values on June 04, 2015.

$$\begin{aligned} cov_{st}(h, \tau; \Theta_{st}) = & C_1 cov_{s1}(h; \Theta_{s1}) cov_{t1}(\tau; \Theta_{t1}) + C_2 cov_{s2}(h; \Theta_{s2}) cov_{t2}(\tau; \Theta_{t2}) \\ & + C_3 cov_{s3}(h; \Theta_{s3}) cov_{t3}(\tau; \Theta_{t3}) \end{aligned} \quad (34)$$

Table 26 Parameters for fitting nested covariance model- hourly PM2.5 BME analysis

$C_1=0.36$	cov_{s1} = Exponential	$\Theta_{s1}=662.63$	cov_{t1} =Exponential	$\Theta_{t1}=7.85$
$C_2=0.05$	cov_{s2} = Exponential	$\Theta_{s2}=7132.61$	cov_{t2} =Exponential	$\Theta_{t2}=12.39$
$C_3=0.06$	cov_{s3} = Exponential	$\Theta_{s3}=7411.57$	cov_{t3} =Exponential	$\Theta_{t3}=15.36$

Similar to hourly PM₁₀ analysis, four time periods were chosen each at six hour intervals to see the spatiotemporal variability of PM_{2.5} values in Eindhoven (Figure 33). Concentration maps for all hourly time periods in June 04 2015 are presented in the appendix (Table 34). The values tend to be low during late night (03:00-04:00) hours and increase through the day. PM_{2.5} concentrations are the highest during 21:00-22:00 hours. Unlike hourly PM₁₀ predictions (Figure 31) which showed highest concentration levels during afternoon rush hour (15:00-16:00) hours and then stabilizes, PM_{2.5} shows an increasing trend in values. Furthermore, locations around ILM measurements have lower concentration than other regions, but in comparison with hourly PM₁₀ predictions (Figure 31), these changes are not so prominent.

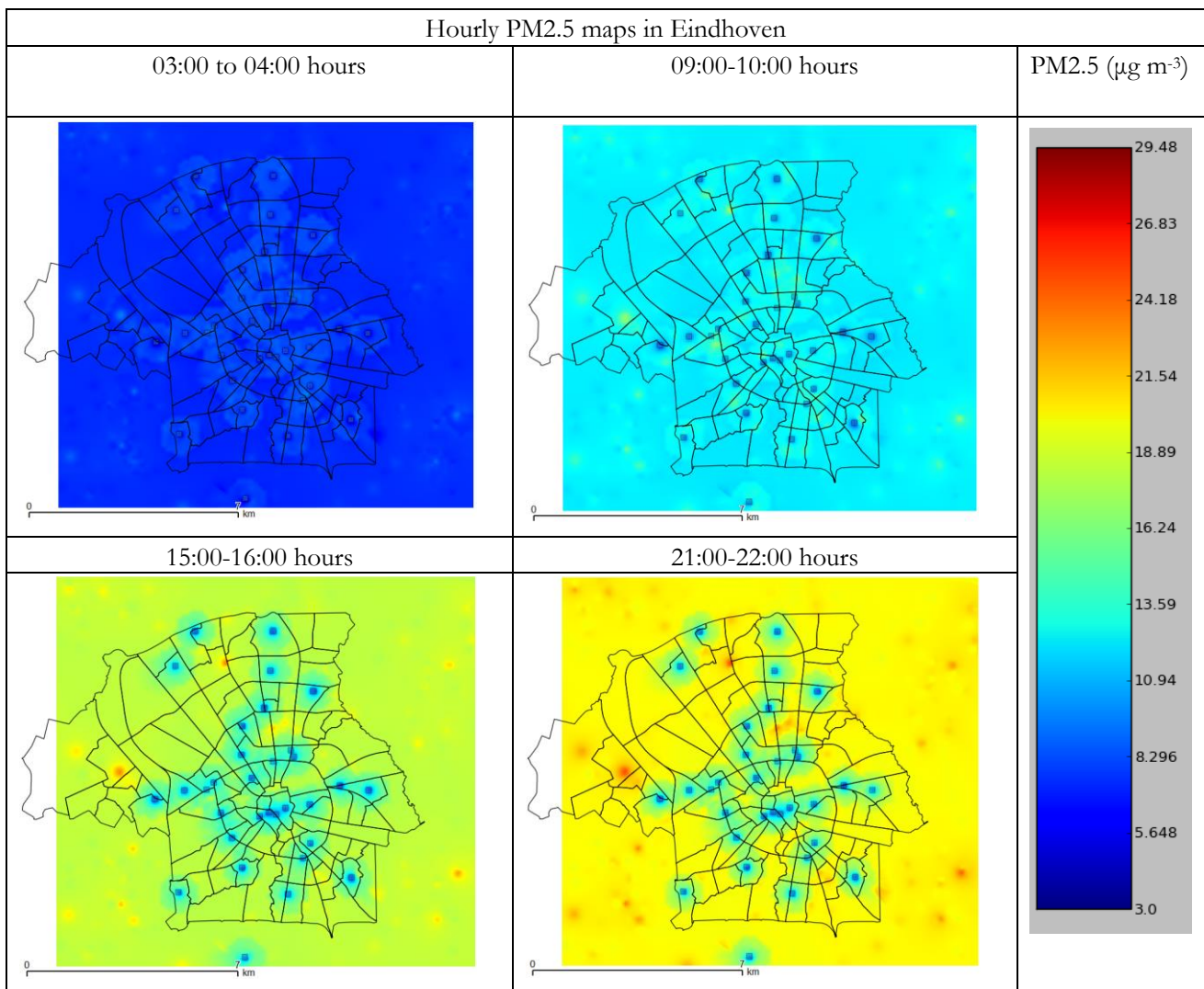


Figure 33 Hourly PM2.5 prediction maps in Eindhoven

5.3.2.3. Cross Validation

To assess the prediction accuracy of BME process, leave-one-out cross validation was carried out taking into consideration 2000 soft and hard data locations (Table 27). PM_{2.5} predictions had a lower RMSE and residual mean as compared to PM₁₀ predictions. PM₁₀ hourly predictions had extremely high value of RMSE and residual standard deviation.

Table 27 Cross validation results- hourly predictions BME

BME analysis	Data	RMSE	Residual Mean	Residual Standard Deviation
PM _{2.5} Hourly	2000 soft and hard	0.95	0.13	0.94
PM ₁₀ Hourly	2000 soft data	3.475	0.57	3.42

5.4. Comparison of mean ILM measurements with averaged LML for background PM

As discussed in Section 5.1, relatively lower value of ILM mean measurements against that of LML background values (Table 12 and Figure 15) and no discernible differences in the mean PM values across the categories of airbox locations (Figure 16 and Figure 17) can suggest that mean values of ILM can also be assumed as the background value of PM in Eindhoven. Timeseries plot (Figure 34) shows that mean ILM PM_{2.5} values at a daily level tend to remain between 5- 10 µg m⁻³ and show less fluctuations as compared to averaged background from LML stations

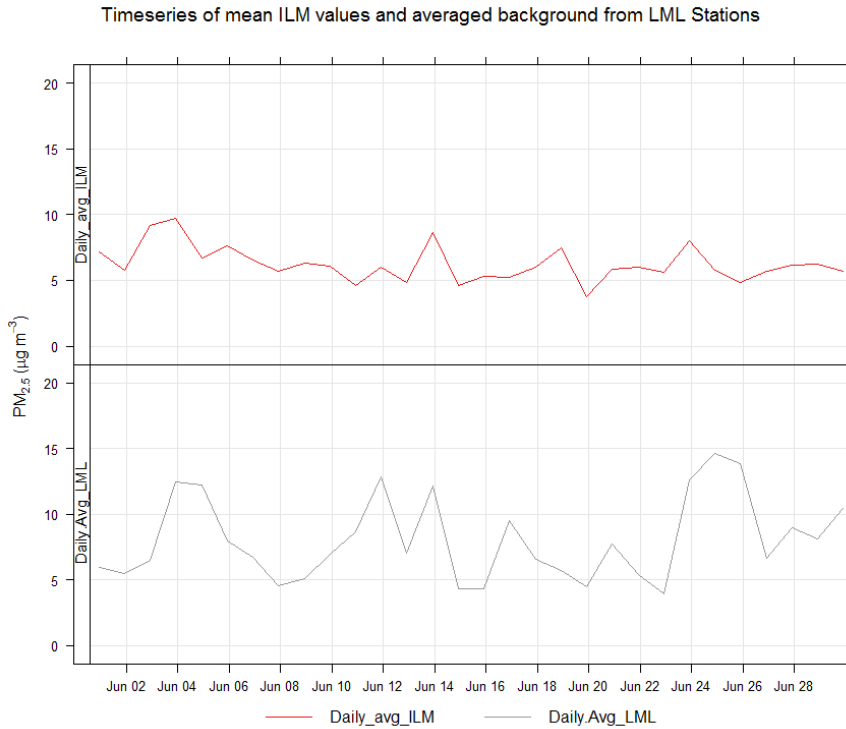


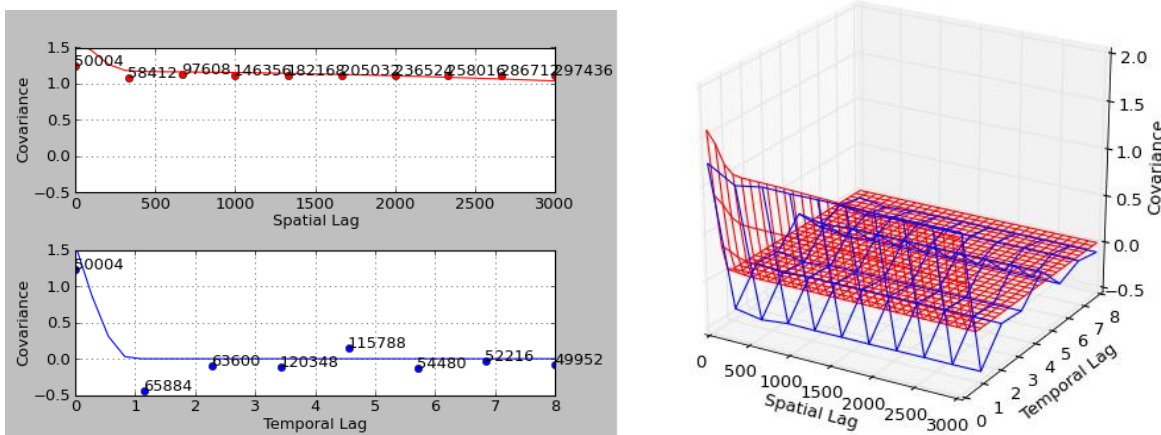
Figure 34 Timeseries of mean ILM values and averaged background from LML stations

To compare the effect of PM background values on performance of URBIS predictions and on BME analysis, one special case was considered. Mean PM_{2.5} ILM measurements were used as background values for URBIS background predictions instead of averaged PM_{2.5} LML measurements. This was done for daily values of PM_{2.5} and the results were compared with corresponding results obtained by taking averaged LML measurements as background value (Section 5.3.1.2 and Section 5.2.5).

5.4.1.1. Spatiotemporal predictions of daily PM_{2.5} using mean ILM as background

Aggregated daily values of PM_{2.5} URBIS foreground predictions were added to averaged ILM measurements (PM_{2.5}) at 32 airbox locations to obtain new URBIS predictions at 500 locations. Uncertainty in these URBIS predictions was kept constant at 25%, that corresponded to maximum allowable uncertainty in daily PM_{2.5} measurements as set by air quality guidelines (EU, 2008). Soft data at these locations was thus generated by using the bounds of ± 25% of the URBIS prediction values. Hard data comprised of daily aggregated PM_{2.5} ILM measurements at 32 locations.

BME was then performed to generate spatiotemporal predictions of daily PM_{2.5} values in Eindhoven. The empirical covariance function in spatial domain and temporal domain were estimated from the data (Figure 35 and Table 28). A high value of spatial covariance is seen for 3000 meters while the temporal covariance reduces to zero approximately at 1 day lag. The units of spatial lag is meters and that of temporal lag is days.

Figure 35 Covariance analysis for BME predictions of daily PM_{2.5} (using ILM as background)Table 28 Estimates of empirical covariance functions- Daily PM_{2.5} BME analysis (using ILM as background)

Estimates for Empirical covariance function	
Spatial distance limit: 3000	Temporal distance limit: 8
Number of spatial lags: 10	Number of temporal lags: 8
Spatial lag tolerance: 200	Temporal lag tolerance: 0.7

The modelled space-time covariance function consisted of three space time separable covariance functions and its parameters are depicted in Table 29. This was used to generate spatiotemporal maps of PM_{2.5} for daily values.

$$\begin{aligned} cov_{st}(h, \tau; \Theta_{st}) = & C_1 cov_{s1}(h; \Theta_{s1}) cov_{t1}(\tau; \Theta_{t1}) + C_2 cov_{s2}(h; \Theta_{s2}) cov_{t2}(\tau; \Theta_{t2}) \\ & + C_3 cov_{s3}(h; \Theta_{s3}) cov_{t3}(\tau; \Theta_{t3}) \end{aligned} \quad (35)$$

Table 29 Parameters for fitting nested covariance model– Daily PM_{2.5} BME analysis (using ILM as background)

$C_1=0.28$	cov_{s1} = Gaussian	$\Theta_{s1}=300$	cov_{t1} =Spherical	$\Theta_{t1}=1.11$
$C_2=1.17$	cov_{s2} = Gaussian	$\Theta_{s2}=15000$	cov_{t2} =Spherical	$\Theta_{t2}=0.87$
$C_3=0.13$	cov_{s3} = Gaussian	$\Theta_{s3}=300$	cov_{t3} =Spherical	$\Theta_{t3}=0.8$

Spatiotemporal prediction maps for daily PM_{2.5} values in Eindhoven were plotted for four dates (June 01, June 04, June 20 and June 30, 2015). These dates were chosen for comparison with daily PM_{2.5} BME predictions that was previously done using LML measurements as background stations for URBIS predictions (Section 5.3.1.2). From the plots (Figure 36) it can be seen that PM_{2.5} values are comparatively high for June 04 and lowest for June 20. One striking feature that can be noticed while comparing these plots with corresponding plots in Figure 29, is that, there is no such distinguishable difference in PM_{2.5} values around the airbox locations (shown as dots). This is in contrast with observations from Figure 29, where differences in PM_{2.5} values around airbox locations were prominent and can suggests that fluctuations in these values were mainly due to averaged LML measurements used as background concentrations.

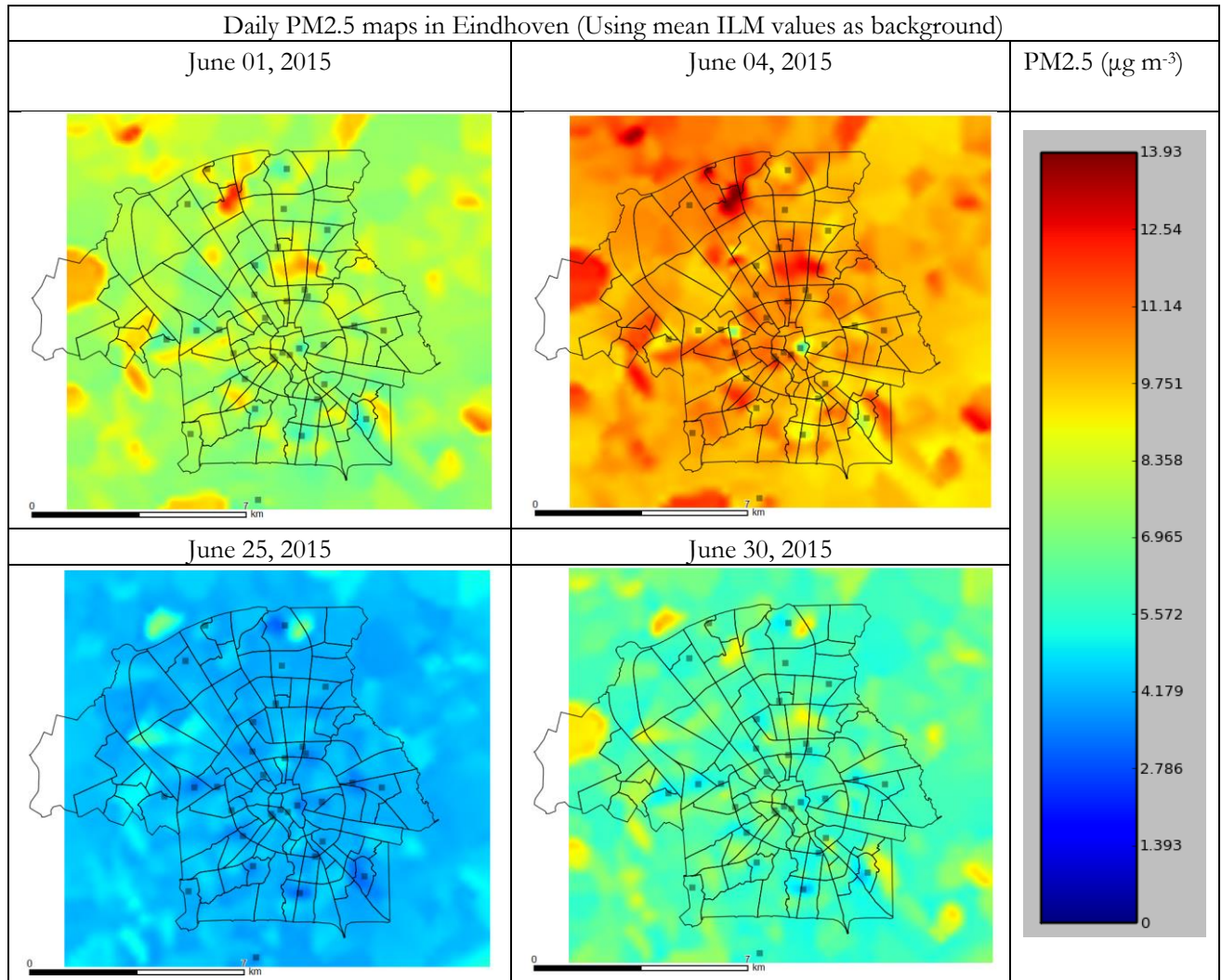


Figure 36 Daily PM2.5 prediction maps in Eindhoven (using ILM as background)

Cross validation of the BME process was done using leave-one out method in the similar manner as described in Section 5.3.1.3 and it was found that RMSE associated with the prediction was 0.89, the residual mean was 0.16 and residual standard deviation was 0.87. This was found to be comparable with cross validation results of BME predictions where averaged LML measurements were used as background values, which had RMSE of 0.85, the residual mean as 0.05 and residual standard deviation as 0.85.

Equal tolerance graphs, described in Section 5.2.5 were plotted to assess the conformance of daily PM_{2.5} values of URBIS predictions against daily PM_{2.5} values of ILM measurements. Here uncertainty levels for both URBIS model predictions and ILM measurements are kept constant at 25%. These were plotted for four different locations (Figure 37)- airbox location 1 (City background), airbox location 2 (Busy road), airbox location 3 (Residential area) and airbox location 31 (City background –outside Eindhoven). These plots show that there is a high conformance in URBIS predictions and ILM measurements. Particularly at airbox location 2, URBIS predictions and ILM measurements are almost identical for all dates of June 2015. For airbox location 3, which corresponds to busy road, URBIS predictions are higher than that of ILM measurements and this can be attributed to URBIS foreground values. Thus it can be asserted that mean values of ILM measurements can be used as background values for PM_{2.5} in Eindhoven and facilitate integration of URBIS predictions with ILM measurements.

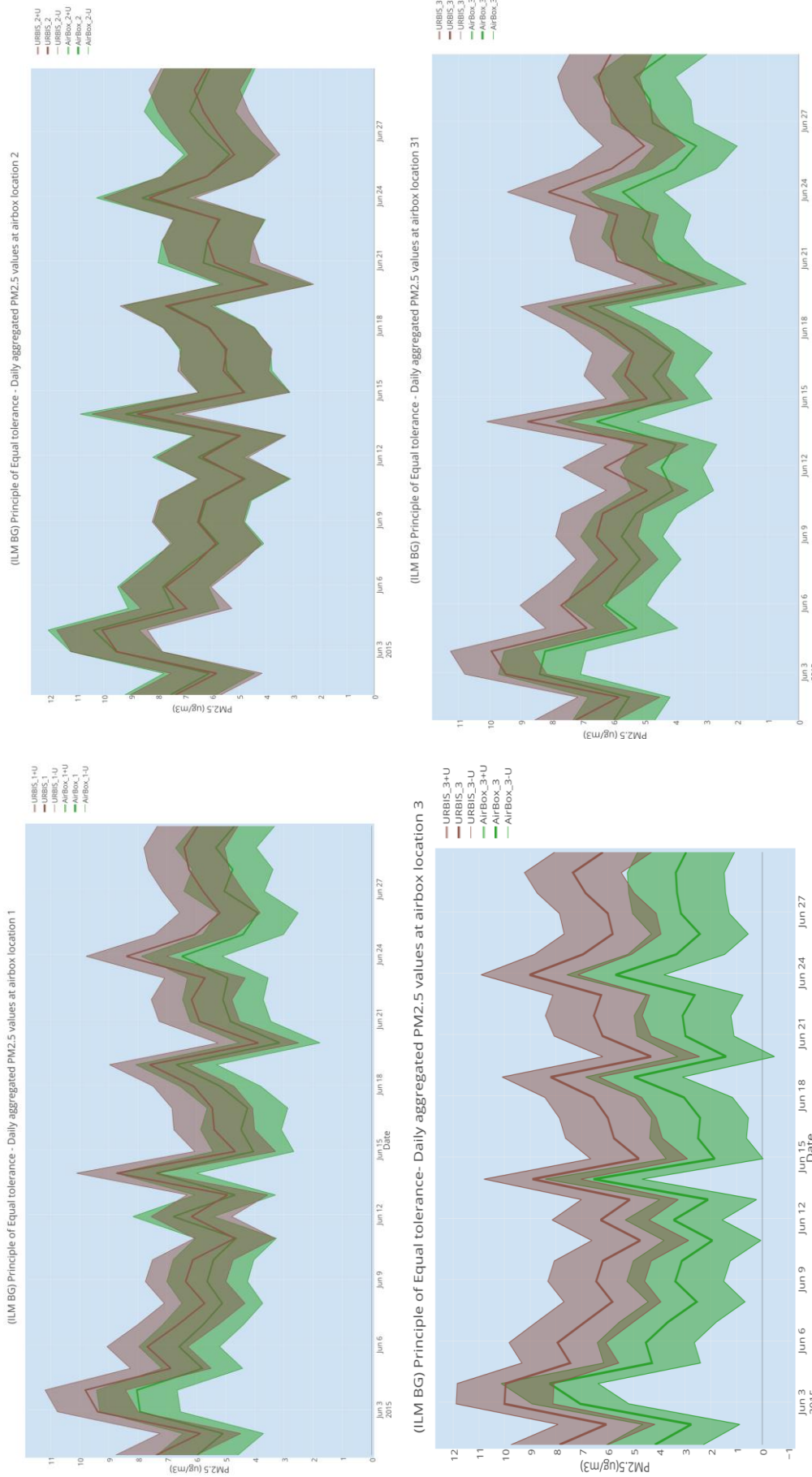


Figure 37 Principle of equal tolerance - daily aggregated PM2.5 (using ILM as background in URBIS predictions)

6. DISCUSSION

This chapter discusses some of the key findings of the research. It includes discussions in particular about the data quality of URBIS predictions and ILM measurements, estimation of background PM values, levels of uncertainty in PM measurements, interpretation of performance evaluation results and feasibility of BME method in integration of URBIS and ILM.

6.1.1. Data quality of URBIS and ILM

ILM dataset contained missing measurements for a prolonged time periods at some airboxes (Table 3; Figure 18 and Figure 19) due to which evaluation of URBIS predictions at these time points was not possible. MPC values were calculated for only those time points at which ILM measurements and URBIS predictions were both available. Reduction in these modelled-concentration pairs thus influenced MPC results at those airbox locations. URBIS dataset only consisted of foreground predictions of PM which were mainly traffic contributions from highways and streets canyons (Table 4). It lacked contributions from emissions by point and area sources, such as industries, building construction sites, agricultural land which amongst other have substantial impact on PM values in a city. Thus it was deemed necessary to account for background PM values for adequate representation of URBIS predictions prior evaluating them against ILM measurements.

6.1.2. Estimation of background values of PM

To account for contribution of background levels in the PM values in Eindhoven, measurements from three LML stations were averaged and its mean value was considered. These stations were classified as background stations and were located in vicinity of Eindhoven (Section 3.2.3.2). By analysing the PM values at these stations (Figure 8, Figure 9 and Figure 10), it was noticed that average value can be the approximation of values at these three stations. This was also confirmed from Table 7 where averaged background showed almost similar values with individual LML stations. Averaged PM values from LML stations were high as compared to the URBIS foreground predictions. This is described in Section 5.1 (Table 12 and Figure 15). Low values of URBIS foreground predictions as compared to ILM measurements and averaged LML background were in accordance with Matthijsen & ten Brink, (2007) suggesting low contribution of local traffic sources to PM_{2.5} values in the Netherlands. Heavier dominance of this background concentration in URBIS predictions can also be seen in the temporal visualization of URBIS predictions at airbox locations (Figure 20 and Figure 21).

From Table 12 and Figure 15, it can also be noticed that the averaged LML measurements (mean value) were also larger than mean of ILM measurements. It might lead to the following conclusions. Firstly, averaging measurements from these three available LML stations might not be adequate representation of background values in Eindhoven. Furthermore, abrupt hourly fluctuations in PM measurements at any individual LML station (Figure 9, Figure 10), missing values, discarding of negative values (Section 3.2.3.2) while averaging can lead to a biased estimation of average. Secondly, ILM instruments might record lower values of PM as compared to LML stations. Recent analysis performed by the AiREAS Calibration/Validation working group has shown that the ILM instruments often record lower values of PM relative to LML station located at Genovevalaan, Eindhoven (Otjes, 2016). It is early to say how widespread the problem is. However, it may explain why the background values recorded by the LML stations located outside Eindhoven contribute to URBIS predictions that are often larger than spatially coincident ILM measurements. Thirdly, relatively lower value of mean ILM measurements against averaged

LML background stations as discussed above and similarity in PM levels for different categorizes of airboxes (Figure 16 and Figure 17) might lead to the fact that mean ILM measurements can also be used as background values in place of averaged LML measurements in the URBIS model. Mean ILM measurements also showed less fluctuations in their values as compared to averaged LML measurements (Figure 34).

6.1.3. Uncertainty levels in PM values

Uncertainty associated with measurements of PM values were assumed to be 25% of their values for ILM network at all temporal scales of aggregation (Section 4.1) due to inadequate information on its exact value. This was based on relative uncertainty of 25% in mean PM measurements (PM_{10} and $PM_{2.5}$) which is a reference value that stems from the European air quality directive and is considered for daily values (EU, 2008). It is because PM values tend to fluctuate and other systematic and random errors associated with measurements which makes it difficult to impose a reference value of uncertainty for lower temporal scales. Changing the temporal scale to hourly or 6-hourly or 24-hourly may result in the increase of uncertainty but the exact value could not be ascertained.

To elucidate principle of equal tolerance which assumes model to exhibit similar levels in uncertainty in PM values as compared to measurements, URBIS model predictions were also assumed to have 25 % uncertainty in their values. This assumption is justifiable owing to that fact that major contribution in URBIS prediction was from the background values which were from the LML stations. These measurements have 16% uncertainty associated with them and is explained in Section 3.2.3.2 and also established by reports of (Hoogerbrugge et al., 2010). Assumption of averaged LML measurements as background value also incorporate additional uncertainties in the PM values of URBIS. Inherent uncertainties associated in the dispersion modelling frameworks employed in the URBIS also account for additional uncertainties. Possibility of performing a sensitivity analysis on URBIS model could have led to discerning these uncertainties but outside the scope of the research. Thus, based on these factors led to the assumption of uncertainty of 25% in URBIS data. This value was kept constant for all temporal scales (hourly and daily level) for the analysis due to lack of information about exact levels of uncertainty of PM predictions in URBIS at these temporal aggregations.

6.1.4. Performance evaluation of URBIS model

Measurement uncertainty were calculated for each airbox, taking into consideration relative uncertainty of 25% for measurement of PM values as set by air quality directives. These values were found to be high for PM_{10} and lower for $PM_{2.5}$ values at all temporal scales of aggregation. From Section 5.2 , it can be seen that aggregation of ILM measurements and URBIS predictions from hourly to 24-hourly resulted in almost no change in measurement uncertainty values. This might be due to the fact that aggregation tends to smooth out variations and the mean value of observations remains approximately the same. Furthermore, assumption of 25% relative measurement uncertainty for PM values at all temporal scales might have resulted in no change in measurement uncertainty at these airboxes. Model performance criteria for RMSE was found to be consistently violated at all representative airbox locations for $PM_{2.5}$ at all temporal aggregations, except in case of busy road (for 12-hourly and daily aggregations). The MPC for RMSE and NMB was violated only in city background locations for PM_{10} . MPC for RMSE values remains low at locations which represent busy roads, owing to fact that URBIS predictions are generally better for locations near to traffic sources and these values were high for regions such as city background which have fewer traffic. Model performance criteria for R remains fulfilled at all locations whilst MPC for NMSD remains violated for all locations in hourly and 6-hourly aggregations. For 12 hourly and daily aggregations, these are only violated in city background (PM_{10}) and only adhered in busy road locations.

The analysis finds that URBIS predictions are consistent with ILM measurements for locations that have substantial traffic contributions and is justifiable based on inherent modelling of URBIS It performs poorly at locations which are considered as city background. Thus, even though the background concentration dominates URBIS foreground predictions, it still does not conform to ILM measurements at locations which do not have heavy traffic. From the equal tolerance graphs, it can be deduced that increasing temporal resolutions tends to reduce the difference between ILM measurements and URBIS predictions, however due to fluctuations in the background values these do not overlap for all time periods. URBIS predictions for PM10 show more overlap to ILM measurements as compared to PM2.5 (discussed in Section 5.2.5). The amount of overlap is also highest for daily aggregations for locations near busy road and is least for background locations (Section 5.2.5.4).

Using mean ILM PM2.5 measurements as an alternative for background values in the URBIS model led to more overlap at all the representative stations (Section 5.4-Figure 37). The temporal trend of PM2.5 predictions from URBIS model were found to match the temporal trend of ILM measurements which were previously not found when averaged LML measurements were taken as background values for URBIS model (Figure 24). From this experiment, that mean ILM measurements can be considered as a better alternative to represent background values than averaged LML measurements and be used in the URBIS model. Although, this case was considered for daily values of PM2.5, it can be further extended to check the overlap patterns for PM10 and hourly values of PM10 and PM2.5, which could not be done due to limitations in resources.

Thus employing multiple statistical indicators and using measurement uncertainty associated with ILM measurements, the study was able to distinguish which spatial locations URBIS predictions conformed to ILM measurements. Furthermore, usage these indicators at different temporal aggregations along with equal tolerance graphs, it can be assessed at which temporal instances and URBIS predictions overlap with ILM measurements. These two criteria were found comprehensively adequate for performance evaluation of URBIS predictions.

6.1.5. BME predictions

Bayesian maximum entropy framework was found a feasible method to integrate URBIS predictions and ILM measurements for spatiotemporal modelling of PM values in Eindhoven. It incorporated URBIS predictions as soft data, characterized by its uncertainty level of 25% and ILM measurements as hard data. Spatiotemporal maps obtained at hourly values and daily average values were able to depict the variability in space and time of PM values in Eindhoven. BME integrates data from multiple sources (such as URBIS predictions and ILM measurements) with their levels of uncertainty which is crucial in mapping applications like air quality for adequate representation of PM values.

Two key aspects can be concluded from the BME predictions. Firstly, BME prediction maps were able to show the variation of PM values in space and time (depicted in Table 31 and Table 32). Variation of PM values were analysed for four dates (Figure 27 and Figure 29). Furthermore, time series analysis of PM values from ILM measurements showed abrupt increase of PM values on 4th June (Section 5.1.1), and using BME approach, these were validated to see patterns in PM values throughout the date of June 04 (Table 33 and Table 34). It was seen that there was a constant increase in PM₁₀ values till afternoon and then it tends to remain stabilized resulting in overall increased values of PM for the next day (Figure 31). Similarly for PM_{2.5} these value tend to gradually increase throughout the day (Figure 33) and this also explains the increased levels of PM_{2.5} in consecutive dates around June 04, 2015.

Secondly, BME was able to discern the local variability in PM values at regions near airboxes. This variation in PM values were prominent for both PM10 and PM2.5 at hourly and daily scales (Section 5.3). This is due to high values of URBIS predictions as compared to ILM measurements. These high values of URBIS predictions, as discussed in Section 6.1.2 is primarily due to averaged LML measurements that was considered as background values for URBIS model. This change in values is most prominent in hourly PM₁₀ predictions (Figure 31). Another possible reason behind this variability can be the use of kernel smoothing filter that is employed in STAR-BME to remove spatiotemporal mean trend. Modification of values for this kernel smoothing filter might have led to a low differences in PM values in the adjacent regions of airboxes. However, this modification was not possible currently and can be considered in future. The cross validation results for BME were seen to acceptable for PM2.5 (RMSE of 0.85 for daily predictions and 0.95 for hourly predictions but these RMSE values were comparatively high for PM10 predictions (Table 22 and Table 27). Specifically for hourly PM10 RMSE value was 3.7 which might raise a question on BME's effectiveness for PM10 modelling. This can be addressed by comparing BME predictions with those obtained by other interpolation methods (such as regression kriging) and can be considered as future scope.

In order to assess the effect of background value on BME predictions, mean ILM measurements were taken as background for URBIS predictions (Section 5.4) and used for daily predictions of PM2.5. From the results, (Figure 36), it can be seen that there were relatively less variations in PM2.5 values near airbox locations, as compared to the predictions where averaged LML measurements were taken as background values for URBIS (Figure 29). This further ascertains that mean ILM measurements can be used as an alternative to averaged LML measurements as background levels of PM2.5 in Eindhoven. The cross validation results for the case where mean ILM measurements were taken as background value was found to be comparable with daily PM2.5 predictions (RMSE value of 0.89). Although this was only one experimental case which was considered (for daily values of PM2.5 predictions), it could be further extended for daily PM10 predictions and hourly predictions. Based on these results, it can be concluded that ILM measurements can be incorporated with URBIS model predictions for spatiotemporal modelling and mapping of PM values in Eindhoven.

7. CONCLUSIONS

Based on research identification outlined in Section 1.3, this research comprised firstly of evaluation of PM predictions (PM10 and PM2.5) from the downscaled URBIS against PM measurements (PM10 and PM2.5) from the ILM to assess at which temporal resolution URBIS predictions resembled ILM measurements. This was done by means of statistical metrics utilizing uncertainty levels associated with PM measurements in the ILM. Conceptual description of the methodologies for performance evaluation have been outlined in Section 4.1.1. Four recommended statistical metrics for air quality evaluation, namely, root mean square error (RMSE), normalized mean bias (NMB), normalized mean standard deviation (NMSD) and correlation co-efficient (R) were used with measurement uncertainty of PM (assumed to be 25% of the measured PM values), lead to formulation of model performance criteria (MPC). Assessment of URBIS predictions against ILM was carried out at 32 ILM measurement locations and at four different temporal scales were done at four different temporal scales- hourly, 6-hourly, 12-hourly and daily values for June 2015. These results are described in Section 5.2.

Secondly, this study employed BME method to integrate URBIS predictions with ILM measurements for spatiotemporal mapping of PM values (PM10 and PM2.5) in Eindhoven. PM values from 500 URBIS prediction locations and 32 ILM locations for June 2015 were used for BME mapping. Predictions were done at two temporal scales - aggregated daily values (entire month of June, 2015) and hourly values (for June 4th, 2015). Conceptual description of BME method is described in Section 4.2.1. Intermediary process and spatiotemporal maps at these temporal scales are depicted in Section 5.3.

7.1. Answer to research questions

Questions related to objective 1:

- a) *What are the key statistical indicators that are needed to evaluate URBIS model?*

After an extensive literature review focussing on evaluating air quality models (Section 2.3) and based on conceptual description (Section 4.1.1), it was found that application of multiple statistical indicators are required for evaluating URBIS model. These were root mean square error (RMSE), Normalized mean bias (NMB), Normalized mean standard deviation (NMSD) and correlation coefficient (R). These were considered as they can be used with measurement uncertainty of airboxes in the ILM network and can facilitate evaluation of URBIS model at different temporal aggregation scales.

- b) *How to formulate and interpret model performance criteria (MPC) to evaluate URBIS model based on statistical indicators and measurement uncertainty of ILM network?*

This was based on the methodology proposed by (Pernigotti et al., 2013; Thunis et al., 2015, 2012a) which considers usage of measurement uncertainty in measurements to assess the predictions of air quality models. This has been the key point in my research and has been addressed in (Section 4.1.1). Based on the statistical indicators answered in question (a) were used with measurement uncertainty of PM in the ILM network to generate model performance criteria and the results have been described in (Section 5.2).

- c) *What are suitable space-time scales for representing PM concentration levels?*

Four different temporal aggregations were chosen to represent PM values from URBIS predictions and ILM measurements. These were hourly, 6-hourly, 12-hourly and daily for data pertaining to June 2015.

To characterize the spatial representativeness of PM values, four different categories of airbox locations were used. These were based on (Hamm et al., 2016) and were city background, residential area, busy road and public hospital (described in Section 3.2.1.1). Performance of URBIS predictions were considered at an airbox location representing the above. URBIS predictions conformed to ILM measurements within the levels of uncertainty at daily aggregations of PM10 especially for locations near to traffic sources (airbox locations 2 and 3 -Figure 25). These overlaps were not so prominent for PM2.5 (Figure 24). However, by taking mean ILM measurements as background values instead of averaged LML measurements, these overlaps regions increased for PM2.5. Thus daily values can be considered as suitable space-time scales for representation of PM concentration levels.

Questions related to objective 2:

- a) *Which data should be considered as soft (data with uncertainty) and hard (certain data)?*

URBIS predictions were considered as soft data with uncertainty value of 25% associated with their values. ILM measurements were considered as hard data for BME analysis. This distinction in soft and hard data has been described in (Section 4.2.2.1).

- b) *How to model the space-time dependence of PM?*

Space time dependence structure of PM was modelled by means of a nested space-time separable covariance model in STAR-BME. This has been discussed in (Section 4.2.2.3). Based on available data, empirical covariance functions were estimated. Then these were modelled by iterative method of PSO (particle swarm optimization) technique in BME to fit a nested space-time separable covariance model and the accuracy was assessed by means of AIC value.

- c) *How to integrate space-time dependence of PM with available data from URBIS model and ILM measurements to generate prediction maps?*

Space-time covariance function is used to generate prior PDF. Then using available data, Bayesian conditionalization is done which integrates attribute values from available data (hard and soft) to generate posterior PDF. In this sense, every node in the output grid consists of a distribution function. Spatiotemporal prediction maps consists of mean values of these distribution functions. This has been described in (Section 4.2.1) and the results are presented in (Section 5.3). Prediction maps for daily PM values for June 2015 can be found in (Table 31 and Table 32) and those for hourly PM values for June 04 2015 can be found in (Table 33 and Table 34).

- d) *How can the accuracy of BME process be assessed?*

Leave-one-out cross validation method is employed on set of 2000 hard and soft data locations to assess the prediction accuracy of BME process. The cross validation results in terms of RMSE, residual mean and residual standard deviation are used to compare the effectiveness of BME in prediction. Prediction accuracy were acceptable for PM2.5 predictions (RMSE value of 0.85 for daily predictions and 0.95 for hourly predictions) whilst these were comparatively higher for PM10 (RMSE value of 1.48 for daily predictions and 3.47 for hourly predictions). Using mean ILM PM2.5 measurements as background values for URBIS model, daily predictions yielded an RMSE of 0.89. Thus it can be said that BME predictions were better for PM2.5 as compared to PM10. This research did not consider any other interpolation method to compare the accuracy of BME predictions. These comparisons could ascertain whether predictions from BME process are accurate enough or not, and could essentially might help to explain the high RMSE value associated with daily PM10 BME predictions.

7.2. Limitations and Recommendations

The following points can be considered as some limitations and recommendations of the research.

- a) Accurate representation of background levels of PM can lead to a better understanding of spatiotemporal variability of PM in Eindhoven. For this research, averaged measurements from 3 LML stations were used. However, it was seen that these values were higher than mean ILM measurements, so this is important to ascertain which values can adequately represent background variability of PM.
- b) Information about measurement uncertainty of PM sensors in the ILM network at different temporal aggregation levels like hourly, 6-hourly, 12-hourly and daily values could help in proper evaluation of performance of URBIS model. For this research, it was considered constant at 25% which is only applicable at daily levels.
- c) Knowledge pertaining to uncertainties in URBIS model can be used to approximate its characterization as soft data for BME process.
- d) BME predictions were carried out at hourly values for one day and for daily values due to limitation in resources. This can be further developed for hourly values for all dates.
- e) Comparison of BME predictions with other interpolation techniques can further help in understanding the accuracy of BME predictions
- f) Downscaled URBIS model, whose data was initially available for June 2015, can be analysed for weekly, monthly and 6-monthly to check for its conformance with ILM predictions.
- g) Integration of ILM measurements, URBIS prediction output with other geographic predictor variables can be used for an improved modelling of spatiotemporal variability of PM values in Eindhoven.

LIST OF REFERENCES

- Adam-poupart, A., Brand, A., Fournier, M., Jerrett, M., & Smargiassi, A. (2014). Spatiotemporal modeling of ozone levels in Quebec (Canada): a comparison of kriging, land-use regression (LUR), and combined Bayesian Maximum Entropy–LUR approaches. *Environmental Health Perspectives*, 970(January 2013), 1–19. doi:10.1289/ehp.1306566
- AiREAS. (2014). AiREAS. Retrieved July 19, 2015, from <http://www.aireas.com/>
- Akita, Y., Baldasano, J. M., Beelen, R., Cirach, M., de Hoogh, K., Hoek, G., Nieuwenhuijsen, M., Serre, M., & de Nazelle, A. (2014). Large scale air pollution estimation method combining land use regression and chemical transport modeling in a geostatistical framework. *Environmental Science & Technology*, 48(8), 4452–9. doi:10.1021/es405390e
- Alam, M. S., & McNabola, A. (2015). Exploring the modeling of spatiotemporal variations in ambient air pollution within the land use regression framework: Estimation of PM₁₀ concentrations on a daily basis. *Journal of the Air & Waste Management Association*, 65(5), 628–640. doi:10.1080/10962247.2015.1006377
- Altman, N. S. (1990). Kernel Smoothing of Data With Correlated Errors. *Journal of the American Statistical Association*, 85(411), 749–759. doi:10.2307/2290011
- Amato, F., Zandveld, P., Keuken, M., Jonkers, S., Querol, X., Reche, C., van der Gon, H.A.C.D., & Schaap, M. (2015). Improving the modelling of road dust levels for Barcelona at urban scale and street level. *Atmospheric Environment*. doi:10.1016/j.atmosenv.2015.10.078
- Annau, M. (2015). CRAN package “h5.” Retrieved from <https://cran.r-project.org/web/packages/h5/h5.pdf>
- AQICN. (2016). Shinyei-PPD42NS inside. Retrieved January 22, 2016, from <http://aqicn.org/aqicn/view/images/sensors/Shinyei-PPD42NS-inside.jpg>
- Araujo, I. P. S., Costa, D. B., & de Moraes, R. J. B. (2014). Identification and characterization of particulate matter concentrations at construction jobsites. *Sustainability (Switzerland)*, 6(11), 7666–7688. doi:10.3390/su6117666
- Arslan, S., & Aybek, A. (2012). Particulate matter exposure in agriculture. In B. Haryanto (Ed.), *Air Pollution - A Comprehensive Perspective* (Vol. 10, pp. 73–104). doi:10.5772/50084
- Beckerman, B. S., Jerrett, M., Serre, M., Martin, R. V., Lee, S.-J., van Donkelaar, A., Ross, Z., Su, J., & Burnett, R. T. (2013). A hybrid approach to estimating national scale spatiotemporal variability of PM2.5 in the contiguous United States. *Environmental Science & Technology*, 47, 7233–7241. doi:10.1021/es400039u
- Beelen, R., Voogt, M., Duyzer, J., Zandveld, P., & Hoek, G. (2010). Comparison of the performances of land use regression modelling and dispersion modelling in estimating small-scale variations in long-term air pollution concentrations in a Dutch urban area. *Atmospheric Environment*, 44(36), 4614–4621. doi:10.1016/j.atmosenv.2010.08.005
- Bencala, K. E., & Seinfeld, J. H. (1979). An air quality model performance assessment package. *Atmospheric Environment*, 13(8), 1181–1185. doi:10.1016/0004-6981(79)90043-X
- Bennett, N. D., Croke, B. F. W., Guariso, G., Guillaume, J. H. A., Hamilton, S. H., Jakeman, A. J., Marsili-Libelli, S., Newham, L.T.H., Norton, J.P., Perrin, C., Pierce, S.A., Robson, B., Seppelt, R., Voinov, A.A., Fath, B.D., & Andreassian, V. (2013). Characterising performance of environmental models. *Environmental Modelling and Software*, 40, 1–20. doi:10.1016/j.envsoft.2012.09.011
- Bernard, S. M., Samet, J. M., Grambsch, a, Ebi, K. L., & Romieu, I. (2001). The potential impacts of climate variability and change on air pollution-related health effects in the United States. *Environmental Health Perspectives*, 109 Suppl (May), 199–209. doi:10.2307/3435010
- Boogaard, H., Kos, G. P. A., Weijers, E. P., Janssen, N. A H., Fischer, P. H., van der Zee, S. C., de Hartog, J.J., & Hoek, G. (2011). Contrast in air pollution components between major streets and background locations: Particulate matter mass, black carbon, elemental composition, nitrogen oxide and ultrafine particle number. *Atmospheric Environment*, 45(3), 650–658. doi:10.1016/j.atmosenv.2010.10.033

- Borrego, C., Monteiro, A., Ferreira, J., Miranda, A. I., Costa, A. M., Carvalho, A. C., & Lopes, M. (2008). Procedures for estimation of modelling uncertainty in air quality assessment. *Environment International*, 34(5), 613–620. doi:10.1016/j.envint.2007.12.005
- Boylan, J. W., & Russell, A. G. (2006). PM and light extinction model performance metrics, goals, and criteria for three-dimensional air quality models. *Atmospheric Environment*, 40(26), 4946–4959. doi:10.1016/j.atmosenv.2005.09.087
- Bruneekreef, B., & Holgate, S. T. (2002). Air pollution and health. *Lancet*, 360, 1233–1242. doi:10.1016/S0140-6736(02)11274-8
- Carslaw, D. C., & Ropkins, K. (2012). openair - An R package for air quality data analysis. *Environmental Modelling & Software*, 27-28, 52–61. doi:10.1016/j.envsoft.2011.09.008
- CBS. (2016a). CBS StatLine - Land use; all categories, municipalities. Retrieved January 22, 2016, from <http://statline.cbs.nl/Statweb/publication/?DM=SLEN&PA=70262eng&D1=0,2,6,16,20,25,28,31,41&D2=76,99,271&D3=3-6&LA=EN&VW=T>
- CBS. (2016b). CBS StatLine - Population; region per month. Retrieved January 22, 2016, from <http://statline.cbs.nl/StatWeb/publication/?DM=SLNL&PA=37230ned&D1=17&D2=57-100&D3=l&LA=EN&HDR=G2&STB=G1,T&VW=T>
- Chang, J. C., & Hanna, S. R. (2004). Air quality model performance evaluation. *Meteorology and Atmospheric Physics*, 87(1-3), 167–196. doi:10.1007/s00703-003-0070-7
- Cheung, K., Daher, N., Kam, W., Shafer, M. M., Ning, Z., Schauer, J. J., & Sioutas, C. (2011). Spatial and temporal variation of chemical composition and mass closure of ambient coarse particulate matter (PM10-2.5) in the Los Angeles area. *Atmospheric Environment*, 45(16), 2651–2662. doi:10.1016/j.atmosenv.2011.02.066
- Christakos, G. (1990). A Bayesian/maximum-entropy view to the spatial estimation problem. *Mathematical Geology*, 22(7), 763–777. doi:10.1007/BF00890661
- Christakos, G. (1998). Spatiotemporal information systems in soil and environmental sciences. *Geoderma*, 85(2-3), 141–179. doi:10.1016/S0016-7061(98)00018-4
- Christakos, G. (2000). *Modern Spatiotemporal Geostatistics*. Oxford University Press. doi:10.1016/S0016-7061(02)00104-0
- Christakos, G., Bogaert, P., & Serre, M. L. (2002). *Temporal GIS: Advanced functions for field-based applications* (First edit). Springer Berlin Heidelberg. doi:10.1007/978-3-662-04482-7
- Christakos, G., & Serre, M. L. (2000). BME analysis of spatiotemporal particulate matter distributions in North Carolina. *Atmospheric Environment*, 34(20), 3393–3406. doi:10.1016/S1352-2310(00)00080-7
- Close, J.-P., (Ed.). (2016). *AiREAS : Sustainocracy for a Healthy City The Invisible made Visible Phase 1*. Springer Dordrecht. doi:10.1007/978-3-319-26940-5
- Colls, J., & Tiwary, A. (2009). Air Pollution : Measurement, Modelling and Mitigation, Third Edition. Hoboken: CRC Press. Retrieved from <http://itc.eblib.com/patron/FullRecord.aspx?p=446716>
- Cox, W. M., & Tikvart, J. a. (1990). A statistical procedure for determining the best performing air quality simulation model. *Atmospheric Environment. Part A. General Topics*, 24(9), 2387–2395. doi:10.1016/0960-1686(90)90331-G
- Cressie, N. (1985). Fitting variogram models by weighted least squares. *Journal of the International Association for Mathematical Geology*, 17(5), 563–586. doi:10.1007/BF01032109
- Daly, A., & Zannetti, P. (2007). Air Pollution Modeling – An Overview. *Ambient Air Pollution*, I(2003), 15–28. Retrieved from <http://envirocomp.org/books/chapters/2AAP.pdf>
- de Hoogh, K., Wang, M., Adam, M., Badaloni, C., Beelen, R., Birk, M., Birk, M., Cesaroni, G., Cirach, M., Declercq, C., Dedele, A., Dons, E., de Nazelle, A., Eeftens, M., Eriksen, K., Eriksson, C., Fischer, P., Grazuleviciene, R., Gyparis, A., Hoffmann, B., Jerret, M., Katsouyanni, K., Iakovides, M., Lanki, T., Lindley, S., Madsen, C., Molter, A., Mosler, G., Nador, G., Nieuwenhuijsen, M., Pershagen, G., Peters, A., Phuleria, H., Probst-Hensch, N., Raaschou-Nielsen, O., Quass, U., Ranzi, A., Stephanou, E., Sugiri, D., Schwarze, P., Tsai, M., Yli-Tuomi, T., Varro, M.J., Vinneau, D., Weinmayr, G., Bruneekreef, B. & Hoek, G. (2013). Development of land use regression models for particle composition in twenty study areas in Europe. *Environmental Science & Technology*, 47(11), 5778–86. doi:10.1021/es400156t
- Den Boeft, J., Eerens, H. C., Den Tonkelaar, W. A M., & Zandveld, P. Y. J. (1996). CAR International: A simple model to determine city street air quality. *Science of the Total Environment*, 189-190, 321–326. doi:10.1016/0048-9697(96)05226-6

- Denby, B., & Larssen, S. (2010). *Guidance on the Use of Models for the European Air Quality Directive (ETC/ACC Version 6.2)*. FAIRMODE. Retrieved from http://www.calidaddelaire.es/descargas/Model_guidance_v5_1a.pdf
- Duyzer, J., van den Hout, D., Zandveld, P., & van Ratingen, S. (2015). Representativeness of air quality monitoring networks. *Atmospheric Environment*, 104, 88–101. doi:10.1016/j.atmosenv.2014.12.067
- EEA. (2014a). *Air pollution fact sheet 2014 Netherlands*. Retrieved from <http://www.eea.europa.eu/themes/air/air-pollution-country-fact-sheets-2014/netherlands-air-pollutant-emissions-country-factsheet/view>
- EEA. (2014b). *Air quality in Europe: 2014 Report*. Copenhagen. doi:10.2800/22847
- EEA. (2014c). AirBase database. Retrieved July 19, 2015, from <http://acm.eionet.europa.eu/databases/airbase>
- EEA. (2015a). *Exceedance of air quality limit values in urban areas (CSI 004)*. Retrieved from <http://www.eea.europa.eu/data-and-maps/indicators/exceedance-of-air-quality-limit-3/assessment>
- EEA. (2015b). Road Vehicles - Transport - Air - Environment - European Commission. Retrieved February 4, 2016, from <http://ec.europa.eu/environment/air/transport/road.htm>
- EEA. (2015c). Standards - Air Quality - Environment - European Commission. Retrieved November 12, 2015, from <http://ec.europa.eu/environment/air/quality/standards.htm>
- Eerens, H. C., Sliggers, C. J., & van den Hout, K. D. (1993). The CAR model: The Dutch method to determine city street air quality. *Atmospheric Environment. Part B. Urban Atmosphere*, 27(4), 389–399. doi:10.1016/0957-1272(93)90016-Y
- EPA. (2015). National Ambient Air Quality Standards (NAAQS) | Technology Transfer Network | US EPA. Retrieved November 12, 2015, from <http://www3.epa.gov/ttn/naaqs/criteria.html>
- EU. (2008). Directive 2008/50/EC of the European Parliament and of the Council of 21 May 2008 on ambient air quality and cleaner air for Europe. *Official Journal of the European Communities*, 1–43.
- EU. (2010). *Guide to the demonstration of equivalence of ambient air monitoring methods*. Retrieved from <http://ec.europa.eu/environment/air/quality/legislation/pdf/equivalence.pdf>
- Fritz, J. B., & Borst, H. C. (1999). *URBIS-Instrument for Local Environmental Surveys*. Retrieved from http://ec.europa.eu/environment/life/project/Projects/PDF/LIFE96_ENV_NL_000203_LAYM_AN.pdf
- Gräler, B., Gerharz, L., & Pebesma, E. (2012). Spatio-temporal analysis and interpolation of PM10 measurements in Europe. *ETC/ACM Technical Paper 2011/10*, (November 2011), 37. Retrieved from http://acm.eionet.europa.eu/reports/ETCACM_TP_2011_10_spatio-temp_AQinterpolation
- Hamm, N. A. S., Finley, A. O., Schaap, M., & Stein, A. (2015). A spatially varying coefficient model for mapping PM10 air quality at the European scale. *Atmospheric Environment*, 102, 393–405. doi:10.1016/j.atmosenv.2014.11.043
- Hamm, N. A. S., Lochem, M. Van Hoek, G., Otjes, R., van der Sterren, S., & Verhoeven, H. (2016). AiREAS: Sustainocracy for a Healthy City. In J.-P. Close (Ed.), *AiREAS: Sustainocracy for a Healthy City* (pp. 51–77). Springer. doi:10.1007/978-3-319-26940-5
- Hoek, G., Beelen, R., de Hoogh, K., Vienneau, D., Gulliver, J., Fischer, P., & Briggs, D. (2008). A review of land-use regression models to assess spatial variation of outdoor air pollution. *Atmospheric Environment*, 42(33), 7561–7578. doi:10.1016/j.atmosenv.2008.05.057
- Hoogerbrugge, R., Denier van der Gon, H. A. C., van Zantem, M. C., & Matthijsen, J. (2010). *Trends in Particulate Matter*. Retrieved from <http://www.pbl.nl/en/publications/2010/Trends-Particulate-Matter>
- Hwa-Lung, Y., & Chih-Hsin, W. (2010). Retrospective prediction of intraurban spatiotemporal distribution of PM2.5 in Taipei. *Atmospheric Environment*, 44(25), 3053–3065. doi:10.1016/j.atmosenv.2010.04.030
- ISO. (2013). *Geographic information — Data quality ISO/FDIS 19157. Iso/Tc 211*. Retrieved from http://www.iso.org/iso/iso_catalogue/catalogue_tc/catalogue_detail.htm?csnumber=32575
- Janssen, S., Dumont, G., Fierens, F., & Mensink, C. (2008). Spatial interpolation of air pollution measurements using CORINE land cover data. *Atmospheric Environment*, 42(20), 4884–4903. doi:10.1016/j.atmosenv.2008.02.043
- Jerrett, M., Arain, A., Kanaroglou, P., Beckerman, B., Potoglou, D., Sahsuvaroglu, T., Morrison, J., & Giovis, C. (2005). A review and evaluation of intraurban air pollution exposure models. *Journal of Exposure Analysis and Environmental Epidemiology*, 15(2), 185–204. doi:10.1038/sj.jea.7500388

- Jha, D. K., Sabesan, M., Das, A., Vinithkumar, N. V., & Kirubagaran, R. (2011). Evaluation of Interpolation Technique for Air Quality Parameters in Port Blair, India. *Universal Journal of Environmental Research and Technology*, 1(3), 301–310.
- JRC. (2015). DELTA Benchmarking: Fairmode tools and software. Retrieved February 14, 2016, from <http://aqm.jrc.ec.europa.eu/index.aspx>
- Juda-Rezler, K., Reizer, M., & Oudinet, J. P. (2011). Determination and analysis of PM10 source apportionment during episodes of air pollution in Central Eastern European urban areas: The case of wintertime 2006. *Atmospheric Environment*, 45(36), 6557–6566. doi:10.1016/j.atmosenv.2011.08.020
- Kanevski, M. (2010). Advanced Mapping of Environmental Data: Introduction. *Advanced Mapping of Environmental Data: Geostatistics, Machine Learning and Bayesian Maximum Entropy*, 1–17. doi:10.1002/9780470611463.ch1
- Keuken, M., Zandveld, P., van den Elshout, S., Janssen, N. a H., & Hoek, G. (2011). Air quality and health impact of PM10 and EC in the city of Rotterdam, the Netherlands in 1985–2008. *Atmospheric Environment*, 45(30), 5294–5301. doi:10.1016/j.atmosenv.2011.06.058
- Kim, K.-H., Kabir, E., & Kabir, S. (2015). A review on the human health impact of airborne particulate matter. *Environment International*, 74, 136–143. doi:10.1016/j.envint.2014.10.005
- Knotters, M., Heuvelink, G. B. M., Hoogland, T., & Walvoort, D. J. J. (2010). *A disposition of interpolation techniques*. Wageningen: Statutory Research Tasks Unit for Nature & the Environment, Wageningen UR. Retrieved from www.wotnatuurenmilieu.nl
- Knox, A., Mykhaylova, N., Evans, G. J., Lee, C. J., Karney, B., & Brook, J. R. (2013). The expanding scope of air pollution monitoring can facilitate sustainable development. *Science of the Total Environment*, 448, 189–196. doi:10.1016/j.scitotenv.2012.07.096
- Kumar, P., Morawska, L., Martani, C., Biskos, G., Neophytou, M., Di Sabatino, S., Bell, M., Norford, L., & Britter, R. (2015). The rise of low-cost sensing for managing air pollution in cities. *Environment International*, 75, 199–205. doi:10.1016/j.envint.2014.11.019
- Lazaridis, M. (2011). *First Principles of Meteorology and Air Pollution* (Vol. 19). doi:10.1007/978-94-007-0162-5
- Lee, S. J., Yeatts, K. B., & Serre, M. L. (2009). A Bayesian Maximum Entropy approach to address the change of support problem in the spatial analysis of childhood asthma prevalence across North Carolina. *Spatial and Spatio-Temporal Epidemiology*, 1(1), 49–60. doi:10.1016/j.sste.2009.07.005
- Lee, S.-J., Balling, R., & Gober, P. (2008). Bayesian Maximum Entropy Mapping and the Soft Data Problem in Urban Climate Research. *Annals of the Association of American Geographers*, 98(2), 309–322. doi:10.1080/00045600701851184
- Lenschow, P. (2001). Some ideas about the sources of PM10. *Atmospheric Environment*, 35(1), 23–33. doi:10.1016/S1352-2310(01)00122-4
- Li, J., & Heap, A. D. (2011). A review of comparative studies of spatial interpolation methods in environmental sciences: Performance and impact factors. *Ecological Informatics*, 6(3-4), 228–241. doi:10.1016/j.ecoinf.2010.12.003
- Li, J., & Heap, A. D. (2014). Spatial interpolation methods applied in the environmental sciences: A review. *Environmental Modelling & Software*, 53, 173–189. doi:10.1016/j.envsoft.2013.12.008
- Li, L., Wu, J., Ghosh, J. K., & Ritz, B. (2013). Estimating spatiotemporal variability of ambient air pollutant concentrations with a hierarchical model. *Atmospheric Environment*, 71, 54–63. doi:10.1016/j.atmosenv.2013.01.038
- Liu, L., Ruddy, T., Dalipaj, M., Poon, R., Szyszkowicz, M., You, H., Dales, R.E., & Wheeler, A. J. (2009). Effects of indoor, outdoor, and personal exposure to particulate air pollution on cardiovascular physiology and systemic mediators in seniors. *Journal of Occupational and Environmental Medicine / American College of Occupational and Environmental Medicine*, 51(9), 1088–1098. doi:10.1097/JOM.0b013e3181b35144
- MacKay, K. P., & Bornstein, R. D. (1982). *Statistical evaluation of air quality model*. Retrieved from <https://statistics.stanford.edu/sites/default/files/SIMS%2056.pdf>
- Matthijssen, J., & Koelemeijer, R. B. a. (2010). *Policy research programme on particulate matter Main results and policy consequences*. Retrieved from <http://www.pbl.nl/en/publications/2010/Policy-research-programme-particulate-matter-Main-results-and-policy-consequences>
- Matthijssen, J., & ten Brink, H. M. (2007). *PM 2.5 in the Netherlands: Consequences of the new European air quality standards*.
- Miller, H. J. (2004). Tobler's First Law and Spatial Analysis. *Annals of the Association of American Geographers*, 94(2), 284–289. doi:10.1111/j.1467-8306.2004.09402005.x

- Murad, M. H. (2012). Main Air Pollutants and Myocardial Infarction- A Systematic Review and Meta-analysis. *The Journal of the American Medical Association*, 307(7), 713–721. doi:10.1001/jama.2012.126
- Nazelle, A. De, Arunachalam, S., & Serre, M. L. (2010). Bayesian maximum entropy integration of ozone observations and model predictions: An application for attainment demonstration in North Carolina. *Environmental Science and Technology*, 44(15), 5707–5713. doi:10.1021/es100228w
- Nguyen, D. L. (2014). A Brief Review of Air Quality Models and Their Applications. *Open Journal of Atmospheric and Climatic Change*, 1(2), 60–81.
- Nielinger, J., Rockle, R., Hans-Chrisitan, H., & Kost, W.-J. (2004). Lagrange Versus Eulerian Dispersion Modeling Comparison for Investigations Concerning Air Pollution Caused By Traffic. In *9th International Conference on Harmonisation within Atmospheric Dispersion Modelling for Regulatory Purposes* (pp. 129–132). Retrieved from http://www.harmo.org/Conferences/Proceedings/_Garmisch/publishedSections/5.29.pdf
- Otjes, R. (2016). CalVal 2.
- Pang, W., Christakos, G., & Wang, J.-F. (2009). Comparative spatiotemporal analysis of fine particulate matter pollution. *Environmetrics*, (April). doi:10.1002/env
- Peng, R. D. (2008). A Method for Visualizing Multivariate Time Series Data. *Journal of Statistical Software*, 25(1), 1–17.
- Pernigotti, A. D., Thunis, P., & Gerboles, M. (2013). Modeling quality objectives in the framework of the FAIRMODE project : working document ., 2013.
- Pernigotti, D., Gerboles, M., Belis, C. a, & Thunis, P. (2013). Model quality objectives based on measurement uncertainty. Part II: NO₂ and PM10. *Atmospheric Environment*, 79, 869–878. doi:10.1016/j.atmosenv.2013.05.018
- QGIS Development Team. (2015). QGIS Pisa 2.10.1. Open Source Geospatial Foundation. Retrieved from <http://qgis.org/>
- R Core Team, R. C. (2014). R: A language and environment for statistical computing. Vienna, Austria: R Foundation for Statistical Computing. Retrieved from <http://www.r-project.org/>
- Rajasegarar, S., Havens, T. C., Karunasekera, S., Leckie, C., Bezdek, J. C., Jamriska, M., Gunatilaka, A., Skvortsov, A., & Palaniswami, M. (2014). High-resolution monitoring of atmospheric pollutants using a system of low-cost sensors. *IEEE Transactions on Geoscience and Remote Sensing*, 52(7), 3823–3832. doi:10.1109/TGRS.2013.2276431
- Raz, R., Roberts, A. L., Lyall, K., Hart, J. E., Just, A. C., Laden, F., & Weisskopf, M. G. (2014). Autism Spectrum Disorder and Particulate Matter Air Pollution before, during, and after Pregnancy: A Nested Case–Control Analysis within the Nurses’ Health Study II Cohort. *Environmental Health Perspectives*, 123(3), 264–70. doi:10.1289/ehp.1408133
- Riccio, a., Barone, G., Chianese, E., & Giunta, G. (2006). A hierarchical Bayesian approach to the spatio-temporal modeling of air quality data. *Atmospheric Environment*, 40(3), 554–566. doi:10.1016/j.atmosenv.2005.09.070
- RIVM. (2015). Home - National Institute for Health and the Environment. Retrieved February 4, 2016, from <http://www.rivm.nl/>
- Romanowicz, R., Higson, H., & Teasdale, I. (2000). Bayesian uncertainty estimation methodology applied to air pollution modelling., 240–260. doi:10.1002/(SICI)1099-095X(200005/06)11:3<351::AID-ENV424>3.0.CO;2-Z
- Ryan, P. H., & LeMasters, G. K. (2007). A review of land-use regression models for characterizing intraurban air pollution exposure. *Inhalation Toxicology*, 19 Suppl 1(2), 127–33. doi:10.1080/08958370701495998
- Schaap, M., Timmermans, R. M. A., Roemer, M., Boersen, G. A. C., Builtjes, P. J. H., Sauter, F. J., Velders, G.J.M., & Beck, J. P. (2008). The LOTOS EUROS model: description, validation and latest developments. *International Journal of Environment and Pollution*, 32(2), 270. doi:10.1504/IJEP.2008.017106
- Serre, M. L., & Christakos, G. (1999). Modern geostatistics : computational BME analysis in the light of uncertain physical knowledge - the Equus Beds study. *Stochastic Environmental Research and Risk Assessment*, 13(1), 1–26. doi:10.1007/s004770050029
- Shah, A. S. , Langrish, J. P., Nair, H., McAllister, D. A., Hunter, A. L., Donaldson, K., ... Mills, N. L. (2013). Global association of air pollution and heart failure: A systematic review and meta-analysis. *The Lancet*, 382(9897), 1039–1048. doi:10.1016/S0140-6736(13)60898-3
- Shah, A., Zeileis, A., & Grothendieck, G. (2005). zoo Quick Reference. *Package Vignette*. Retrieved from <http://debian.bjtu.edu.cn/cran/web/packages/zoo/vignettes/zoo-quickref.pdf>

- Shinyei Technologies. (2010). *Specification Sheet of Particle Sensor PPD42NS* (Vol. 2010). Retrieved from <http://www.sca-shinyei.com/pdf/PPD42NS.pdf>
- Srimuruganandam, B., & Shiva Nagendra, S. M. (2012). Source characterization of PM10 and PM2.5 mass using a chemical mass balance model at urban roadside. *The Science of the Total Environment*, 433, 8–19. doi:10.1016/j.scitotenv.2012.05.082
- Tessum, C. W., Hill, J. D., & Marshall, J. D. (2015). Twelve-month, 12km resolution North American WRF-Chem v3.4 air quality simulation: performance evaluation. *Geoscientific Model Development*, 8(2012), 957–973. doi:10.5194/gmd-8-957-2015
- Thi, N., Oanh, K., Permadi, D. A., Bao-ning, Z., Huy, T.N.Q., Phuong, N.L., Kanabkaew, T., & Iqbal, A. (2012). Applications of Photochemical Smog Models for Assessment of Ozone, Particulate Matter Air Quality, and Acid Deposition in Asian Cities. In *Integrated Air Quality Management: Asian Case Studies* (pp. 151–198). CRC Press. doi:10.1201/b12235-8
- Thunis, P., Cuvelier, C., Pederzoli, A., Georgieva, E., Pernigotti, D., Degraeuwe, B., & Marioni, M. (2015). *DELTA Version 5 . 1 Concepts / User 's Guide / Diagrams Authors*. Ispra. Retrieved from http://fairmode.jrc.ec.europa.eu/document/fairmode/WG1/DELTA_UserGuide_V5_1.pdf
- Thunis, P., Pederzoli, a., & Pernigotti, D. (2012a). Performance criteria to evaluate air quality modeling applications. *Atmospheric Environment*, 59, 476–482. doi:10.1016/j.atmosenv.2012.05.043
- Thunis, P., Pederzoli, A., & Pernigotti, D. (2012b). *FAIRMODE SG4 Report Model quality objectives Template performance report DELTA updates*. Retrieved from http://fairmode.jrc.ec.europa.eu/document/fairmode/WG1/FAIRMODE_SG4_Report_March2012.pdf
- Thunis, P., Pernigotti, D., & Gerboles, M. (2013). Model quality objectives based on measurement uncertainty. Part I: Ozone. *Atmospheric Environment*, 79, 861–868. doi:10.1016/j.atmosenv.2013.05.018
- TNO. (2015). Urbis: Instrument for local environmental exploration. Retrieved August 29, 2015, from <https://www.tno.nl/nl/aandachtsgebieden/leefomgeving/environment-sustainability/gebiedsontwikkeling/urbis-instrument-voor-lokale-milieuverkenning/>
- Tobler, A. W. R. (1970). A Computer Movie Simulation Urban Growth in Detroit Region. *Economic Geography*, 46(332), 234–240. doi:10.1126/science.11.277.620
- US-EPA. (2015). Basic Information-Particulate Matter. Retrieved February 13, 2016, from <http://www3.epa.gov/pm/basic.html>
- van de Kassteele, J., & Stein, A. (2006). A model for external drift kriging with uncertain covariates applied to air quality measurements and dispersion model output. *Environmetrics*, 17(4), 309–322. doi:10.1002/env.771
- van de Kassteele, J., Stein, A., Dekkers, A. L. M., & Velders, G. J. M. (2009). External drift kriging of NO_x concentrations with dispersion model output in a reduced air quality monitoring network. *Environmental and Ecological Statistics*, 16(3), 321–339. doi:10.1007/s10651-007-0052-x
- Vardoulakis, S., Fisher, B. E. A., Pericleous, K., & Gonzalez-Flesca, N. (2003). Modelling air quality in street canyons: A review. *Atmospheric Environment*, 37(2), 155–182. doi:10.1016/S1352-2310(02)00857-9
- Visser, H., Buringh, E., & van Breugel, P. B. (2001). Composition and Origin of Airborne Particulate Matter in the Netherlands, 787. Retrieved from <http://hdl.handle.net/10029/257110>
- VROM. (2008). *Bijlage 3: Explanatory note to the NL forms 02/07/2008*. Den Haag. Retrieved from https://circabc.europa.eu/sd/a/e04b4781-78c1-46b8-9cbd-fb7da9a0efdc/NL_EL_Notification_3_Summary.pdf
- Wang, M., Beelen, R., Bellander, T., Birk, M., Cesaroni, G., Cirach, M., ... Brunekreef, B. (2014). Performance of multi-city land use regression models for nitrogen dioxide and fine particles. *Environmental Health Perspectives*, 122(8), 843–849. doi:10.1289/ehp.1307271
- Wesseling, J., den Boeft, J., Boersen, G. A. C., Hollander, K., van den Hout, K. D., Keuken, M. P., Spoelstra, H., Teeuwisse, S.D., Weinhold, O., & Zandveld, P. Y. J. (1996). Development and validation of the new TNO models for the dispersion of traffic emissions. In *8th International Conference on Harmonisation within Atmospheric Dispersion Modelling for Regulatory Purposes* (pp. 456–460). Retrieved from http://www.harmo.org/conferences/Proceedings/_Sofia/publishedSections/Pages456to460.pdf
- WHO. (2006). *WHO Air quality guidelines for particulate matter, ozone, nitrogen dioxide and sulfur dioxide: global update 2005: summary of risk assessment*. Geneva: World Health Organization. Retrieved from http://whqlibdoc.who.int/hq/2006/WHO_SDE_PHE_OEH_06.02_eng.pdf?ua=1

- WHO. (2013). *Health Effects of Particulate Matter: Policy implications for countries in eastern Europe, Caucasus and central Asia*. World Health Organization (Vol. 50). doi:10.5124/jkma.2007.50.2.175
- Williams, M., & Bruckmann, P. (2002). *Guidance To Member States on Pm10 Monitoring and Intercomparisons With the Reference Method. EC Working Group on Particulate Matter*. Retrieved from <http://ec.europa.eu/environment/air/pdf/finalwgreporten.pdf>
- Wong, D. W., Yuan, L., & Perlin, S. A. (2004). Comparison of spatial interpolation methods for the estimation of air quality data. *Journal of Exposure Analysis and Environmental Epidemiology*, 14(5), 404–415. doi:10.1038/sj.jea.7500338
- Yadav, R., Sahu, L. K., Beig, G., & Jaaffrey, S. N. . (2014). Temporal Variation of Particulate Matter (PM) and Potential Sources at an Urban Site of Udaipur in Western India. *Aerosol and Air Quality Research*, 1–17. doi:10.4209/aaqr.2013.10.0310
- Yip, F. Y., Keeler, G. J., Dvonch, J. T., Robins, T. G., Parker, E. A., Israel, B. A., & Brakefield-Caldwell, W. (2004). Personal exposures to particulate matter among children with asthma in Detroit, Michigan. *Atmospheric Environment*, 38(31), 5227–5236. doi:10.1016/j.atmosenv.2004.06.006
- Yu, H., Wang, C., & Wu, Y. (2009). An automatic approach to the mean and covariance estimations of spatiotemporal nonstationary processes. In *STATGIS 2009*. Milos. Retrieved from https://www.stat.aau.at/Tagungen/statgis/2009/StatGIS2009_Yu_1.pdf
- Yu, H.-L. (2014). STAR-BME. Retrieved February 15, 2016, from <http://140.112.63.249/STARBME/index.html>
- Yu, H.-L., Ku, S.-C., & Kolovos, A. (2015). A GIS tool for spatiotemporal modeling under a knowledge synthesis framework. *Stochastic Environmental Research and Risk Assessment*. doi:10.1007/s00477-015-1078-5
- Yu, H.-L., Ku, S.-J., & Kolovos, A. (2012). Advanced space-time predictive analysis with STAR-BME. In *Proceedings of the 20th International Conference on Advances in Geographic Information Systems - SIGSPATIAL '12* (p. 593). doi:10.1145/2424321.2424424

APPENDICES

Table 30 Appendix 1: Measurement uncertainty in the ILM

AirBox Location	Measurement Uncertainty in ILM sensors							
	PM10 ($\mu\text{g}/\text{m}^3$)				PM2.5 ($\mu\text{g}/\text{m}^3$)			
Hourly	6-Hourly	12-Hourly	Daily	Hourly	6-Hourly	12-Hourly	Daily	
1	3.21	3.17	3.15	3.11	1.43	1.42	1.40	1.38
2	4.32	4.26	4.23	4.18	1.74	1.72	1.70	1.68
3	4.60	4.54	4.52	4.46	1.94	1.92	1.91	1.89
4	3.73	3.69	3.66	3.63	1.57	1.55	1.54	1.52
5	3.28	3.24	3.22	3.19	1.49	1.47	1.46	1.44
6	2.30	2.29	2.27	2.31	0.90	0.90	0.88	0.90
7	3.58	3.56	3.54	3.50	1.87	1.86	1.84	1.81
8	4.00	3.96	3.94	3.90	1.69	1.68	1.66	1.65
9	2.80	2.77	2.75	2.73	1.34	1.33	1.32	1.30
11	3.11	3.07	3.05	3.03	1.50	1.49	1.48	1.46
12	3.16	3.13	3.11	3.08	1.61	1.60	1.58	1.56
13	3.81	3.77	3.74	3.70	1.76	1.74	1.72	1.70
14	4.19	4.12	4.08	4.02	1.74	1.72	1.70	1.68
16	5.32	5.25	5.21	5.15	2.03	2.01	1.99	1.96
17	4.13	4.05	4.02	4.00	1.63	1.61	1.59	1.58
19	4.31	4.23	4.18	4.13	1.77	1.75	1.73	1.70
20	3.16	3.12	3.10	3.07	1.55	1.54	1.52	1.50
23	2.37	2.38	2.41	2.37	1.25	1.25	1.27	1.24
24	4.30	4.25	4.22	4.16	1.80	1.78	1.76	1.74
25	2.54	2.52	2.48	2.42	1.26	1.25	1.24	1.21
26	3.57	3.53	3.50	3.47	1.57	1.55	1.54	1.52
27	3.53	3.46	3.43	3.39	1.51	1.49	1.47	1.45
28	4.03	3.98	3.95	3.90	1.59	1.57	1.55	1.53
29	4.18	4.13	4.10	4.05	1.70	1.68	1.66	1.64
30	3.61	3.57	3.55	3.51	1.57	1.55	1.53	1.51
31	2.73	2.70	2.67	2.65	1.37	1.36	1.35	1.33
32	4.48	4.42	4.37	4.31	1.85	1.83	1.81	1.78
34	4.05	4.00	3.96	3.92	1.69	1.68	1.66	1.64
35	3.37	3.32	3.30	3.28	1.71	1.69	1.68	1.66
36	3.53	3.54	3.60	3.75	1.64	1.63	1.63	1.63
37	3.09	3.06	3.04	3.01	1.45	1.43	1.42	1.40
39	3.59	3.60	3.61	3.71	1.85	1.87	1.92	2.02

Table 31 Appendix 2: Daily PM10 maps in Eindhoven

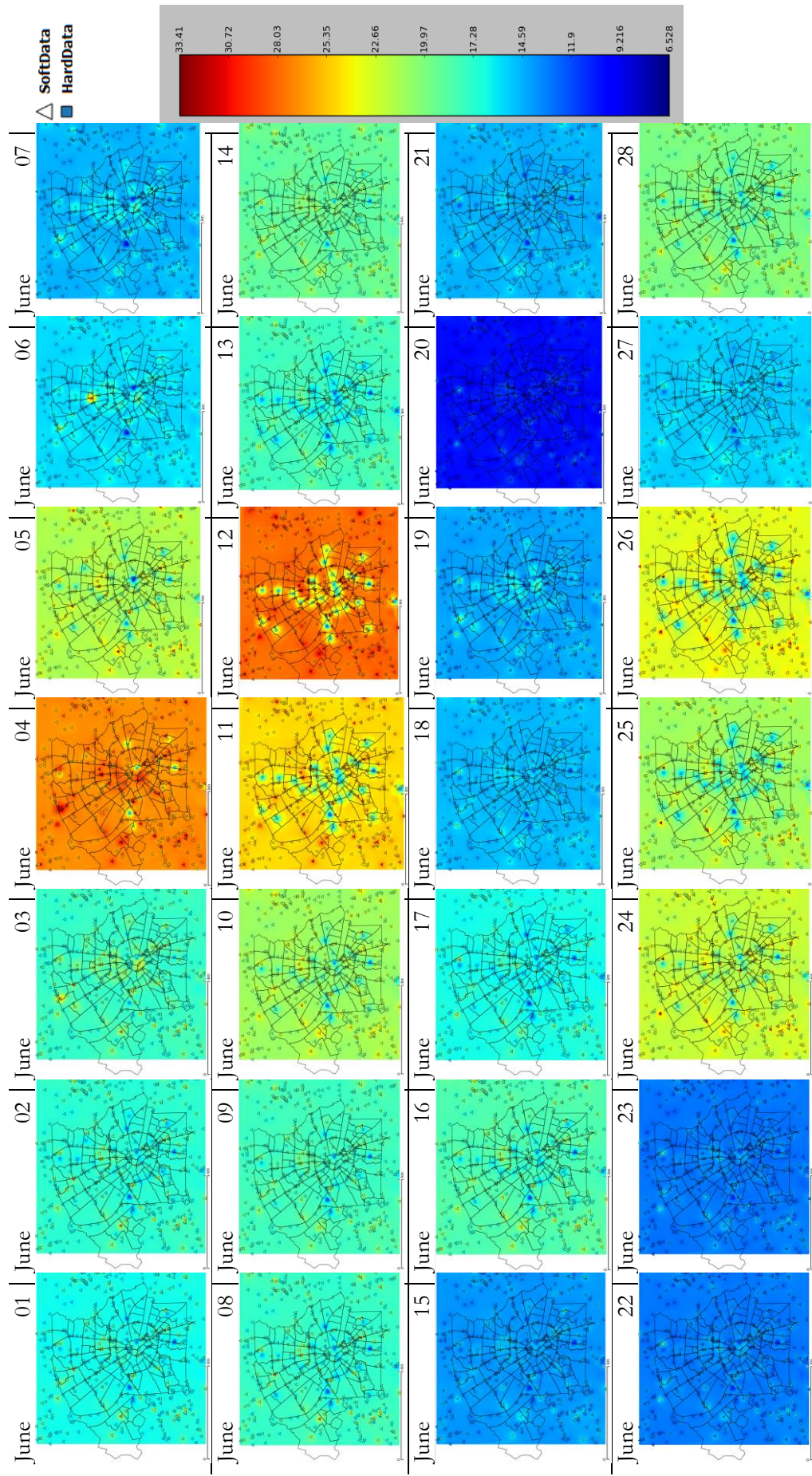


Table 32 Appendix 3 -Daily PM2.5 maps in Eindhoven

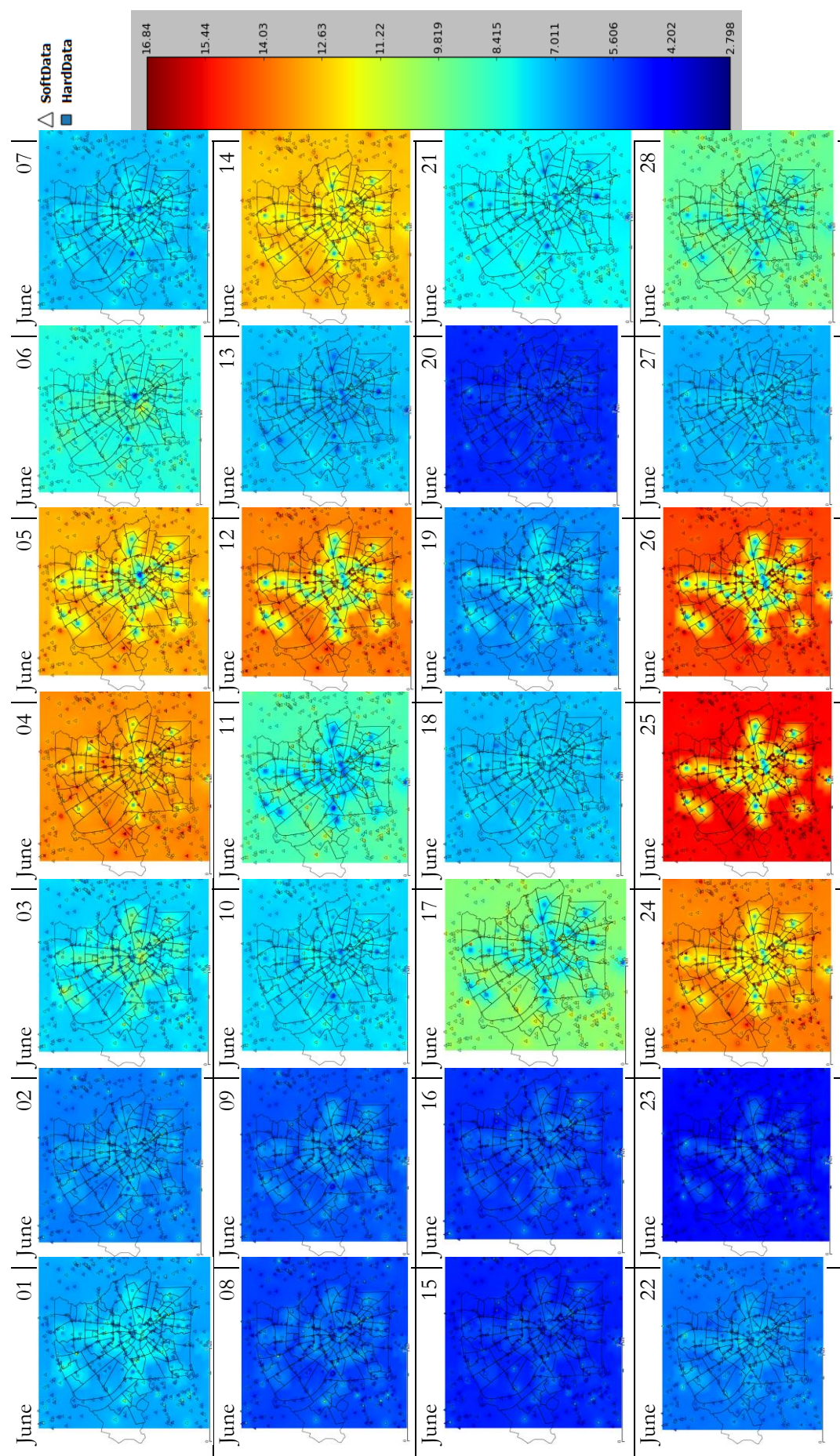


Table 33 Appendix 4-Hourly PM10 maps for June 04 in Eindhoven

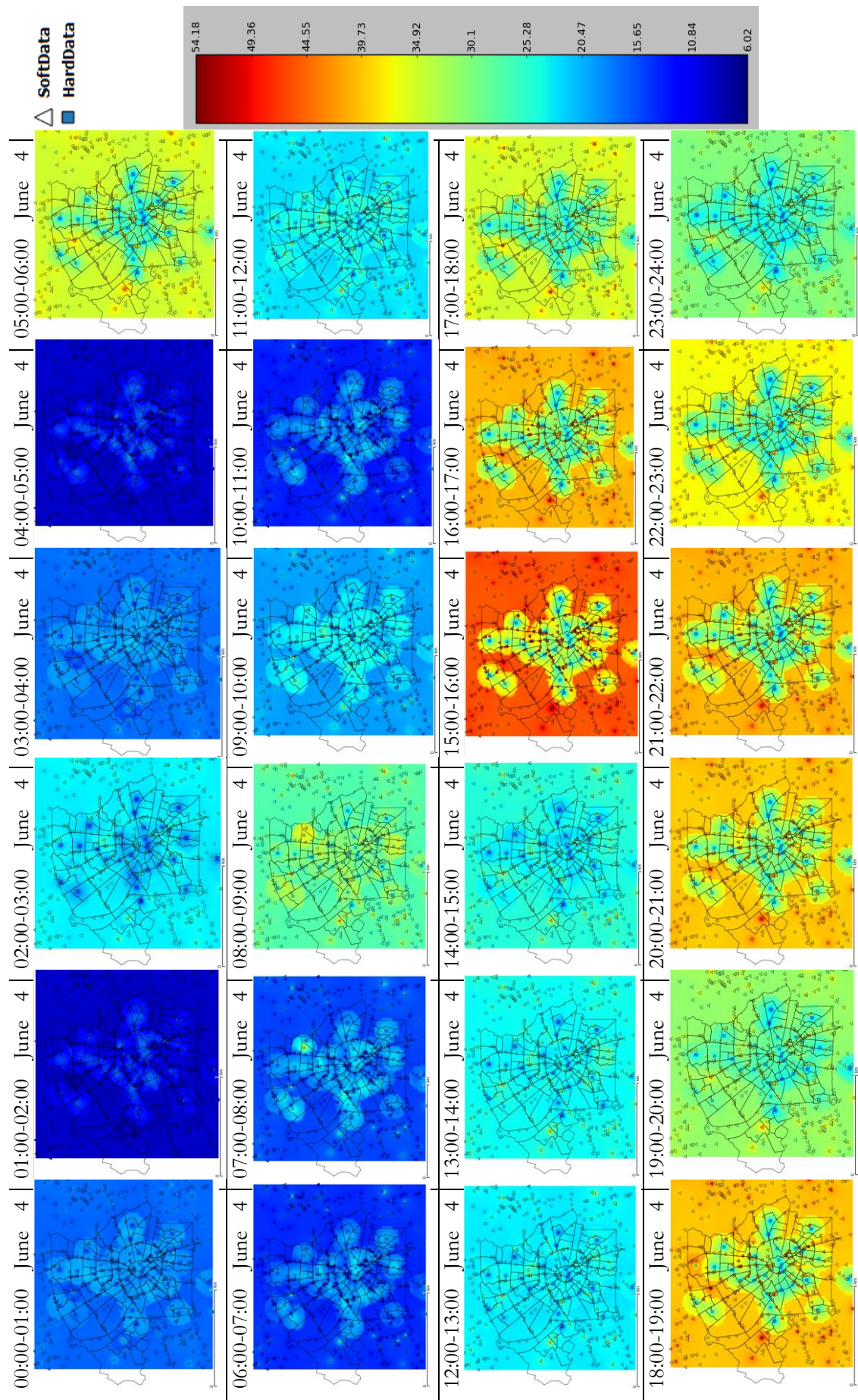


Table 34 Appendix 5 - Hourly PM2.5 maps for June 04 in Eindhoven

